

**Static and dynamic beam intensity modulation
in radiotherapy using a multileaf collimator**

Cover: Generation of an intensity modulated field by using
dynamic multileaf collimation.

Druk: Optima, Rotterdam

Static and dynamic beam intensity modulation in radiotherapy using a multileaf collimator

Statische en dynamische intensiteitsmodulatie in de radiotherapie
middels een multileaf collimator

PROEFSCHRIFT

ter verkrijging van de graad van doctor
aan de Erasmus Universiteit Rotterdam
op gezag van de Rector Magnificus

Prof.dr.ir. J.H. van Bommel

en volgens besluit van het College voor Promoties.

De openbare verdediging zal plaatsvinden op
vrijdag 8 december 2000 om 13:30 uur
door

Maarten Lucas Petrus Dirkx

geboren te Goirle

Promotiecommissie

Promotor: Prof.dr. P.C. Levendag

Overige leden: Dr. B.J.M. Heijmen (tevens co promotor)
Prof.dr.ir. J.J.W. Lagendijk
Prof.dr. J.W. Oosterhuis
Prof.dr.ir. P.F.F. Wijn

This thesis has been prepared at the Division of Clinical Physics,
Department of Radiotherapy, Daniel den Hoed Cancer Center,
University Hospital Rotterdam, The Netherlands.

Address for correspondence:

M.L.P. Dirkx

University Hospital Rotterdam, Daniel den Hoed Cancer Center

Department of Radiotherapy, Division of Clinical Physics

P.O. Box 5201, 3008 AE Rotterdam, The Netherlands

phone: (31) 10 4391183, fax: (31) 10 4391012, E-mail: dirkx@kfh.azr.nl

*In dierbare herinnering
aan mijn vader*

Contents

Chapter 1	Introduction	1
1.1	Radiotherapy.....	2
1.2	Realization of intensity modulated beam profiles	3
1.3	The MM50 Racetrack Microtron.....	4
1.4	Objective of this study.....	5
Chapter 2	Daily dosimetric quality control of the MM50 Racetrack Microtron using an Electronic Portal Imaging Device	7
2.1	Introduction	8
2.2	Materials and methods.....	8
2.2.1	<i>The electronic portal imaging device</i>	<i>8</i>
2.2.2	<i>Reproducibility, stability and linearity of the EPID</i>	<i>9</i>
2.2.3	<i>Daily quality control measurements</i>	<i>10</i>
2.3	Results and discussion.....	12
2.3.1	<i>Reproducibility, stability and linearity of the EPID</i>	<i>12</i>
2.3.2	<i>Daily quality control measurements</i>	<i>14</i>
2.3.3	<i>Protocol for daily quality control measurements.....</i>	<i>17</i>
2.4	Conclusions	17
Chapter 3	Field margin reduction using intensity modulated X-ray beams formed with a multileaf collimator	19
3.1	Introduction	20
3.2	Materials and methods.....	21
3.2.1	<i>Intensity modulated X-ray beams for treatment of prostate cancer patients: the applied technique.....</i>	<i>21</i>
3.2.2	<i>Evaluation of the IM technique based on 3D treatment planning</i>	<i>24</i>
3.2.3	<i>Accuracy of dose calculations</i>	<i>24</i>
3.2.4	<i>Implementation on the MM50 Racetrack Microtron</i>	<i>25</i>
3.3	Results and discussion.....	26
3.3.1	<i>Evaluation of the IM technique based on 3D treatment planning</i>	<i>26</i>
3.3.2	<i>Accuracy of dose calculations</i>	<i>29</i>
3.3.3	<i>Implementation on the MM50 Racetrack Microtron</i>	<i>31</i>
3.4	Summary and conclusions.....	31

Chapter 4	Beam intensity modulation for penumbra enhancement in the treatment of lung cancer.....	33
4.1	Introduction	34
4.2	Methods and materials.....	36
4.2.1	<i>The BIM technique.....</i>	36
4.2.2	<i>Evaluation of the BIM technique</i>	37
4.3	Results	39
4.3.1	<i>Dose distributions in the PTV.....</i>	39
4.3.2	<i>Dose distributions in normal tissues.....</i>	41
4.4	Conclusions and discussion.....	43
Chapter 5	Beam intensity modulation for penumbra enhancement and field length reduction in lung cancer treatments; a dosimetric study	45
5.1	Introduction	46
5.2	Material and methods	47
5.2.1	<i>The BIM technique.....</i>	47
5.2.2	<i>Dosimetric measurements.....</i>	48
5.2.3	<i>Treatment planning.....</i>	50
5.3	Results	50
5.3.1	<i>Sensitometric curve for polystyrene and lung.....</i>	50
5.3.2	<i>Comparison of dose distributions in polystyrene and lung for standard flat fields</i>	50
5.3.3	<i>Optimization of lengths and weights of boost fields used for BIM in lung</i>	52
5.3.4	<i>Comparison of dose distributions in the lung geometry for standard fields and intensity modulated fields</i>	52
5.3.5	<i>Comparison of dose distributions in the tumor geometry for standard fields and intensity modulated fields.....</i>	56
5.4	Conclusions	58
Chapter 6	Leaf trajectory calculation for dynamic multileaf collimation to realize optimized fluence profiles.....	59
6.1	Introduction	60
6.2	Iterative algorithm for leaf trajectory calculation	61
6.3	Materials and methods.....	63
6.3.1	<i>Measurement of collimator scatter factors</i>	63
6.3.2	<i>Measurement of transmission through the leaves.....</i>	64
6.3.3	<i>Realization of fluence profiles at the MM50 Racetrack Microtron.....</i>	65
6.3.4	<i>Dosimetric verification of leaf trajectory calculations</i>	66

6.4	Results and discussion.....	66
6.4.1	<i>Collimator scatter factors needed for leaf trajectory calculation.....</i>	66
6.4.2	<i>Verification of predicted collimator scatter factors for irregularly shaped fields and off-axis positions.....</i>	67
6.4.3	<i>Effective transmission through the leaves.....</i>	69
6.4.4	<i>Iterative calculation of leaf trajectories.....</i>	69
6.4.5	<i>Dosimetric verification of leaf trajectory calculation.....</i>	71
6.5	Conclusions	74

Chapter 7	Testing of the stability of intensity modulated beams generated with dynamic multileaf collimation, applied to the MM50 Racetrack Microtron.....	75
7.1	Introduction	76
7.2	Methods and materials.....	76
7.2.1	<i>Dynamic multileaf collimation at the MM50 Racetrack Microtron.....</i>	76
7.2.2	<i>Stability of leaf positioning in DMLC mode</i>	78
7.2.3	<i>Long term dosimetric stability</i>	79
7.2.4	<i>Dosimetric stability under gantry rotation</i>	80
7.2.5	<i>Sensitivity to treatment interrupts.....</i>	80
7.3	Results and discussion.....	81
7.3.1	<i>Stability of leaf positioning in DMLC mode</i>	81
7.3.2	<i>Long term dosimetric stability</i>	82
7.3.3	<i>Stability under gantry rotation</i>	84
7.3.4	<i>Sensitivity to treatment interrupts.....</i>	86
7.4	Conclusions	88

Chapter 8	Dosimetric verification of intensity modulated beams produced with dynamic multileaf collimation using an electronic portal imaging device.....	89
8.1	Introduction	90
8.2	Materials and methods.....	92
8.2.1	<i>EPID and ionization chamber dose measurements</i>	92
8.2.2	<i>Calculation of the dose distribution at the detector.....</i>	93
8.2.3	<i>Realization and verification of fluence profiles.....</i>	94
8.3	Results	95
8.4	Discussion and conclusions.....	98

Chapter 9	General discussion	101
9.1	Introduction	102
9.2	Clinical implementation of IMRT techniques using a multileaf collimator	102
9.2.1	<i>Static intensity modulation techniques.....</i>	<i>102</i>
9.2.2	<i>Dynamic intensity modulation</i>	<i>103</i>
9.2.3	<i>Rotational intensity modulation techniques.....</i>	<i>103</i>
9.2.4	<i>Comparison of techniques for intensity modulation with a MLC</i>	<i>104</i>
9.3	Impact of treatment uncertainties in IMRT	105
9.3.1	<i>Delineation of the target volume.....</i>	<i>105</i>
9.3.2	<i>Set-up accuracy and organ motion.....</i>	<i>106</i>
9.3.3	<i>Geometrical misalignment of the treatment unit parameters.....</i>	<i>107</i>
9.4	Dosimetrical verification of IMRT	109
9.4.1	<i>Verification by dose measurements.....</i>	<i>109</i>
9.4.2	<i>Independent verification of monitor units for IMRT.....</i>	<i>110</i>
9.5	Concluding remarks.....	110
Summary.....		111
Samenvatting.....		117
Bibliography		123
List of abbreviations, symbols and units.....		141
Nawoord.....		145
Curriculum vitae.....		147
List of publications.....		148

Chapter 1

Introduction

1.1 Radiotherapy

Radiotherapy is widely used for the treatment of cancer, either as a single modality or in combination with other treatments, like surgery or chemotherapy. The aim of radiotherapy is the eradication of tumor cells by means of ionizing radiation. Radiation can induce, either directly or indirectly, irreparable DNA damage in the cells, resulting in cellular kill directly or in a so-called apoptosis, i.e. cellular suicide. Because radiation damage is not restricted to tumor cells only, but affects normal cells as well, it is essential that the dose delivered to healthy tissues is as low as achievable to minimize the risk of side effects of the treatment.

Most frequently, radiation is delivered by external beam radiotherapy using a linear accelerator. For this kind of radiotherapy, possibilities to minimize the dose delivery to normal tissues have largely been extended in the past few decades. First of all, the introduction of CT, and later MRI, allowed for a more accurate definition of tumor volumes and sensitive structures. Secondly, the availability of user-friendly and fast, 3D treatment planning tools extended the possibilities to optimize treatment plans for a particular patient within a reasonable time, by a proper, manual selection of the number of treatment fields and, for each particular field, the beam direction, energy, weight and, if necessary, wedge angle. Thirdly, after introduction of multileaf collimators (MLC) the shape of treatment fields could be conformed easily and fast to the beam's eye view projection of the tumor volume, thereby reducing the dose delivery to surrounding healthy tissues [112]. Finally, investigations on computer optimization of radiotherapy treatment planning demonstrated that dose distributions could often be conformed more tightly to a target volume by customizing the beam intensity profiles within the treatment field (intensity modulated radiotherapy (IMRT)). The use of patient-specific intensity modulated beams makes it possible to correct for variations in patient contours and for tissue inhomogeneities. It allows for the generation of concave shaped dose distributions and the sparing of organs at risk in complex treatment geometries. For calculation of intensity modulated beam profiles, different inverse treatment planning techniques have been proposed in the literature [12,16,17,56,68,91, 104,114,134,137,164,166-168], but improved treatment plans using beam intensity modulation have also been realized by advanced, computer-assisted forward planning techniques [36,36,50].

Treatment planning techniques aiming at tailoring the high dose volume strictly to the tumor volume, while simultaneously delivering as low a radiation dose as possible to surrounding normal structures are classified as 3D conformal radiotherapy. A main impact of conformal radiotherapy is that it allows for a reduction in the dose delivered to sensitive healthy tissues, thereby reducing the risk of (severe) side effects, like

xerostomia in the treatment of head and neck cancer. For other tumors, like lung cancer and prostate cancer, application of advanced conformal treatment techniques makes escalation of the target dose possible, without increasing the risk of normal tissue complications, in an attempt to improve the probability of local tumor control and overall survival [86].

1.2 Realization of intensity modulated beam profiles

Patient-specific intensity modulated beam profiles can be realized in several ways. A rather straightforward method is the use of compensators [66], but this has several drawbacks. First of all, their production is labor-intensive. Since they have to be changed manually for each treatment field, their use is time consuming during treatment delivery as well. For this reason, only a limited number of compensators can generally be used in clinical practice. Another drawback is the need for models to accurately include scattered photons and beam hardening, as produced by the compensators, in the dose calculations.

As an alternative, several methods for realization of intensity modulated beams using a multileaf collimator have been suggested. Bortfeld *et al* [13] and Galvin *et al* [51] have investigated the use of static multileaf collimation. This technique is based on the superpositioning of a number of partially overlapping, static, irregularly shaped MLC fields. A second technique is the use of dynamic multileaf collimation. So far the 'sliding window' technique has received most attention in the literature. This technique is based on the independent movement of leaf pairs across the treatment field while the radiation is on, effectively sweeping apertures of variable widths across the field [29, 135,138,147]. Convery and Roosenbloom [29] published the basic algorithm to derive leaf motions to realize an optimized intensity modulated profile. Faster, analytical solutions to the problem were independently published by Spirou *et al* [135], Stein *et al* [138] and Svensson *et al* [147].

At the MM50 Racetrack Microtron, described in the next section, beam intensity modulation can also be realized by using scanning photon beams. Due to the width of the scanned photon beams (10 cm for a 50 MV beam [11,148], and even larger for lower energies), only fields with moderate gradients can presently be realized by beam scanning alone. For the 50 MV photon beam the capability of beam scanning to deliver more heterogeneous dose distributions could be improved by replacing the standard W/Cu target by a 3 mm thick Be target, reducing the width of the scanned photon beams to 3.5 cm only [148]. Beam scanning may effectively be used in combination with dynamic multileaf collimation, first adjusting as good as possible the incoming

fluence profile to the optimized fluence profile by beam scanning, after which dynamic multileaf collimation is required for fine adjustments only [57,136]. In this way, the time required for an IMRT treatment may be reduced significantly with respect to the use of dynamic multileaf collimation alone, but the complexity of the treatment is increased significantly.

A special kind of collimator which has been implemented clinically for the realization of intensity modulated beam profiles is the Peacock MiMiC [22,55]. This device produces a fan beam (1.7 or 3.4 cm wide) with an intensity profile that is modulated continuously while rotating the gantry. Generally, this fan beam does not cover the entire PTV in one gantry rotation, requiring the treatment couch with the patient to be moved precisely along the axis of rotation after each gantry rotation. For larger tumors, this results in much longer treatment times than are presently used in most radiotherapy departments.

A similar approach, which is still in a developmental phase, is the tomotherapy unit described by Mackie *et al* [102,103]. Like the Peacock system, the tomotherapy unit uses a fan-beam for irradiation of the patients. However, while in the Peacock system patients are sequentially irradiated and translated, radiation and translation take place simultaneously in the tomotherapy unit, similar to a spiral scans CT. An advantage of this technique is that the risk of underdosages due to beam-junction artifacts will be reduced. Another important issue is that a CT capability will be available in the tomotherapy unit, providing accurate information for patient set-up verification [49] and allowing for a reconstruction of the actual dose distribution delivered to a patient [109].

Yu *et al* [176] introduced the concept of intensity modulated arc therapy (IMAT). Instead of using a slit beam to treat a patient slice by slice, IMAT uses MLC-shaped fields, which change shape during gantry rotation. By employing multiple arc rotations, an optimized intensity profile is delivered from each gantry angle. For most clinical sites generally less than five arc rotations are required [15,178].

1.3 The MM50 Racetrack Microtron

An on-going research project involving the development and clinical introduction of conformal radiotherapy was started in the Daniel den Hoed Cancer Center at the time of the clinical introduction of a dual gantry MM50 Racetrack Microtron [70,93,105, 108,130] in March 1994. This device, manufactured by Scanditronix Medical AB, is a fully computer-controlled treatment unit, suited for advanced three-dimensional conformal radiation techniques. Photon beams in the range of 10 up to 50 MV can be

produced in steps of 5 MV. Electron beams are available from 7.5 up to 50 MeV in steps of 2.5 MeV. Flat beam profiles are created by scanning of elementary beams according to fixed scanning patterns. Due to the beam scanning, flattening filters for photon beams can be omitted or be very thin, yielding extremely flat beam profiles at all depths [70,93]. For electron beams, the scattering foil is very thin due to the scanning beam principle [69]. In combination with the helium atmosphere in the treatment head, this enables the use of isocentric irradiation techniques, applying the double focussed multileaf collimator for beam shaping, like for photon beams [46,71]. The MM50 can be used in a fully computer-controlled multi-segment treatment mode [38,105]. Using this mode only the set-up of the first segment (field) of a patient treatment needs direct interference of the technicians; all parameters of the next segments, like the gantry and collimator angles, couch positions, field shape, beam energy and monitor units, are set-up by the treatment computer. Customized intensity modulated beams can be generated by computer-controlled superpositioning of MLC-defined fields (static intensity modulation), by scanning of elementary beams according to individualized scanning patterns and by dynamic multileaf collimation [28,57,135,136,147,158].

1.4 Objective of this study

In the past decade much attention has been paid to the development of algorithms to calculate customized intensity modulated beam profiles for a particular patient by using inverse treatment planning techniques [12,16,17,56,68,91,104,114,134,137,164, 166-168]. On the other hand, clinical implementation of intensity modulated treatments, with one of the techniques described in section 1.2, has just been started in a limited number of institutes around the world.

The main objective of this study was the development and clinical implementation of intensity modulated conformal radiation techniques on the MM50 Racetrack Microtron using the multileaf collimator. Both techniques for static and dynamic beam intensity modulation using a multileaf collimator have been investigated.

For complex treatment machines like the MM50 and for advanced treatment techniques using intensity modulation, more extensive quality control is definitely required to ensure accurate and safe dose delivery to the patients. Therefore, a second objective of this work was the development of fast methods for dosimetric quality control using a camera based fluoroscopic electronic portal imaging device (EPID), as part of the overall quality control system.

Chapter 2 describes a daily dosimetric quality control procedure for the MM50, verifying the output (cGy/MU) and the beam profile for open and wedged fields of

scanning photon beams at different gantry angles. The suitability of the applied EPID for dosimetrical quality control is demonstrated.

In chapters 3 and 4 a technique for penumbra enhancement is presented using static beam intensity modulation (BIM) with a multileaf collimator, which allows for a reduction in the field length of all treatment fields used for co-planar treatments of prostate and lung cancer patients in our clinic. Based on 3D treatment planning, the benefits of this new technique in terms of dose delivery to the target volume and the normal tissues were assessed by comparison with our standard technique without BIM. Dose measurements were performed to assess the dosimetrical accuracy of the technique. Due to the limited accuracy of our treatment planning system in lung tissue, special attention had to be paid to the use of BIM for the treatment of lung cancer patients. Therefore, a more extensive dosimetrical study, which is presented in chapter 5, was performed on the use of BIM for this tumor site.

Chapter 6 describes an algorithm for the calculation of the required leaf trajectories to generate optimized intensity modulated beam profiles by means of dynamic multileaf collimation. In addition to algorithms published before [135,138,147,158], leaf transmission and collimator scatter were included and tongue-and-groove underdosages were fully avoided. The accuracy of this method in combination with our treatment planning system was assessed based on absolute dose measurements.

Before implementing dynamic multileaf collimation in clinical practice, tests were performed to investigate the stability of intensity modulated beam profiles realized with DMLC. Based on the results, described in chapter 7, the effects of gravity and of acceleration and deceleration of the leaves on the stability of the delivered dose profiles were derived.

Chapter 8 deals with a procedure for pre-treatment verification for each individual patient of absolute, intensity modulated beam profiles, realized using dynamic multileaf collimation, by applying our EPID. In contrast to previously published methods [5,65,100,118], this procedure simultaneously verifies (i) the calculation of the dose distribution by the treatment planning system, resulting from the derived leaf trajectories, (ii) the transfer of the leaf sequencing file to the treatment unit, and (iii) the mechanical and dosimetrical performance of the treatment machine.

Finally in chapter 9 a general discussion on the use of IMRT in clinical practice is presented.

Chapter 2
**Daily dosimetric quality control of the MM50 Racetrack
Microtron using an Electronic Portal Imaging Device**

Adopted from the original article by MLP Dirkx, M Kroonwijk, JCJ de Boer
and BJM Heijmen published in *Radiother. Oncol.* 37: 55-60, 1995.

2.1 Introduction

The dual gantry MM50 Racetrack Microtron that has been installed in the Daniel den Hoed Cancer Center consists of a separate electron accelerator and two gantries. Through an evacuated beam line of about 6 meters the accelerated electrons are transported to one of both gantries where clinical photon and electron beams are generated by computer-controlled scanning of elementary beams according to fixed scanning patterns [69,70]. A constant flow of a helium/nitrogen mixture (99% He, 1% N₂) runs through the MM50 monitor chambers and the treatment heads to reduce electron scattering, yielding very narrow elementary electron beams [69].

The complex lay-out with a separate accelerator serving two gantries, the application of beam scanning and the continuous gas flow through the monitor chamber and the treatment head definitely require a *daily* dosimetric quality control program in addition to more extensive checks on a two weekly basis. Therefore a method has been developed to perform *fast*, dosimetric checks under different gantry angles using the Philips SRI-100 electronic portal imaging device (EPID) fitted to each of both gantries of the MM50. Measurements take place every morning before patient treatment starts.

This chapter deals with a description of the daily quality control measurements and demonstrates the suitability of the EPID for this purpose. The stability of the absolute output and the relative fluence profile of the 25 MV scanned photon beam of the MM50 has been assessed. A protocol for quality control measurements, based on the results of this study, is described.

2.2 Materials and methods

2.2.1 The electronic portal imaging device

The SRI-100 is a fluoroscopic system: radiation incident on a fluorescent screen (at a distance of 160 cm from the focus) is converted into an optical image, which is digitized using a CCD camera. The CCD-chip consists of 512 x 256 pixels, with a pixel size projected at isocenter¹ of about 0.05 x 0.08 cm², resulting in a maximum field size of 25 x 19 cm² for imaging. In order to improve the signal to noise ratio, the signals of the CCD camera are accumulated on the CCD-chip and averaged in a frame grabber. The final image is stored in a PC using gray scale values in the range of 0 to

¹ All pixel and field sizes mentioned in this thesis are defined at isocenter level, i.e. at a distance of 100 cm from the focus.

255. The technical details of the EPID have been described by Visser *et al* [163].

Prerequisites for dosimetric quality control measurements with an EPID are adequate reproducibility, stability and linearity of the measured gray scale values. To ensure the response of the EPID, defined as the ratio of a measured gray scale value and the applied portal dose, to be as unequivocal as possible, some precautions have been taken. The gain and offset of the CCD camera have been set to fixed values and a fixed data acquisition time has been used. In addition, the images have only been corrected for dark current, which is measured just before irradiation starts.

The fluorescent screen of the EPID is a 0.165 cm thick stainless steel plate coated with a fluorescent layer [163]. For a 25 MV photon beam this screen is not thick enough to establish a full charged particle build-up. In the present study this is not a problem since the EPID has only been used for dosimetric constancy checks.

A fixed field size of 18 x 18 cm² has been used for all measurements in this study. For data reduction, average gray scale values have been calculated for 49 areas of 1.5 x 1.5 cm² inside the measured EPID-image, yielding dosimetric data for the beam axis and for 48 off-axis points (see figure 2.1). All software used for acquiring and analyzing the images has been written in the macro command language of the SRI-100 system.

In addition to the daily dosimetric checks with the EPID for the 18 x 18 cm² field, the field flatness and symmetry are also checked for the maximum field size (31 x 40 cm²) as part of our two weekly quality control program. These measurements are performed along the two main axes using a linear detector array consisting of 32 ionization chambers.

2.2.2 Reproducibility, stability and linearity of the EPID

The reproducibility, stability and linearity of the EPID have been assessed by comparing measured gray scale values with absolute dose measurements at the beam axis. The dose measurements were performed with a NE-2571 ionization chamber in a PMMA phantom at the depth of maximum dose with a source to surface distance of 100 cm. Since EPID and ionization chamber measurements could not be performed simultaneously, the two types of measurements were always performed sequentially, keeping the interval time as short as possible.

2.2.3 Daily quality control measurements

For the open 25 MV scanning photon beam, EPID images were obtained on a daily basis for four different gantry angles (0, 90, 180 and 270 degrees). For gantry angle 0, a 60° wedged field image was measured as well to verify the wedge position and to check the beam penetrative quality. All images were acquired using a fixed dose of 150 monitor units. The five fields (four open fields and one wedged field) were set-up under computer control using the MM50 multi-segment treatment mode which was described in chapter 1.3.

To determine deviations in the absolute beam output and in the relative 2D fluence profile, each image has been compared with a corresponding reference image. This reference image reflects the *absolute* 2D fluence profile at the time of beam commissioning for a fixed dose of 150 MU and a cGy/MU value of 1 for the 10 x 10 cm² field. Both the absolute output and the 2D fluence profile of the 25 MV photon beam of the MM50 are slightly gantry angle dependent. For clinical practice these dependencies are within acceptable levels and for treatment planning the beam data for gantry angle 0 are used. The use of a separate reference image for each field in the daily dosimetric constancy checks eases a fast interpretation of these measurements: for each field, constancy means zero deviations with regard to its corresponding reference image.

For each of the 49 areas defined in the measured images, the percentual difference in measured gray scale value compared to the corresponding area in the related reference image has been determined. Figure 2.1 shows the screen output of a typical measurement. Observed differences at the beam axis (1.4% in this example) relate to deviations in the *absolute* output of the photon beam. Deviations in the *relative* 2D fluence profile have been determined by correcting the 49 percentual differences for the observed deviation in absolute output at the beam axis (compare figures 2.1 and 2.2).

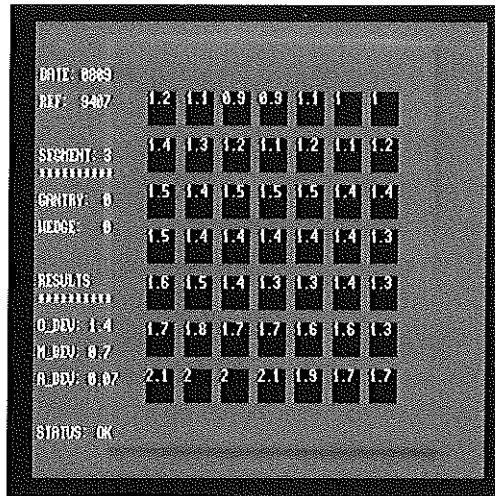


Figure 2.1 Screen output showing the definition of the 49 areas of $1.5 \times 1.5 \text{ cm}^2$ in an EPID-image. The numbers represent an example of observed percentual deviations of measured absolute gray scale values from the corresponding values in the related reference image.

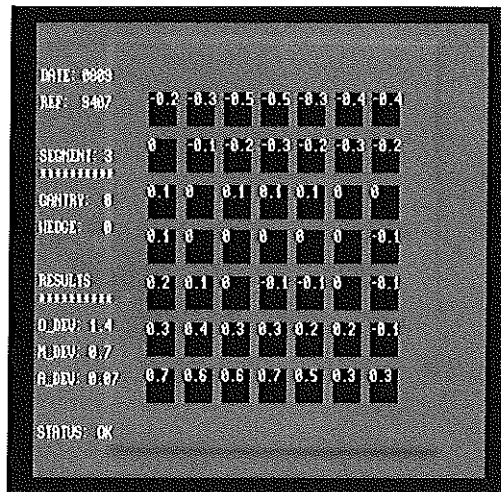


Figure 2.2 Percentual deviations in the relative 2D fluence profile from the reference image, derived by renormalization of the data in figure 2.1, assuming zero deviation at the beam axis.

2.3 Results and discussion

2.3.1 Reproducibility, stability and linearity of the EPID

The short term reproducibility of dosimetric EPID-measurements has been assessed by sequential measurement of images and ionization chamber readings at the beam axis under identical conditions in a short overall period of time (typically 15 minutes). Both for the on-axis and off-axis points the EPID-measurements show a reproducibility of the measured gray scale values of 0.5% (1 SD); the fluctuations in the ionization chamber readings were negligible. A significant correlation exists between on-axis and off-axis fluctuations: after correcting the gray scale values in the off-axis points for the observed on-axis fluctuations, the remaining image-to-image variation for off-axis points decreases to only 0.2% (1 SD).

To assess the day-to-day sensitivity stability of the SRI-100, its response at the beam axis has been determined, usually twice a day, for a period of twenty days. Measurements of *one* EPID-image and a few ionization chamber readings were performed for gantry angle 0 in a short overall period of time. The results depicted in figure 2.3 reveal a variation in the on-axis EPID-response of 0.6% (1 SD), which is only slightly larger than the above mentioned short-term reproducibility.

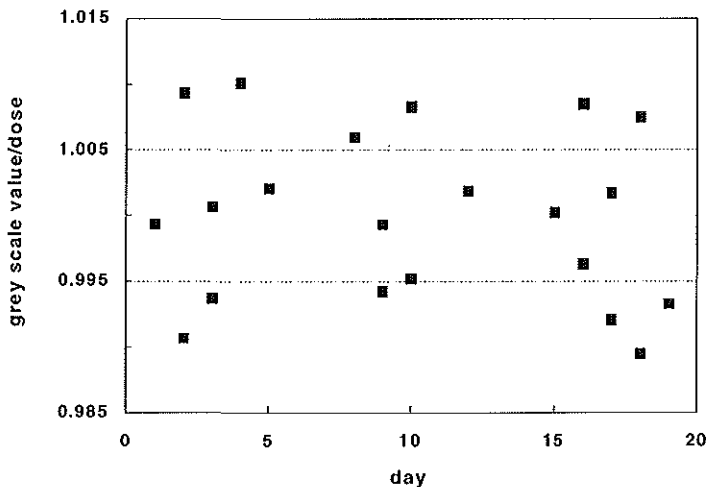


Figure 2.3 Day-to-day on-axis sensitivity stability of the EPID.

To assess the long-term sensitivity stability of the SRI-100, the response measurements have been repeated in a second period of twenty days. The time interval between the first and the second period was 60 days. Also for this second period a variation in the EPID-response of 0.6% (1 SD) was measured. However, the average response in the second period was 0.5% lower than in the first period, probably due to radiation damage in the CCD-chip.

The linearity of the EPID has been assessed for doses between 40 and 180 monitor units (MU). From the results in figure 2.4, showing the measured response at the beam axis as a function of MU, it is clear that the response does not significantly depend on the applied dose. In other words, the measured gray scale value increases linearly with the delivered dose.

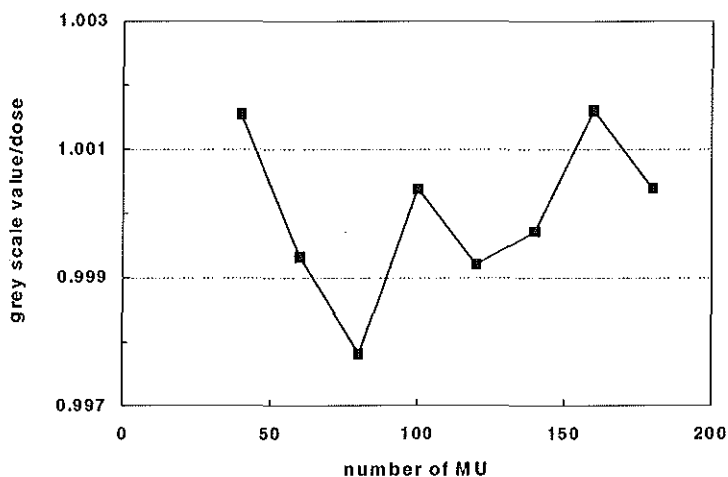


Figure 2.4 Linearity of the measured gray scale value with applied portal dose.

It may be concluded that the SRI-100 is suitable for daily dosimetric quality control measurements. No adverse interference effects related to the combined use of the MM50 scanning beams and the slow scan mode of the CCD-camera have been observed. For at least a period of several weeks it is possible to derive the output at the beam axis from a *single* EPID-measurement with an accuracy of 0.6% (1 SD), while the relative 2D fluence profile can be determined even more accurately. After a period of several weeks a recalibration of the EPID might be necessary to correct for changes in sensitivity.

2.3.2 Daily quality control measurements

The observed deviations in absolute on-axis output for gantry angle 0, measured with the EPID during a period of 300 days, are depicted in figure 2.5. The sudden change in output deviation on day 142 is related to a recalibration of the MM50 monitor chamber. Table 2.1 summarizes the results of 1300 measured images, equally spread over the five different fields.

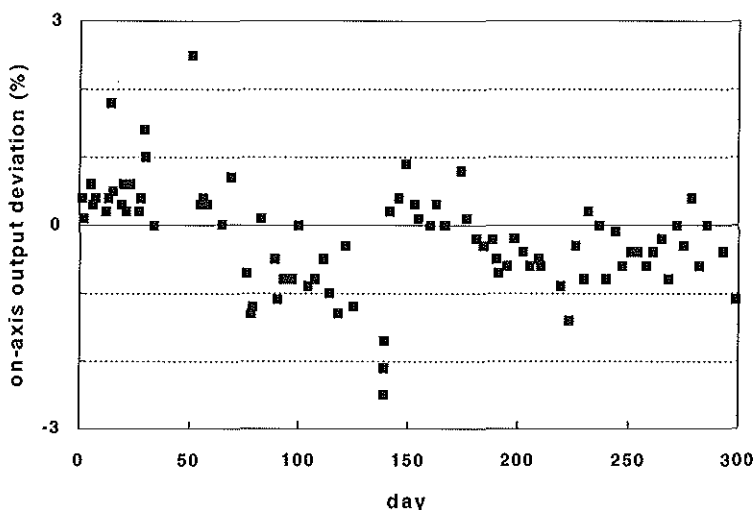


Figure 2.5 *Deviations in absolute on-axis output of the 25 MV photon beam, measured with the EPID for gantry angle 0. The deviation of 6% has been omitted (see text for further explanation).*

Once an output deviation of about 6% was detected for each field. (In order to stick to an appropriate ordinate scale in figure 2.5, this value has not been included). Checks with an ionization chamber showed an output deviation of the same amount. This large deviation was a consequence of a human error related with the helium/nitrogen flow in the monitor chamber. For historical reasons two separate bottles are used to supply each gantry with this mixture: one while the MM50-system is switched on, the other when the system is off. During the weekend the 'system-off bottle' for one gantry became empty because the responsible person forgot to change it before the weekend. For this reason the constant gas flow stopped, the overpressure in the treatment head went down and air could leak into the treatment head and therefore also into the monitor chamber. When the machine was switched on after the weekend, the 'system-

Table 2.1 Overview of observed deviations from corresponding reference images. The incidence rates indicate the percentage of the total number of analyzed fields ($N = 1300$) in which a certain deviation occurred.

	deviations	incidence rate
absolute on-axis output deviations	$< \pm 2.0 \%$	94 %
	$\pm(2.0 - 3.0)\%$	5 %
	$> \pm 3.0 \%$	1 %
average off-axis profile deviations	$< \pm 0.3 \%$	94.7 %
	$\pm(0.3 - 0.5)\%$	5 %
	$> \pm 0.5 \%$	0.3 %
maximum off-axis profile deviations	$< \pm 1.5 \%$	89 %
	$\pm(1.5 - 2.0)\%$	10 %
	$> \pm 2.0 \%$	1 %

on bottle' was automatically connected to the monitor chamber. At that moment the MM50 system observed correct input and return gas flows (since the 'system-on bottle' was not empty) and no interlock occurred. However, it took several hours before all air had disappeared from the monitor chamber, yielding an increased sensitivity of this chamber and therefore a 6% too low beam output.

The observed average and maximum deviations in the relative 2D beam profile, determined from the measurements in the 48 off-axis points, are depicted in figure 2.6 for gantry angle 0 and summarized in table 2.1 for all fields. Because the average off-axis deviation was always less than 0.6% and the maximum observed off-axis deviation was 2.8%, it may be concluded that the relative 2D fluence profile is very stable. Wedge factors have been calculated from measured gray scale values at the beam axis for the open and the wedged field at gantry angle 0. The results, depicted in figure 2.7, show a constancy of 0.7% (1 SD).

On several days, the morning quality control measurements were repeated in the afternoon after patient treatment. No significant differences between results obtained in the morning and in the afternoon have been observed.

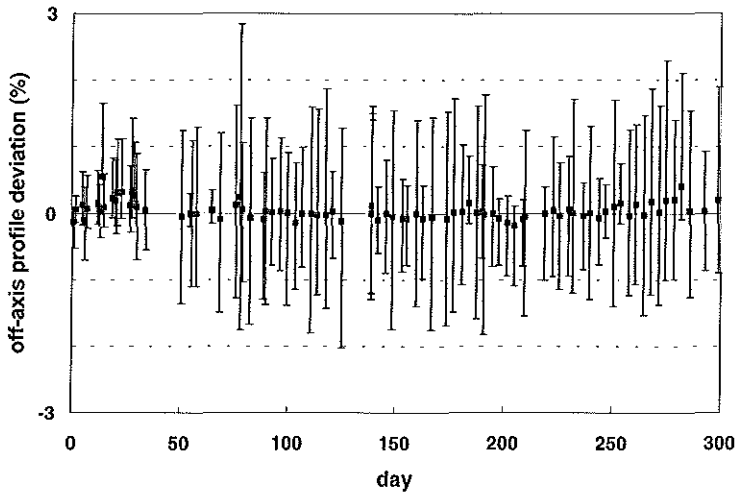


Figure 2.6 *Off-axis deviations in the relative 2D beam profiles for gantry angle 0. The dots indicate the average off-axis deviations for the 48 off-axis points, the bars indicate the maximum deviations.*

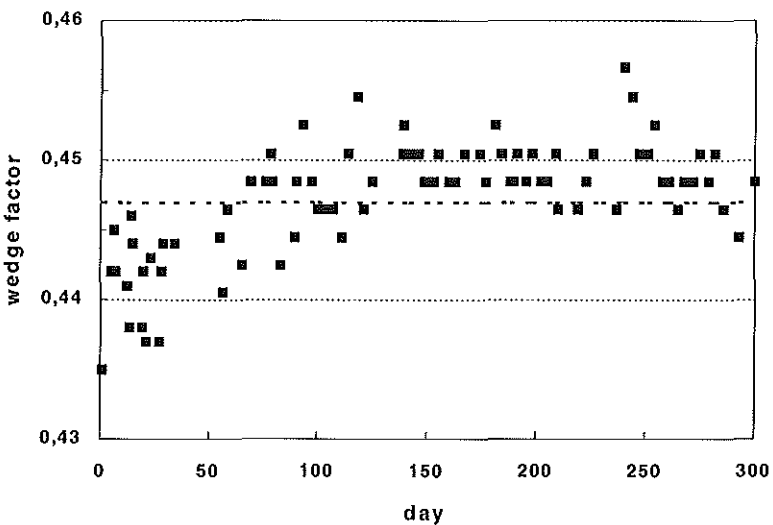


Figure 2.7 *Wedge factors, calculated from measured gray scale values at the beam axis for the open and the wedged field at gantry angle 0. The dashed line indicates the average value.*

2.3.3 Protocol for daily quality control measurements

Based on the results in table 2.1 and on clinical requirements regarding acceptability of deviations, the following practical protocol for daily dosimetric quality control measurements has been adopted:

If

* for each field the on-axis output deviation is smaller than 3%,

and

* for the five fields the *average* output deviation at the beam axis is less than 2%, or between 2% and 2.5% while being below the 2%-level the previous two days,

and

* for each field the maximum off-axis beam profile deviation is less than 2%, or between 2% and 2.5% while being below the 2%-level the previous two days,

and

* for each field the average off-axis deviation is less than 0.5%, or between 0.5% and 0.7% while being below the 0.5%-level the previous two days,

the results are accepted and patient treatment can start.

In all other cases, additional investigations and, if necessary, adjustment of the beam characteristics have to be performed. When this protocol had been applied to the daily quality control measurements described before, patient treatment could have started immediately on 95% of the days.

Daily EPID measurements should be fast. Therefore, only one image is measured per field and the allowed deviations, as described in the protocol above, are somewhat larger than for the checks in our two weekly quality control program.

2.4 Conclusions

Because of its characteristics, the Philips SRI-100 Electronic Portal Imaging Device is suitable for *fast* and *accurate* daily dosimetric quality control of photon beams under different gantry angles. Deviations in the absolute output and in the relative 2D fluence profiles are determined within ten minutes for five fields.

Despite the complexity of the MM50, the 2D fluence profile of the 25 MV scanned photon beam has been very stable for all gantry angles during a period of 10 months: a maximum profile deviation of 2.8% was observed and the average profile deviation

never exceeded 0.6%. Once, a deviation in the cGy/MU-value of 6% has been detected. Only because of the performed morning quality control checks, erroneous dose delivery to patients could be avoided. Based on our experiences, a practical protocol for daily dosimetric quality control measurements has been developed.

This chapter is based on the results of measurements for the 25 MV photon beam of one gantry. However, in the meantime the dosimetric checks are also successfully performed at the other gantry. Moreover, the quality control measurements have been extended to the 10 MV photon beam. Studies on the application of a fluoroscopic portal imaging device for in-vivo dosimetry on the MM50 are in progress [76,77,118-121,123].

Chapter 3

Field margin reduction using intensity modulated X-ray beams formed with a multileaf collimator

Adopted from the original article by MLP Dirkx, BJM Heijmen, GA Korevaar, MJH van Os, JC Stroom, PCM Koper and PC Levendag, published in *Int. J. Radiat. Oncol. Biol. Phys.* 38: 1123-1127, 1997.

3.1 Introduction

In the Daniel den Hoed Cancer Center, prostate cancer patients are treated at the MM50 Racetrack Microtron with a 25 MV photon beam. An isocentric technique is used with one open anterior field and two lateral oblique fields, which are partly delivered with a 60° (motor) wedge inserted. The lateral oblique fields are slightly tilted posteriorly in order to minimize the irradiated rectal volume. All fields contribute equally to the dose in the isocenter. Beam shaping is performed with a multileaf collimator. The intention is to comply with the ICRU-50 recommendations for dose homogeneity [62]: the dose in the 3D PTV is aimed to be between -5% and +7% of the dose in the ICRU-point, i.e. the isocenter. To avoid doses in the PTV of less than 95% resulting from beam penumbrae, beam apertures are defined by adding field margins to the beam's-eye-view projections of the PTV. For all patients, field margins of 0.5 cm and 0.7 cm for, respectively, the lateral borders of the anterior field and the anterior and posterior borders of the lateral oblique fields are sufficient to meet the ICRU-50 recommendations. However, even a field margin of 1.5 cm for definition of the superior and inferior field borders of all fields still yields small underdosages (< 2%) in the superior and inferior ends of the PTV for nearly all patients. In these cases, 1.5 cm margins are used and the underdosages are accepted. Relatively large field margins for definition of the superior and inferior field borders for treatment of prostate cancer patients have also been reported by Leibel *et al* [86].

Recently, Chen *et al* [25] and Mohan *et al* [113] have investigated the influence of phantom scatter on the design of optimized intensity modulated beams; phantom scatter is one of the main causes for the generally observed large 50-95% penumbra width of photon beams. They found that extra beam intensity near the beam boundaries could compensate for beam penumbra effects, yielding a more homogeneous irradiation of the PTV and providing a better protection for normal tissues. For multiple field, axial treatments, extra beam intensity was especially needed near the superior and inferior field borders; this observation was attributed to the overlap of penumbrae of *all* involved treatment fields at the superior and inferior ends of the PTV.

Several devices have been used to reduce the 50-95% penumbra width of X-ray beams. Biggs and Shipley [9] have described the use of lead filters in a 25 MV photon beam, which were positioned in the center part of the fields. In this way the dose in the center of the beam was attenuated relative to the dose in the beam edges, improving the 50-95% penumbra width with 0.4 to 0.7 cm, depending on the field size. For a 4 MV accelerator, improvements in the flatness and the penumbra of small fields (up to 10x10 cm²) have been reported using special tungsten alloy trimmers, attached to a tray below the accelerator head [116]. The lead filters used by Biggs and Shipley have some

disadvantages: for each patient and each treatment field, a separate filter has to be produced. Moreover, in between treatment fields the technicians have to enter the treatment room in order to change the filters. The use of the tungsten alloy trimmers is restricted to rectangular fields.

In this chapter we report on a method for treatment of prostate cancer patients applying intensity modulated (IM) X-ray beams with increased intensity near the superior and inferior field borders in order to reduce the distance between the 50 and 95% isodose surfaces. The intensity modulated beams, produced with a multileaf collimator, include narrow, low weight boost fields superimposed on the superior and inferior ends of regular flat fields. The development of the IM technique was aimed to achieve a reduction in the superior-inferior field length. The technique should meet three constraints: (i) the minimum dose in the entire PTV should be 95% of the isocenter dose, (ii) compared to our standard technique, increases in the maximum rectal and bladder doses should be avoided as much as possible, and (iii) treatment planning and clinical application of the IM technique should be simple, safe and not time consuming. Using 3D treatment plans, the benefits of the technique are demonstrated for ten prostate cancer patients. The accuracy of the dose calculation algorithm in our treatment planning system for the narrow boost fields has been determined by comparison with measurements. For treatments at the M50 Racetrack Microtron, the extra time needed for delivery of the boost fields has been assessed.

3.2 Materials and methods

3.2.1 *Intensity modulated X-ray beams for treatment of prostate cancer patients: the applied technique*

With respect to our standard three field technique, described in the introduction, only two changes are made for the IM technique: 1) for all three involved fields the field margin for definition of the superior and inferior field borders is fixed at 0.7 cm instead of the usual 1.5 cm, and 2) narrow, low weight boost fields are superimposed on the superior and inferior ends of each of the two lateral oblique fields such that the minimum dose in the superior and inferior ends of the PTV just exceeds the 95% level. For field margins smaller than 0.7 cm, a minimum PTV dose of 95% could generally only be achieved at the cost of an increase in the maximum doses delivered to the rectum and the bladder.

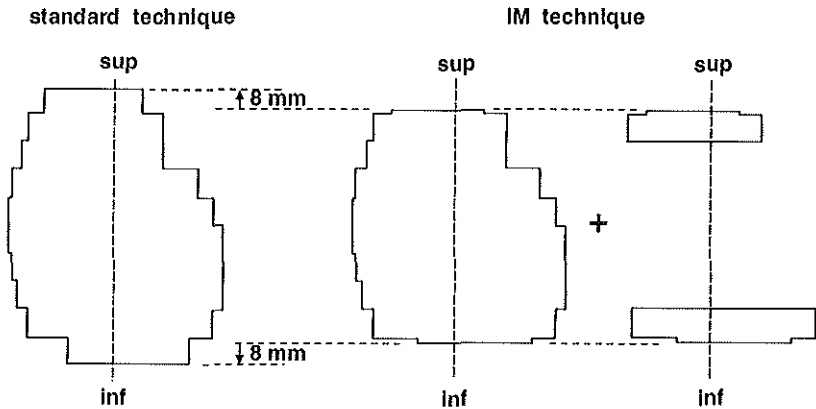


Figure 3.1 Right lateral oblique fields for treatment of patient 4 in table 3.1: (a) for the standard technique using field margins in superior-inferior direction of 1.5 cm; (b) for the IM technique, i.e. superior-inferior field margins of 0.7 cm and addition of a superior and an inferior boost field.

For both lateral oblique beam orientations, the superior and inferior boost fields are generally delivered simultaneously by closing leaf pairs in the central part of the beam while keeping the position of the collimator blocks fixed. See figure 3.1 for an example. To be able to compensate for variations in the patient contour in superior-inferior direction, possibly yielding an increased maximum dose in the rectum or the bladder, the two fields can also be delivered sequentially (see below).

For each patient, all four boost fields have the same superior-inferior length l , obeying the equation $l = (L - n \cdot w) / 2$, with L the field length as defined by the collimator blocks, n the number of central leaf pairs that are closed and w the leaf width (1.25 cm at isocenter for the MM50 Racetrack Microtron). L is fully determined by the superior-inferior PTV length and the applied fixed field margin of 0.7 cm. As a consequence, for each patient, possible lengths l of the boost fields differ by multiples of $w/2$ cm, depending on the choice of n in the equation above. Based on a large number of treatment plans, it was concluded that l should preferably be in the range 1.1 to 1.6 cm. Often, a smaller field length yielded underdosages in the PTV in CT-slices situated next to the most superior and inferior slices with PTV; larger lengths l could lead to unwanted increases in the maximum dose delivered to the rectum or the bladder. For each patient, only one l can fulfil both equations $l = (L - n \cdot w) / 2$ and $1.1 \text{ cm} \leq l \leq 1.6 \text{ cm}$. For the patients in this study, each with a different PTV length, the length l of the applied boost fields for the design of the final IM plan is presented in table 3.1.

Table 3.1 The superior-inferior length of the applied boost fields as a function of the length of the PTV in superior-inferior direction.

patient	length PTV (cm)	length boost fields (cm)
1	7.5	1.3
2	8.0	1.6
3	8.5	1.2
4	9.0	1.5
5	9.5	1.1
6	10.0	1.3
7	10.5	1.6
8	11.0	1.2
9	11.5	1.5
10	12.0	1.1

The only real variables in treatment planning are the weights of the boost fields and the choice whether or not to deliver the superior and inferior boost fields simultaneously (see above). In practice, for each patient, the design of the IM-technique starts with a treatment plan based on a simultaneous delivery of the superior and inferior boost fields for each of the two lateral oblique fields. The weight of the boost fields is such that for both the superior and the inferior ends of the PTV, the delivered dose is at least 95% of the isocenter dose. In case the obtained minimum dose in the most superior or the most inferior parts of the PTV is higher than 95% (e.g. due to variations in patient contour in superior-inferior direction), a modified plan, based on a sequential delivery of the superior and inferior boost fields for one of the two lateral oblique fields with slightly different weights, is considered.

At the MM50 Racetrack Microtron overtravel of the collimator blocks across the central axis is not possible. Therefore, a more flexible field length definition of the boost fields by using both collimator blocks for generation of each of the two boost fields, implying a sequential delivery of these fields, is impossible. The leaves of the multileaf collimator of the MM50 have a maximum overtravel of 14 cm, allowing more flexibility in the choice of l by rotating the collimator 90° prior to the delivery of the boost fields. These fields should then be delivered separately using the leaves for the definition of l and the blocks for definition of the width of the boost field. Because of the good results obtained with the relatively simple technique described above we did not study this more complex and time-consuming technique with collimator rotation.

3.2.2 Evaluation of the IM technique based on 3D treatment planning

To assess the effectiveness of the proposed use of intensity modulated X-ray beams, 3D treatment plans have been made for ten prostate cancer patients with PTV lengths ranging from 7.5 to 12 cm using the Cadplan 3D planning system manufactured by Varian-Dosetek [6,139,140]. For each patient three plans have been compared: *A*) our standard technique with field margins in the superior-inferior direction of 1.5 cm, *B*) the same technique but with field margins in superior-inferior direction of only 0.7 cm, and *C*) the IM technique described in the previous section, based on field margins of 0.7 cm and application of superior and inferior boost fields.

For all patients, CT-slices with 0.5 cm spacing were available. To improve the spatial resolution for penumbra analyses in the superior-inferior direction, dose calculations were also performed for CT-slices generated by interpolation at intermediate positions; within each slice a grid size of 0.5 cm was used for the dose calculations.

For treatment planning, the gross tumor volume (GTV) [62] - i.e. prostate (for patients 1, 2 and 6) or prostate + vesiculae seminalis (other patients) as delineated on CT-slices by the physician - was expanded in 3D [143,144] with a margin of 1.5 cm to render the PTV. For the bladder and the rectum the outer surfaces were contoured. The rectum was contoured from 2.5 cm inferior of the PTV to 2.5 cm superior of the PTV.

Treatment plans were designed and evaluated using 3-dimensional planning tools such as beam's eye view (BEV), dose distributions in coronal and sagittal planes and dose volume histograms of the PTV, the rectum and the bladder. Dose profiles along the superior-inferior axis through the isocenter have been used to quantify the superior and inferior reduction in distance between the 50 % and 95 % isodose surfaces, resulting from the applied boost fields in plan C. For each patient, the percentual changes between the IM plan and the standard plan in rectal and bladder volumes receiving a dose higher than 80% of the isocenter dose and in the maximum rectal and bladder doses have been quantified.

3.2.3 Accuracy of dose calculations

The high accuracy of the implemented dose calculation algorithms in Cadplan (version 2.62) for photon fields larger than $4 \times 4 \text{ cm}^2$ has been demonstrated [6,139,140]. To assess the accuracy of these algorithms for the 25 MV narrow boost fields, calculated relative dose distributions for off-axis fields as small as $1.1 \times 5.0 \text{ cm}^2$ have been compared with distributions measured in a water phantom (RFA-300, manufactured by Scanditronix Medical AB) using a linear detector array consisting of 11 p-type diodes,

and with distributions measured with film, irradiated horizontally in a polystyrene phantom at a depth of 3.5 cm (the depth of maximum dose for the 25 MV photon beam). In the latter case, measured optical densities were converted into doses by applying a sensitometric curve determined for the beam axis of a $10 \times 10 \text{ cm}^2$ field using the same set-up. All measurements were performed with a source to surface distance of 100 cm.

Absolute dose calculations of Cadplan were checked by comparison with dose measurements performed at a depth of 3.5 cm in the center of the narrow boost fields, using a semiconductor detector (manufactured by Scanditronix Medical AB). The readings of the semiconductor were converted to dose by applying a conversion factor measured at the same depth on the beam axis of a $10 \times 10 \text{ cm}^2$ field. Required phantom scatter factors, needed to improve the accuracy of the monitor unit calculations of Cadplan for the small boost fields, were determined from measurements of the head-scatter factor and the total-scatter factor [156] for square fields of 4×4 down to $1 \times 1 \text{ cm}^2$. All scatter factors were determined relative to the $10 \times 10 \text{ cm}^2$ field. The head-scatter factors were measured with an RK-chamber vertically positioned in a brass buildup cap with sidewalls of 2 gcm^{-2} [89,180] and a front-wall of 10 gcm^{-2} . In order to ensure the $1 \times 1 \text{ cm}^2$ radiation field to fully encompass the used buildup cap, the source to surface distance was extended from 100 to 120 cm. Measurements of the total-scatter factors were performed in water at a depth of 10 cm [141] using a semiconductor detector; a source to surface distance of 100 cm was used.

3.2.4 Implementation on the MM50 Racetrack Microtron

As described in section 1.3, the MM50 can be operated in a fully computer-controlled multi-segment treatment mode. In this mode the technicians set-up only the first segment (field) of a patient treatment. All parameters of the next segments, like the gantry and collimator angles, couch positions, field shapes, beam energies and monitor units, are set-up and verified by the treatment computer. In between segments, the technicians do not enter the treatment room. Segments without dose ('dummy' segments) can be used to temporarily displace the treatment table in order to increase the distance between the patient and the treatment head before rotating the gantry. For treatment of prostate cancer patients we use two 'dummy' segments. The extra time needed for delivery of the boost fields has been assessed using the fully computer-controlled multi-segment treatment mode.

3.3 Results and discussion

3.3.1 Evaluation of the IM technique based on 3D treatment planning

A Dose profiles along the superior-inferior axis

For all patients, the dose profiles along the superior-inferior axis through the isocenter have been analyzed for plans A and C (see above) to assess the superior and inferior reduction in distance between the 50% and 95% isodose surfaces resulting from the application of the boost fields. As an example, figure 3.2a shows the dose profiles for patient 3; figure 3.2b shows the dose distributions of the superior and inferior boost fields that are added to plan B, yielding plan C. The average reduction in the superior and inferior 50-95% penumbra widths due to the application of boost fields is 0.66 ± 0.25 cm (1 standard deviation) for all patients.

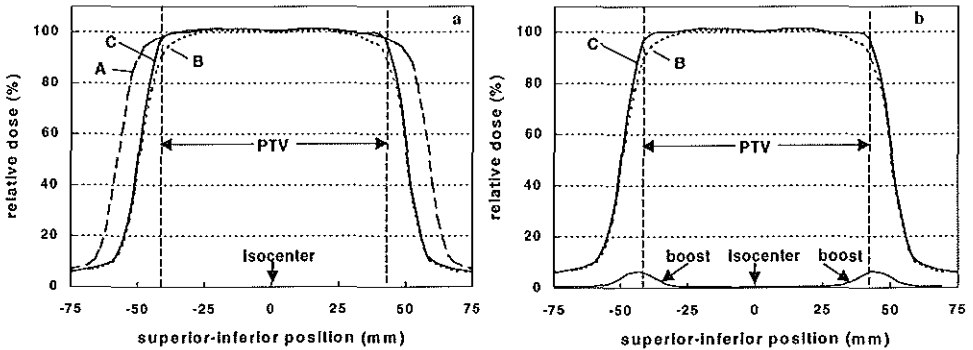


Figure 3.2 a Dose profiles in superior-inferior direction through the isocenter for patient 3 in this study. Curve A: superior-inferior field margins of 1.5 cm; curve B: superior-inferior field margins of 0.7 cm; curve C: superior-inferior field margins of 0.7 cm and boost fields on the superior and inferior ends of the PTV.

b Addition of the boost profiles to curve B yields curve C of the IM technique.

B Dose distribution in the PTV

For the 3-dimensional PTV, minimum doses and dose homogeneities, expressed as the standard deviation (σ) of the observed deviations from the average dose, are summarized in table 3.2. Each dose distribution was normalized to 100% in the isocenter. The data show that for nine of the ten patients a field margin in superior-inferior direction as large as 1.5 cm (plan A) was not enough to fully comply with the ICRU-50 recommendations for dose homogeneity in the PTV [62], i.e. in some parts of the PTV (situated in the superior and inferior ends) the dose is still somewhat less than 95%. With field margins in superior-inferior direction of 0.7 cm and no boost fields (plan B), the minimum dose in the PTV was on average 88.4 % for the 10 patients; for patient 4 the minimum PTV dose was only 86.5 %. Using superior-inferior field margins of 0.7 cm in combination with boost fields (plan C, the IM technique) yielded a minimum PTV dose of 95% for all patients. This technique also yielded the best dose homogeneity, i.e. the smallest values for σ .

Table 3.2 Minimum dose (D_{min}) and dose homogeneity (σ) in the PTV for the three treatment plans described in section 3.2.2.

plan	A		B		C	
	field margin 1.5 cm		field margin 0.7 cm		field margin 0.7 cm + boost fields	
patient	D_{min} (%)	σ (%)	D_{min} (%)	σ (%)	D_{min} (%)	σ (%)
1	95.6	1.3	88.5	2.4	95.6	1.1
2	93.6	1.3	88.5	2.1	95.0	1.2
3	94.5	1.9	89.5	2.7	95.0	1.8
4	92.6	1.8	86.5	2.5	95.0	1.5
5	94.5	1.3	87.6	2.0	95.6	1.2
6	93.6	1.4	89.5	2.2	95.6	1.2
7	93.5	1.6	86.7	2.1	95.6	1.1
8	94.5	1.4	89.6	1.9	95.6	1.2
9	94.5	1.3	88.6	1.9	95.6	1.2
10	93.6	1.3	89.5	1.7	95.6	1.3

C Dose distribution within rectum and bladder

As demonstrated in table 3.2 and explained in subsection B, our standard technique and the IM technique allow, respectively, near and full compliance with the dose homogeneity recommendations mentioned in the ICRU-50 report [62]. Due to the reduction of 1.6 cm in field length for the IM technique relative to the standard technique (see section 3.2.1), reductions in rectal and bladder volumes in the high dose area could be expected for the former technique. In table 3.3, observed percentual decreases in the rectal and bladder volumes that receive a dose higher than 80 % of the isocenter dose are presented. For both the rectum and the bladder, the data show a large variation in the observed high dose volume reductions, strongly depending on the position and the shape of these critical organs relative to the most superior and inferior parts of the radiation fields.

Table 3.3 Differences between our standard technique and the IM technique with respect to rectal and bladder volumes receiving a dose of more than 80% (ΔV) and to the maximum dose delivered to these tissues (ΔD_{\max}). Positive numbers point at reduced values for the IM technique.

patient	rectum		bladder	
	ΔV (%)	ΔD_{\max} (%)	ΔV (%)	ΔD_{\max} (%)
1	4.5	-0.4	15.6	-0.4
2	11.3	-2.2	11.9	-3.0
3	2.5	0.1	14.7	0.3
4	4.1	-0.3	-0.2	-0.6
5	0.1	0.3	1.1	0.6
6	6.6	0.3	0.6	0.3
7	2.3	-1.0	9.0	0.2
8	3.1	0.3	0.5	0.3
9	7.8	0.1	0.4	0.3
10	8.1	-0.4	-0.9	0.5

As explained in section 3.2.1, attention has been paid to avoid increases in the maximum rectal and bladder doses due to the application of the boost fields. Table 3.3 shows that the differences in maximum rectal and bladder doses between the IM technique and the standard technique are small (<1% of the isocenter dose for nine of the ten patients). The observed increases in maximum doses for the IM technique for

patient 2 (2.2 % in the rectum and 3.0% in the bladder) and the increase of 1 % in maximum rectal dose for patient 7 are due to the relatively large superior-inferior length of the applied boost fields (1.6 cm) for these patients (see table 3.1). For both patients the increased maximum doses occurred in one or two CT-slices adjacent to the most superior or the most inferior CT-slice containing PTV (slice distance 0.25 cm). By choosing boost fields with a length of 1.0 cm instead of 1.6 cm for these patients, increased maximum rectal and bladder doses could be avoided. However, as a consequence the calculated minimum PTV dose went down to 94.5% for both patients.

3.3.2 Accuracy of dose calculations

Dose calculations of the Cadplan planning system for the narrow boost fields have been extensively verified by comparison with measurements. The field sizes that were studied ranged from $1.1 \times 5.0 \text{ cm}^2$ up to $1.6 \times 10 \text{ cm}^2$; the fields were positioned off-axis at distances of 3.2 to 6.1 cm from the isocenter. As an example, measured and calculated dose distributions for boost fields of $1.2 \times 5.0 \text{ cm}^2$ and $1.2 \times 10 \text{ cm}^2$, positioned at an off-axis distance of 4.4 cm, are depicted in figure 3.3. The measurements and calculations have been normalized to 100% at a depth of 3.5 cm. For all cases, measured and calculated relative dose distributions agreed within 2% or 0.2 cm. Initially, the Cadplan planning system calculated too high absolute doses (up to 16%) in the normalization point of the boost fields. The largest deviations were observed for boost fields with the smallest lengths. To a very large extent, this discrepancy was caused by the table of phantom scatter factors used in the Cadplan system. For fields larger than $4 \times 4 \text{ cm}^2$, this table is based on data presented by Storchi and van Gasteren [141]. For smaller fields, the values in the table were obtained by a linear extrapolation.

Based on measurements of head-scatter factors and total-scatter factors, we determined phantom scatter factors for square fields down to $1 \times 1 \text{ cm}^2$. In figure 3.4, the results are depicted and compared with the original Cadplan table. For the larger fields, the Cadplan data agree very well with the measurements. However, serious deviations occur for fields smaller than $4 \times 4 \text{ cm}^2$. After modification of the Cadplan phantom scatter table according to our measurements measured and calculated absolute doses for the boost fields generally agreed within 2%. The applied boost fields have a small weight (see subsection B). Therefore, the achieved accuracy of the dose calculations for boost fields is certainly adequate.

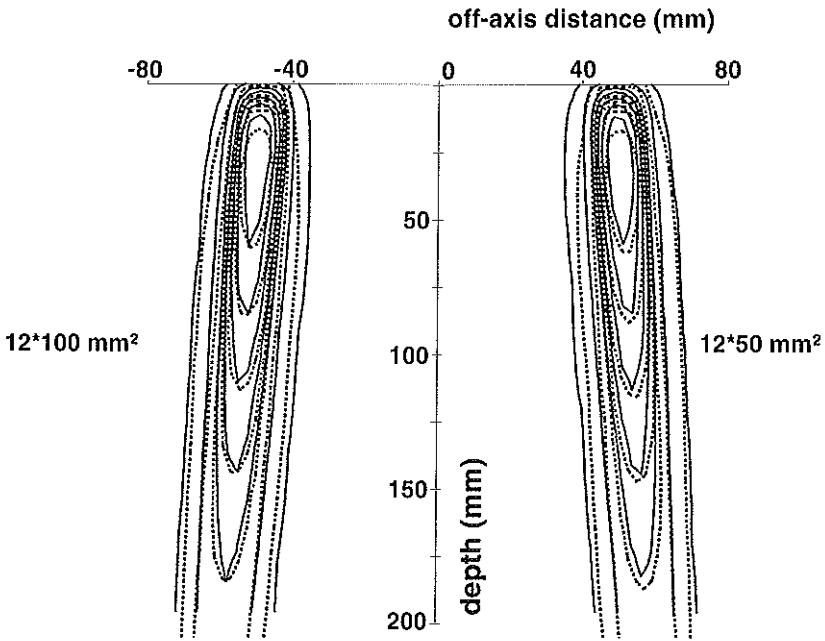


Figure 3.3 Measured (dashed lines) and calculated (solid lines) isodose distributions for boost fields. Depicted isodose lines: 10, 30, 50, 60, 70, 80 and 90%.

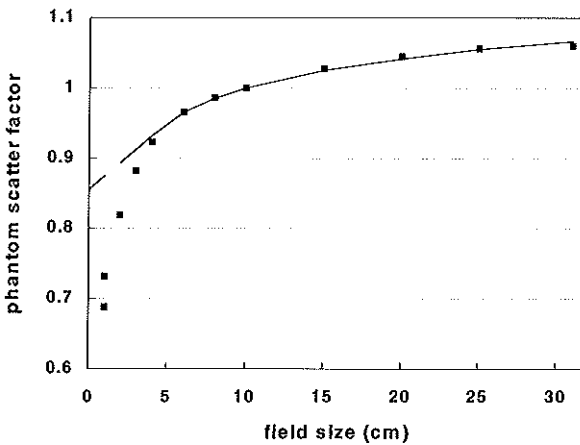


Figure 3.4 Comparison of measured phantom scatter factors for the 25 MV X-ray beam of the MM50 (squares) with the values originally used in the Cadplan planning system (solid line).

3.3.3 Implementation on the MM50 Racetrack Microtron

For all ten patients, the increase in treatment time due to delivery of the boost fields has been assessed by simulation of the treatments using the fully computer-controlled multi-segment treatment mode. For most patients, the observed extra time for delivery of the boost fields was about one minute. For patients 4, 5 and 7 the two boost fields in the left lateral oblique field were delivered sequentially (with different weights) in order to avoid an increase in the maximum dose delivered to the bladder and/or the rectum as much as possible (see also section 3.2.1). For these patients the extra time was about 1.5 minute.

Most of the extra time needed for delivery of the boost fields is used by the MM50 computer for verification of the setup. A modification of the control software of the MM50, which is being developed by the manufacturer, will allow a significant reduction of this overhead time.

3.4 Summary and conclusions

In axial, co-planar treatments with multiple fields, often large field margins are needed for definition of the superior and inferior field borders in order to avoid underdosages in the superior and inferior ends of the PTV. We have investigated the use of intensity modulated beams, generated with a multileaf collimator, to allow reduction of these field margins while fulfilling the ICRU-50 recommendations for dose homogeneity. The intensity modulated beams consist of narrow, low weight boost fields superimposed on the superior and inferior ends of treatment fields that enclose a BEV-projection of the PTV with well-defined, narrow field margins.

For ten prostate cancer patients, computer planning studies have shown that due to the proposed application of the intensity modulated fields the field length can be reduced by 1.6 cm, usually resulting in significant reductions in rectal and/or bladder volumes receiving a high dose. No differences were observed between patients planned to the prostate only or to the prostate and seminal vesicles. The accuracy of the Cadplan planning system for calculation of relative dose distributions for the narrow boost fields is within 2% or 0.2 cm. After a small modification in the Cadplan system, calculated absolute doses of the boost fields at the depth of maximum dose generally agreed within 2% with measurements.

Using the fully computer-controlled multi-segment treatment mode of the MM50 Racetrack Microtron, the application of intensity modulated beams would have led to an increase in treatment time of 1.5 minute maximum.

In this study we have focused on prostate cancer patients treated with our three-field technique. However, we have observed that introduction of boost fields in the often-applied four field box- and six field techniques can also yield significant reductions in field length. Improved dose distributions have also been achieved for a cervix cancer patient. In the next chapter the benefits of the proposed application of boost fields will be demonstrated for the treatment of lung cancer patients.

In the meantime, the technique described in this chapter is used routinely in our clinic for treatment of prostate cancer patients.

Chapter 4

Beam intensity modulation for penumbra enhancement in the treatment of lung cancer

Adopted from the original article by MLP Dirx, M Essers, JR van Sörnsen de Koste, S Senan and BJM Heijmen, published in *Int. J. Radiat. Oncol. Biol. Phys.* 44: 449-454, 1999.

4.1 Introduction

Presently, the outcome after radiotherapy alone in patients treated for non-small cell lung cancer is poor, as evidenced by pathological complete remission rates of only around 20% after doses of 65 Gy [2]. Whilst radiation dose escalation is expected to improve local control [31,43], delivery of higher doses is, especially in advanced (stage III) tumors, often limited by severe complications such as radiation pneumonitis, despite the use of 3D treatment planning techniques [53]. Other approaches to improve local control rates include altered fractionation schemes and concomitant chemoradiotherapy, both of which are complicated by severe oesophagitis. Continuous hyperfractionated, accelerated radiotherapy improved survival over conventional radiotherapy [131] but was accompanied by a higher incidence of severe oesophagitis (19% vs. 3%). With hyperfractionated radiotherapy, the likelihood of severe oesophagitis has been shown to correlate with the length of the oesophagus, which is irradiated [74]. Whilst a survival advantage was seen for patients treated with radiotherapy and daily cisplatin [132], the administration of active new agents such as paclitaxel, gemcitabine and topotecan during radiotherapy has resulted in dose-limiting acute oesophagitis [26,52,54,83]. Consequently, all approaches aiming to improve the results of radiotherapy in non-small cell lung cancer will benefit from steps to limit the volume of irradiated normal tissue.

As a prelude to a future dose escalation study for treatment of patients with a stage III non-small cell lung cancer, a phase II trial of induction chemotherapy, followed by 'involved-field' radiotherapy was recently activated at the Daniel den Hoed Cancer Center. During the radiotherapy treatment, a dose of 70 Gy is delivered in daily fractions of 2 Gy to a planning target volume (PTV), which includes only the primary tumor, enlarged mediastinal lymph nodes with a short axis diameter exceeding 1 cm, and a 3D margin for geometrical uncertainties. As generally known the dose calculation algorithms in most treatment planning systems are less accurate in lung tissue than in other soft tissues, especially at higher energies, due to the influence of reduced electron density on secondary electron transport [45,75]. To minimize this problem the patients are treated at the MM50 Racetrack Microtron with the lowest photon beam energy. The quality index of this beam, defined as the ratio of the dose in water measured at isocenter for a 10 x 10 cm² field at depths of 20 and 10 cm respectively, equals 0.704 and its percentage depth dose curve is similar to a 7 MV photon beam according to *British Journal of Radiology*, supplement 25 [18]. An isocentric irradiation technique is used with one anterior oblique, one posterior oblique and one lateral oblique field (see figure 4.1). For each patient, the beam orientations are optimized to minimize the dose delivery to surrounding healthy tissues, i.e. the



Figure 4.1 Central transversal CT-slice of patient 4 showing the three treatment fields.

contra- and ipsilateral lungs, the spinal cord and the oesophagus. The beams are shaped with a multileaf collimator using the beam's eye view projection of the PTV. The fields may be partly delivered with a 60° motor wedge inserted. The intention is to comply with the ICRU-50 recommendations for dose homogeneity [62]: the dose in the 3D PTV is aimed to be within -5 and $+7\%$ of the dose in the ICRU-point, i.e. the isocenter. To account for beam penumbrae, beam apertures are defined by adding a field margin of 0.8 cm to the lateral, the anterior and the posterior beam's eye view projections of the PTV. Depending on the calculated dose distribution in the superior and inferior ends of the PTV, a margin of at least 1.5 cm is used for definition of the superior and inferior field borders to account for the dose reduction due to the overlap of penumbrae of *all* involved treatment fields [25,39]. However, even with a field margin of 2.5 cm, the 95% isodose is not yet completely encompassing the most superior and inferior parts of the PTV for some patients. An identical treatment technique is also used for stage I lung patients who are treated without elective nodal irradiation.

In the previous chapter, we described a technique using beam intensity modulation (BIM) for penumbra enhancement, which allows a reduction of the large superior and inferior field margins around the PTV. By applying this technique for treatment of prostate cancer patients, the superior-inferior field lengths could be reduced with 1.6

cm compared to the standard technique, while complying with the ICRU-50 dose homogeneity criteria for the PTV, generally yielding smaller volumes of rectum and bladder in the high dose region.

In this chapter, the application of this BIM technique is evaluated for six consecutive stage III patients who participated in the above-described phase II study and for six consecutive stage I patients. Using 3D treatment plans, the potential benefits of the technique are demonstrated. Compared to the standard technique, defined as the previously described technique with fixed field margins in superior and inferior direction of 1.5 cm, the possible dose escalation for the BIM treatment has been estimated, while keeping the calculated risk of pneumonitis constant.

4.2 Methods and materials

4.2.1 The BIM technique

With respect to the standard technique described in the introduction, only two modifications were made: 1) for all three fields the field margin for definition of the superior and inferior field borders was fixed at 0.8 cm instead of 1.5 cm, and 2) for one of the treatment fields used in the standard technique the in-field fluence profile was modified by superimposing narrow, low-weight boost fields on the superior and inferior parts of the treatment field

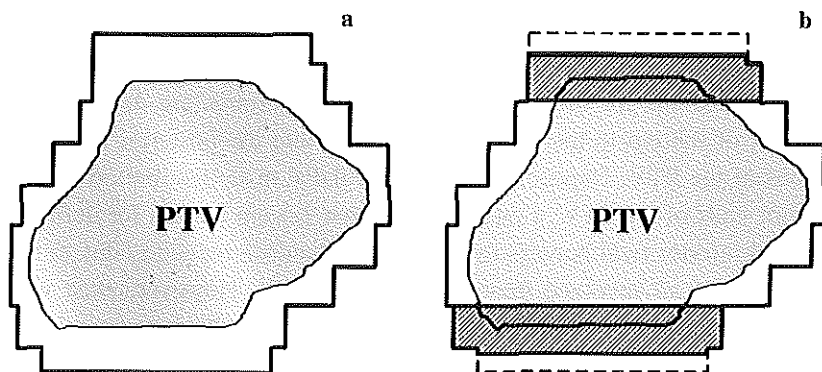


Figure 4.2 Posterior field for patient 4 in this study for the standard technique (a) and the BIM technique (b). For the BIM technique, boost fields (shaded areas) are superimposed on the superior and inferior parts of the treatment field and the total field length is reduced by 1.4 cm. The dashed lines show the field length reduction with respect to the field shown in a.

inferior ends (see figure 4.2). Boost fields were only applied in one beam in order to minimize the increase in treatment time in a future clinical application of the BIM technique. The selection of this beam was determined by the position of the target relative to the normal structures, especially aiming to avoid increased dose delivery to the contralateral lung and the spinal cord. For all patients this aim could be achieved by never adding the boost fields to the lateral oblique field and by avoiding beam orientations showing the spinal cord in the superior and inferior ends of their beam's eye view. When both the anterior and the posterior oblique fields fulfilled this last requirement, the beam orientation for the boost fields was determined by the shortest pathlength through healthy lung tissue from the skin to the target.

Generally, the superior and inferior boost fields were delivered simultaneously by closing leaf pairs in the central part of the beam, while keeping the position of the collimator blocks fixed. The superior-inferior length l of the applied boost fields was related to the field length L as defined by the collimator blocks by:

$$l = (L - n \cdot w) / 2 \quad (4.1)$$

with n the number of central leaf pairs that are closed during delivery of the boost fields and w the leaf width (1.25 cm at the MM50 Racetrack Microtron). L is the sum of the superior-inferior PTV length and the applied fixed field margins of 0.8 cm. As we concluded from our planning study for prostate cancer patients (see previous chapter), the length of the boost fields should be at least 1.1 cm to avoid underdosages in the PTV in CT-slices situated next to the most superior and inferior slices with PTV. In agreement with this requirement, the smallest length l that obeys equation (4.1) was selected, yielding $1.1 \text{ cm} \leq l \leq 1.6 \text{ cm}$.

The weight of the boost fields was chosen such that the minimum dose in the inferior and the superior ends of the PTV was at least 95% of the isocenter dose. In case simultaneous delivery of the boost fields yielded a minimum dose in the most superior or the most inferior part of the PTV that was significantly larger than 95% of the isocenter dose, e.g., due to the shape of the tumor or due to variations in patient contour in superior-inferior direction, a modified plan, based on a sequential delivery of the two boost fields with different weights, was considered.

4.2.2 Evaluation of the BIM technique

To investigate the proposed use of intensity modulated x-ray beams, 3D treatment plans were made for twelve lung cancer patients (see table 4.1) using the Cadplan 3D treatment planning system (version 2.7) manufactured by Varian-Dosetek [139,140].

Table 4.1 Characteristics of the patients in this study. The volume of the healthy lung tissue (column 4) was defined as the total lung volume minus the volume of the GTV.

patient	stage	volume PTV (cc)	volume healthy lung tissue (cc)	length PTV (cm)	length boost fields (cm)
1	III	372	5895	10.0	1.4
2	III	208	3586	6.5	1.5
3	III	456	3847	11.5	1.5
4	III	305	1921	7.5	1.4
5	III	477	3059	8.0	1.1
6	III	648	2876	17.0	1.2
7	I	44	3877	3.5	1.3
8	I	191	5997	9.0	1.6
9	I	372	2702	12.5	1.6
10	I	205	3699	8.0	1.1
11	I	63	3386	5.0	1.4
12	I	218	4377	8.0	1.1

For each patient, three plans were compared: A) the standard plan (field margins in the superior-inferior direction of 1.5 cm), B) a modified standard plan (field margins in the superior-inferior direction of only 0.8 cm), and C) the BIM plan (field margins of 0.8 cm and the application of superior and inferior boost fields in one of the treatment fields, as described in the previous subsection).

For all patients, CT-slices with 0.5 cm spacing were available. For treatment planning, the gross tumor volume (GTV) [62], the ipsilateral lung, the contralateral lung, the spinal cord and the oesophagus were contoured on each CT-slice. To account for the set-up variability and motion due to respiration and heartbeat, a margin to the GTV was automatically added in 3D [143,144], rendering the PTV. In all directions the applied margin was 1 cm, except for tumors located adjacent to the diaphragm for which a margin of 2 cm was used in superior and inferior directions.

In the Cadplan system the generalized Batho method was used to account for lung inhomogeneity effects. Each plan was normalized to 100% at the isocenter, where a total dose of 70 Gy was prescribed. All plans were evaluated using 3-dimensional planning tools such as dose volume histograms for the PTV, the healthy lung tissue (i.e. the contralateral lung plus the ipsilateral lung minus the GTV), the oesophagus and the spinal cord.

The dose distribution in the healthy lung tissue was evaluated using the following parameters: (i) the average normalized total dose (NTD), calculated using an α/β ratio of 3 Gy [82,84,85], (ii) the relative volume receiving an NTD of more than 20 Gy [53], and (iii) the calculated normal tissue complication probability (NTCP), based on the Lyman model [99], and the DVH-reduction algorithm described by Kutcher *et al* [81], using the following parameters: $TD_{50}=28.0$ Gy, $n=0.87$ and $m=0.18$ [107]. In all analyses the two lungs minus the GTV were considered as one functional unit. To estimate the incidence of pneumonitis, two published models were used: the average NTD [82,85] and the calculated NTCP. For stage III patients, treated with chemo-radiotherapy, resulting in the highest risk for severe oesophagitis, the length of the oesophagus, which received a dose of more than 60 Gy was quantified [74,83]. For the BIM plan, possible dose escalations were estimated, keeping the average NTD or the calculated NTCP at the same level as in the standard plan (plan A).

4.3 Results

4.3.1 Dose distributions in the PTV

Figure 4.3 shows dose distributions in the sagittal plane through the isocenter for plans A and C of patient 4 in this study. As a result of the application of the boost fields, the distance between the 50 and 95% isodose surfaces reduced by 0.8 cm both around the

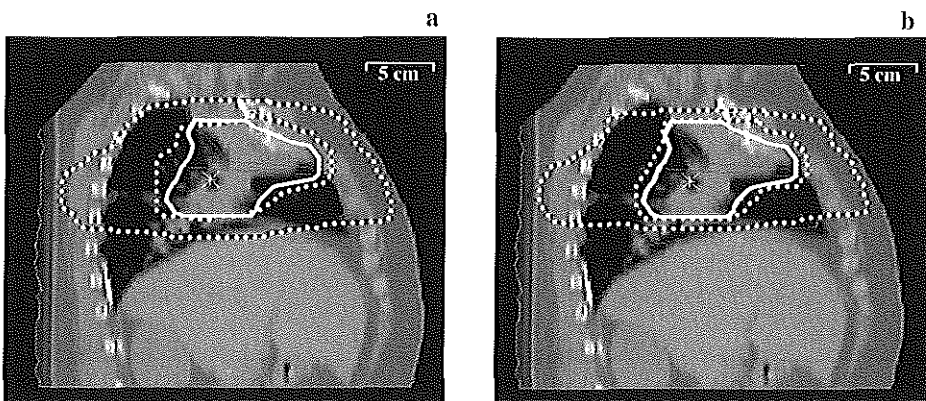


Figure 4.3 Dose distributions in the sagittal plane through the isocenter for patient 4 in this study: a) for the standard technique and b) for the BIM technique. Depicted are the PTV (solid line) and the 50 and 95% isodose lines.

superior and the inferior ends of the PTV. Moreover, while with the standard technique a penumbra margin of 1.5 cm was not sufficient to encompass the superior end of the PTV with the 95% isodose surface, the BIM technique yielded a minimum dose in the entire PTV of 95% with a reduced field length of 1.4 cm.

For all patients in the study, the minimum doses delivered to the superior and inferior ends of the PTV are summarized in table 4.2. The data show that with a field margin of 1.5 cm the minimum dose in the most superior and inferior parts of the PTV was 93.6% on average (range 91.2 to 95.4%) and that for only 4 of the 12 patients a minimum dose of 95% was obtained. With field margins of 0.8 cm and no boost fields (plan B), the minimum dose decreased to 89.4% on average (range 85.5 to 92.9%). Combining field margins of 0.8 cm with the application of boost fields (plan C) resulted in a minimum dose at the superior and inferior ends of the PTV of 95% for all patients.

Table 4.2 Minimum dose (in % of the isocenter dose) in the superior and inferior ends of the PTV for the three techniques described in the text.

patient	Plan A field margin 1.5 cm	plan B field margin 0.8 cm	plan C field margin 0.8 cm + boost fields
1	91.2	87.8	95.0
2	92.9	88.5	95.2
3	94.5	85.5	95.1
4	92.6	89.1	95.2
5	92.6	88.8	95.0
6	95.0	89.3	95.2
7	95.4	92.5	95.4
8	93.4	90.3	95.0
9	91.5	86.8	95.2
10	95.0	91.9	95.0
11	95.4	92.9	95.5
12	93.6	89.4	95.0

4.3.2 Dose distributions in normal tissues

For all patients in this study, the advantages of the BIM technique for sparing the healthy lung tissue are summarized in table 4.3. Relative to the standard technique the patient mean of the average lung NTD reduced by 8.2% (range 1.5 to 20.6%) and the volume of healthy lung tissue receiving an NTD of more than 20 Gy reduced by 9.7% (range 2.2 to 23.1%). With BIM the calculated NTCP was reduced from 10.7% to 7.6% on average.

Table 4.3 Evaluation of the BIM technique (plan C) for the healthy lung tissue using (i) the fraction of lung tissue receiving an NTD of more than 20 Gy ($V_{>20\text{ Gy}}$), (ii) NTD_{avg} , the average NTD, and (iii) the calculated NTCP. $\Delta V_{>20\text{ Gy}}$, ΔNTD_{avg} and $\Delta NTCP$ are the improvements with the BIM technique compared to the standard technique (plan A - plan C).

Patient	$V_{>20\text{ Gy}}(\%)$	$\Delta V_{>20\text{ Gy}}(\%)$	NTD_{avg} (Gy)	ΔNTD_{avg} (Gy)	NTCP (%)	$\Delta NTCP$ (%)
1	24.8	1.7	15.4	0.6	4.8	1.8
2	21.2	2.8	13.4	1.2	1.8	1.7
3	24.1	1.8	15.6	0.8	4.6	1.9
4	32.7	2.5	20.5	1.7	26.2	12.4
5	28.4	3.2	18.0	1.7	11.7	9.4
6	36.3	0.8	25.8	0.4	67.9	3.2
7	16.3	4.9	9.6	2.5	0.2	0.6
8	22.9	1.3	14.9	0.4	3.8	1.2
9	19.3	1.7	12.2	1.2	0.8	0.7
10	20.5	2.0	13.9	1.1	2.1	1.5
11	13.6	3.1	8.7	1.9	0.1	0.2
12	24.6	2.1	15.3	1.0	4.2	2.5

For stage III tumors, the length of the oesophagus that received a dose of 60 Gy or more is indicated in table 4.4. Compared to the standard technique the length of the oesophagus in the high dose region was reduced by 0.7 cm (range 0 to 1.3 cm) on average by application of the BIM technique. For the only patient where no improvement was observed, only 2.2 cm of the oesophagus received a dose higher than 60 Gy.

Table 4.4 Length L of the oesophagus receiving a dose of 60 Gy or more for the BIM technique for the stage III patients. ΔL indicates the reduced length in the high dose region compared to the standard technique.

Patient	L (cm)	ΔL (cm)
1	10.7	0.6
2	7.1	1.3
3	2.2	0.0
4	5.5	0.6
5	8.9	1.3
6	10.0	0.4

As a result of the penumbra enhancement, a dose escalation would be possible with the BIM technique for all patients, whilst keeping the average NTD or the calculated NTCP at the same level as in the standard plan (see figure 4.4). Based on equal NTCPs, the patient mean of the allowed dose escalation was 5.7 Gy (range 1.1 to 16.0 Gy) with the BIM technique. Based on equal mean NTDs, the possible dose escalation would even be slightly higher, i.e. 6.5 Gy on average (range 1.1 to 18.2 Gy). With these dose escalations, the maximum spinal cord dose would be between 1.9 Gy and 41.6 Gy for the patients in this study.

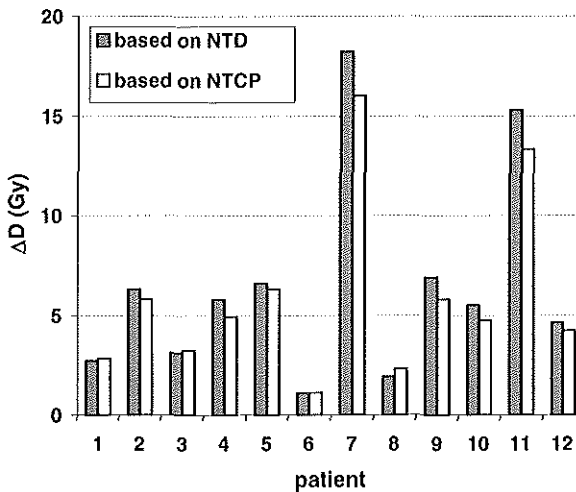


Figure 4.4 Estimated possible dose escalations with the BIM technique, based on equal average NTDs and equal NTCPs as for the standard technique.

4.4 Conclusions and discussion

A treatment planning study for twelve patients with lung cancer has shown that the proposed technique for static beam intensity modulation with an MLC allows a reduction in the field lengths by 1.4 cm, yielding a reduced dose delivery to the surrounding normal tissues. All parameters used to evaluate dose distributions in the healthy lung tissue point at a potential for dose escalation (6-7 Gy on average) with the BIM technique, without increasing the incidence of pneumonitis. For two patients a dose escalation of more than 15 Gy would even be possible. In an on-going dose escalation study, patients are stratified according to the calculated effective lung volume V_{eff} [129] which is directly correlated to the calculated NTCP in our study, because the same parameters (m , n , TD_{50}) are used. In our clinic the BIM technique will first be introduced to reduce the observed normal tissue complication rates. In a second phase, dose escalation will be considered as one of the options to intensify the treatment of lung cancer patients.

It is well known that the dose calculation algorithms in most treatment planning systems are less accurate in lung tissue than in other soft tissues, especially at higher energies, due to the influence of reduced electron density on secondary electron transport [45,75]. Also the Batho algorithm in the Cadplan treatment planning system is of limited accuracy for dose calculations in lung tissue. This was the main reason for selecting a low beam energy for this study. Before implementing the BIM technique for lung patients in clinical practice we have performed an extensive dosimetric study to assess the accuracy of the calculated dose distributions by comparison with dose distributions measured in anthropomorphic phantoms. This dosimetric study, described in the next chapter, yielded recommendations to further optimize the weight and width of the applied boost fields used in the proposed BIM technique to compensate also for the increased lateral secondary electron transport in lung tissue around the superior and inferior ends of the PTV, which especially in these areas might have a significant influence on the delivered dose distribution due to the overlapping penumbrae of all treatment fields.

In all co-planar irradiation techniques, the penumbrae of the superior and inferior field edges of all treatment fields overlap, yielding broad overall penumbrae in these regions [25,39]. Therefore, the reduced dose delivery to critical structures with the proposed BIM technique, related to the decreased superior-inferior field lengths, is not typical for the treatment technique applied in our clinic; improved treatment plans are to be expected for all co-planar techniques. The BIM technique could also be advantageous in the treatment of small cell lung cancer, where early concomitant chemo-radiotherapy has shown to result in improved survival [115], albeit with increased normal tissue

toxicity. BIM is already routinely applied in our clinic for treatment of prostate cancer patients and head and neck cancer patients. The extra time needed for set-up and delivery of the boost fields is usually less than one minute. Treatment plans for the BIM technique are easily obtained by 'forward' treatment planning; sophisticated computer optimization algorithms are not required.

Chapter 5

Beam intensity modulation for penumbra enhancement and field length reduction in lung cancer treatments; a dosimetric study

Adopted from the original article by MLP Dirx and BJM Heijmen, published in *Radiother. Oncol.* 56: 181-188, 2000.

5.1 Introduction

In all axial co-planar irradiation techniques, there is an overlap of the penumbrae of *all* treatment fields around the superior and inferior ends of a planning target volume (PTV), yielding a relatively large distance between the overall 95 and 50% isodose surfaces in these regions [25,39]. Around field corners, the dose fall-off is even shallower due to lateral electronic disequilibrium in both longitudinal and lateral directions. As a result, in superior and inferior direction large field margins should be added to a beam's eye view projection of the PTV to comply with ICRU-50 recommendations for dose homogeneity [62]: a dose in the 3D PTV within -5 and +7% of the dose in the ICRU-point, i.e. the isocenter. While in the three-field technique used in our clinic for treatment of prostate cancer patients field margins of 0.5 to 0.8 cm are adequate for definition of the lateral, anterior and posterior field borders, a margin of 1.5 cm for definition of the superior and inferior field borders still yields underdosages in the superior and inferior ends of the PTV for nearly all patients [39]. Because of the major impact of beam penumbrae on field margins required in superior and inferior directions, we developed an easy and practical technique for penumbra enhancement around the superior and inferior ends of a PTV and field length reduction using static beam intensity modulation (BIM) with a multileaf collimator (see chapter 3). The applied intensity modulated x-ray beams consist of narrow, low-weight boost fields, superimposed on the superior and inferior ends of treatment fields that encompass the beam's-eye-view projection of the PTV with narrow field margins in superior and inferior directions. We demonstrated that application of this technique allows the use of superior and inferior field margins of only 0.7 cm for prostate cancer patients, yielding a field length reduction of 1.6 cm for all fields compared to our (previous) standard technique. Using BIM, the conformity of the dose distribution to the tumor volume is improved, generally reducing the volumes of rectum and bladder in the high dose region. Currently, this BIM technique is routinely applied in our clinic for treatment of prostate cancer patients and head and neck cancer patients.

The results of a treatment planning study for twelve lung cancer patients treated with 'involved field radiotherapy', which were described in the previous chapter, demonstrate that a field length reduction of 1.4 cm, combined with penumbra enhancement by applying the described BIM technique, may result in reduced dose delivery to critical structures in co-planar lung treatments as well. Using the average normalized total dose (NTD) in the healthy lung tissue and the calculated normal tissue complication probability (NTCP) as estimates for the risk of radiation pneumonitis [82,107], it was concluded that a dose escalation of 6 Gy on average would be possible with BIM, without increasing the incidence of radiation pneumonitis. For two patients

in the study the potential for dose escalation even exceeded 15 Gy.

In an experimental study Brugmans *et al* [19] investigated some fundamental dosimetrical aspects of BIM in lung cancer treatments for a set of idealized square fields. They concluded that the use of an 8 MV photon beam is more suitable than the use of an 18 MV beam, due to the increased lateral secondary electron transport in lung tissue at higher energies, requiring larger field margins to get the same target coverage. Because most commercially available treatment planning systems are not capable of predicting penumbra broadening in soft tissues accurately, they stated that patient-specific measurements would generally be required for clinical application of BIM.

Based on the promising results of our treatment planning study, we decided to start an extensive dosimetric study on the use of BIM for superior-inferior field length reduction in lung cancer treatments in order to (i) adapt our BIM technique to properly account for increased lateral secondary electron transport, (ii) compare BIM dose distributions in lung material with dose distributions of standard treatment fields, and (iii) derive practical rules to use our treatment planning system for the design of BIM treatment plans for lung cancer patients. To minimize the increase of lateral secondary electron transport in lung tissue, the investigations were performed for low-energy photon beams [19,45,75], which are also routinely used in our clinic for treatment of lung cancer patients.

5.2 Material and methods

5.2.1 The BIM technique

For the 'standard' technique, treatment fields were designed by adding field margins of 1.5 cm around the beam's-eye-view projection of the PTV. For the BIM technique, two modifications were made: (i) the field margins in the superior and inferior direction were reduced to 0.8 cm and (ii) the in-field fluence profile was modified by superimposing narrow, low-weight boost fields on the superior and inferior ends of the treatment field (see figure 5.1), as explained in the introduction. The superior and inferior boost fields were delivered simultaneously by closing leaf pairs in the central part of the beam while keeping the position of the collimator blocks fixed. The superior-inferior length l of the applied boost fields (see figure 5.1) was related to the field length L as defined by the collimator blocks by

$$l = (L - n \cdot w) / 2 \quad (5.1)$$

with n the number of central leaf pairs that are closed during delivery of the boost fields and w the leaf width (1.25 cm at the MM50 Racetrack Microtron and 1 cm at the

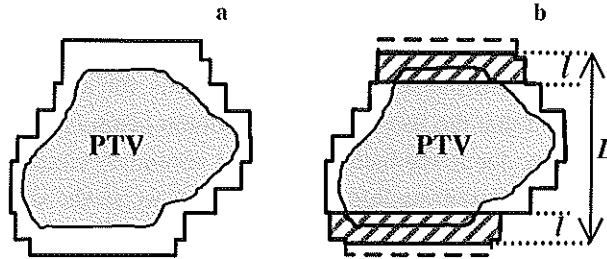


Figure 5.1 Beam's eye view projections of a treatment field used in the 'standard' technique (a) and the BIM technique (b). For the BIM technique, boost fields with length l (shaded areas) are superimposed on the superior and inferior ends of the PTV and the total field length L is reduced by 1.4 cm. The dashed lines in (b) illustrate the field size reduction with respect to the field shown in (a).

Siemens KD2). L equals the superior-inferior PTV length plus two times the applied field margin of 0.8 cm.

In our planning study for prostate cancer patients, described in chapter 3, it was concluded that the length of the boost fields should be at least 1.1 cm to avoid underdosages in the PTV in CT-slices situated next to the most superior and inferior slices with PTV. Accounting for this requirement, the smallest length l that obeys equation 5.1 was selected, yielding $1.1 \text{ cm} \leq l \leq 1.6 \text{ cm}$. The weight of the boost fields was chosen such that the minimum dose in the inferior and the superior ends of the PTV was at least 95% of the isocenter dose. Similar values for the length and the weight of the boost fields were found in our *treatment planning* study for lung cancer patients, described in chapter 4. In the present study, dose distributions *measured* in lung equivalent material were used to experimentally optimize the lengths and the weights of the boost fields to account for the increased lateral secondary electron transport in lung tissue.

5.2.2 Dosimetric measurements

Film dosimetry was performed in three phantoms. The first phantom ('water geometry') consisted of only polystyrene, the second one ('lung geometry') consisted of slabs of polystyrene (in total 5 cm thick), lung equivalent material (Gammex, $\rho \approx 0.3 \text{ gcm}^{-3}$, in total 12.5 cm thick) and again polystyrene (in total 5 cm thick). The third phantom ('tumor geometry') consisted of 3 cm polystyrene, 10 cm lung equivalent

material and again 3 cm polystyrene. A tumor volume (GTV), composed of polystyrene, with a cylindrical cross section with axes of 6 and 10 cm and a thickness of 5 cm was situated in the lung material (see figure 5.2). For this phantom a PTV was defined by expanding the GTV in 3D [143,144] with a margin of 1 cm to account for set-up inaccuracies and internal organ motion due to breathing, as encountered in clinical practice [42].

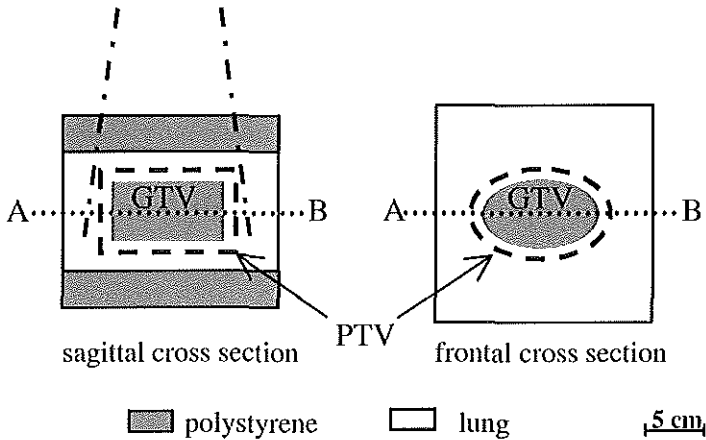


Figure 5.2 Sagittal and frontal cross sections through the center of the GTV in the 'tumor geometry' (along line A-B). The PTV, indicated by a dashed line, was defined by expanding the GTV in 3D with a margin of 1 cm.

The film measurements were performed for the 6 MV photon beam of a Siemens KD2 and for the 10 MV beam of an MM50 Racetrack Microtron (Scanditronix Medical AB). The 6 MV beam has a quality index, defined as the ratio of the dose in water measured at the isocenter for a $10 \times 10 \text{ cm}^2$ field at depths of 20 and 10 cm respectively, equal to 0.675. The applied 10 MV photon beam of the Racetrack Microtron has a quality index of 0.704 and a percentage depth dose curve similar to a 7 MV photon beam according to *British Journal of Radiology*, Supplement 25 [18].

Films (Kodak XV) were positioned in the phantoms perpendicular to the beam axis at depths ranging from 7.5 to 15 cm. Measured optical densities were converted into doses by applying a sensitometric curve determined in polystyrene at the depth of dose maximum in a $10 \times 10 \text{ cm}^2$ field using a focus to surface distance of 100 cm. 2D dose distributions for 'standard' flat fields were compared with 1.4 cm shorter, intensity modulated fields in which boosts fields were superimposed on the most superior and most inferior parts of a flat field for penumbra enhancement. All dose distributions were normalized to 100% in the center of the treatment field.

5.2.3 Treatment planning

For both the standard fields and the intensity modulated fields, 2D dose distributions were calculated using our Cadplan 3D treatment planning system (version 2.7.9) manufactured by Varian-Dosetek [139,140]. The generalized Batho method was used to account for lung inhomogeneity effects. Each plan was normalized to 100% in the field center.

In Cadplan, a table of phantom scatter factors is used, based on data for square fields larger than $4 \times 4 \text{ cm}^2$, as presented by Storchi and van Gasteren [141]. For smaller fields the values in the table were originally obtained by linear extrapolation, but to improve the accuracy of the predicted dose delivered by the boost fields, these values were modified into the ratio of total-scatter factors measured in water and head-scatter factors measured in a brass mini-phantom [39].

5.3 Results

5.3.1 Sensitometric curve for polystyrene and lung

To verify that the same sensitometric curve could be used in polystyrene and in lung equivalent material, films were irradiated at a depth of 10 cm in the water geometry or in the lung geometry to prescribed doses at the central axis ranging from 10 to 70 cGy using a $10 \times 10 \text{ cm}^2$ field. For both phantoms the required number of monitor units was calculated using our treatment planning system and the delivered dose at the central axis was verified by measurements with a NE 2571 ionization chamber. Prescribed doses and doses measured using the ionization chamber agreed within 2%, whilst the agreement between optical densities measured in both phantoms was within 1%.

5.3.2 Comparison of dose distributions in polystyrene and lung for standard flat fields

To demonstrate the effect of increased lateral electron transport on the beam penumbrae, dose distributions measured in polystyrene and in lung equivalent material were compared. In figure 5.3a dose profiles for the 10 MV photon beam along a central axis of a $10 \times 10 \text{ cm}^2$ field are depicted. The 95-50% dose fall-off is 1.2 cm in polystyrene and 1.9 cm in lung. This increase in 50-95% penumbra is comparable to the results for 10 MV reported by Ekstrand and Barnes [45]. Figure 5.3b compares

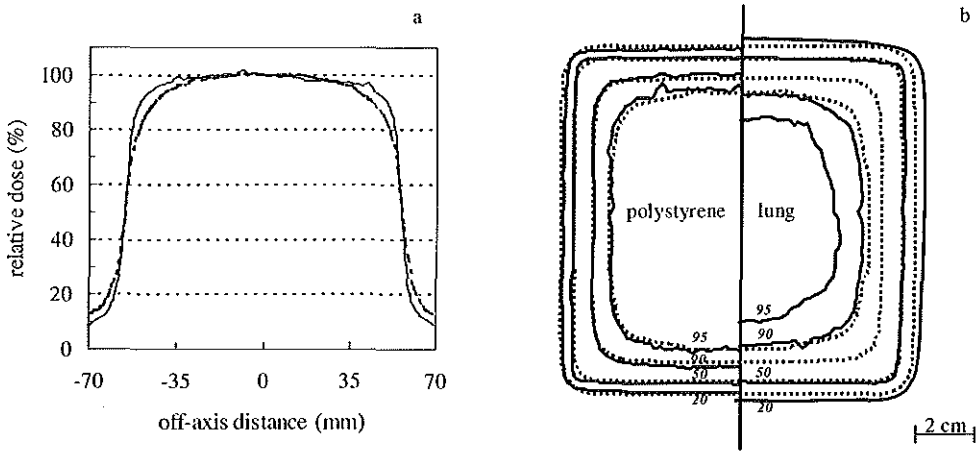


Figure 5.3 a Dose profiles along a central axis of a $10 \times 10 \text{ cm}^2$ field measured in polystyrene (solid line) and in lung equivalent material (dotted line) for the 10 MV photon beam at a depth of 10 cm using a focus to surface distance of 100 cm.

b Measured and calculated isodose distributions (solid and dashed lines respectively) for this $10 \times 10 \text{ cm}^2$ field in polystyrene (left) and lung equivalent material (right). Depicted are the 20, 50, 90 and 95% isodose levels.

measured and calculated 2D dose distributions for this $10 \times 10 \text{ cm}^2$ field in polystyrene and lung equivalent material. The measurements show that, due to the lateral transport of secondary electrons in *two* directions in the field corner, the distances between the 95 and 50% isodose levels increase to 2.1 cm in polystyrene and even 3.7 cm in lung. For the 10 MV photon beam the 90% isodose line in lung is similar to the 95% isodose line in polystyrene. At 0.8 cm within the field borders, where the most superior and inferior parts of the PTV are located when applying the BIM technique (see section 5.2.1), the difference in relative dose between polystyrene and lung equals 10%. Due to a lower secondary electron transport, the differences between dose profiles measured in polystyrene and lung are smaller for the 6 MV beam, ranging up to 5% at 0.8 cm within the field borders.

Since Cadplan does not account for the increased lateral secondary electron transport in lung material, a dose distribution for water is predicted for both phantoms (see figure 5.3b). Therefore, for lung cancer treatments, the borders of the PTV are generally underdosed compared with calculations by our treatment planning system.

5.3.3 Optimization of lengths and weights of boost fields used for BIM in lung

In order to avoid underdosages in the superior and inferior parts of the PTV when applying BIM in lung cancer treatments, both the lengths l and the weights of the applied boost fields have to be increased with respect to the values mentioned in section 5.2.1, while keeping the total field length L , as defined in section 5.2.1 and depicted in figure 5.1, constant. In agreement with the observed differences between calculated and measured doses at 0.8 cm from the field border (see previous section), the weight of the boost fields should be chosen such that the treatment planning system predicts a minimum dose of 100% of the isocenter dose at the most superior and most inferior ends of the PTV for 6 MV and of 105% of the isocenter dose for 10 MV. In reality the minimum PTV dose then just exceeds 95%. Due to the broader beam penumbra in lung, shown in the previous section, the lengths of the boost fields should be increased as well in order to avoid underdosages in CT-slices next to the most superior and inferior slices with PTV. Obeying equation 5.1, a length l of 1.6 or 1.8 cm should be selected for 6 MV and a value in the range of $2.0 \leq l \leq 2.5$ cm for 10 MV.

5.3.4 Comparison of dose distributions in the lung geometry for standard fields and intensity modulated fields

In the lung geometry, 2D dose distributions for standard fields and for 1.4 cm shorter fields with BIM were compared for a number of PTVs at different depths in the phantom. Figure 5.4a shows an isodose distribution measured for 10 MV at a depth of 12.5 cm. The superior-inferior length of the PTV is 10.5 cm, so, conform to the rules mentioned in the previous subsection, boost fields with a length of 2.3 cm were used in the BIM technique. For the standard field, the minimum dose in the superior and inferior parts of the PTV is less than 90%, while this value increases to 95% when applying BIM, in spite of a reduction in field length of 1.4 cm. Due to BIM, the 50-95% penumbra is reduced by 1.2 cm around the inferior part of the PTV and by 2.0 cm in superior direction (see figure 5.4b). Moreover, BIM allows an effective compensation for the reduced dose delivery in the field corners: the 50-95% penumbra is reduced from 3.7 to 2.0 cm (see figure 5.4a). In lateral direction the isodose distributions are similar for the standard field and the intensity modulated field (except around the superior and inferior field corners), since in our present study no attempts were made to improve the penumbra in that direction.

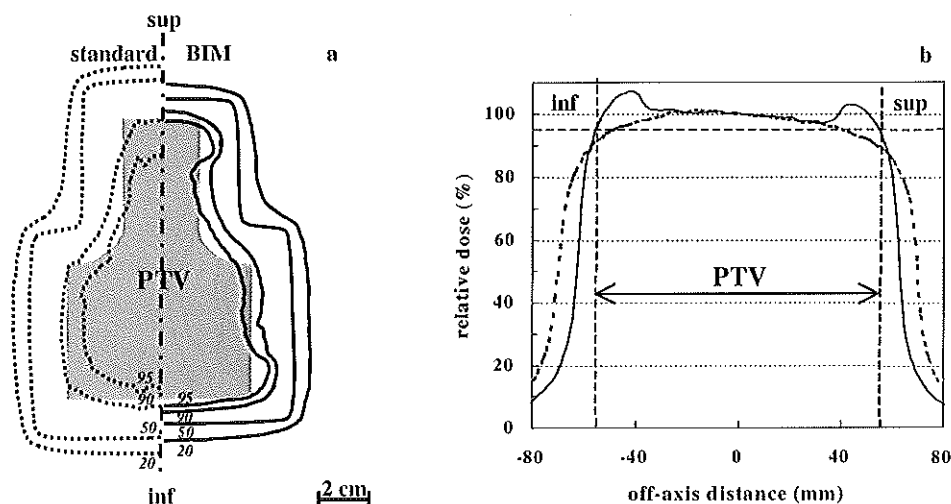
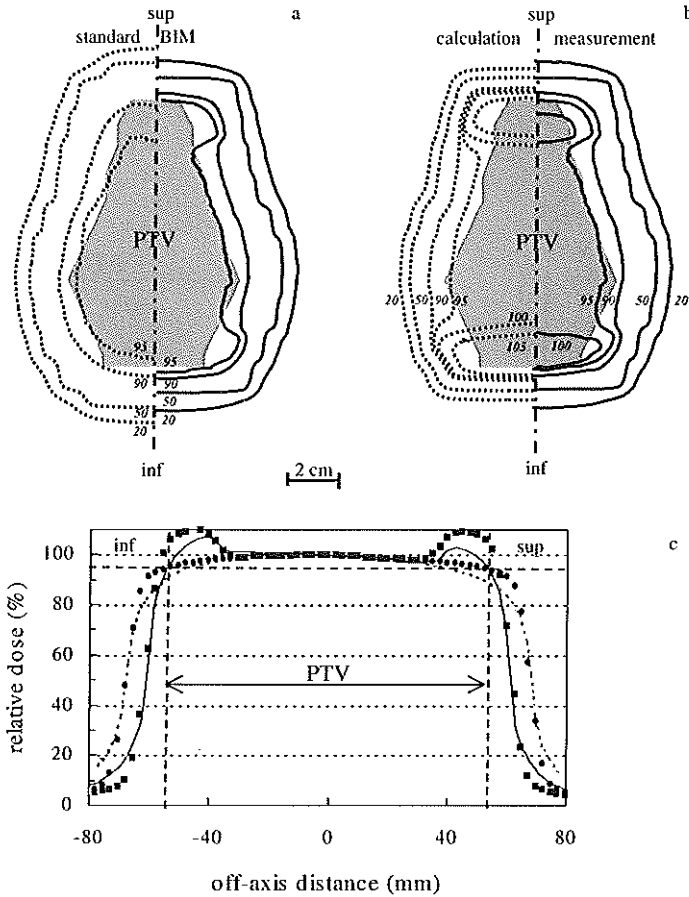


Figure 5.4 *a* Measured isodose distributions in lung equivalent material at a depth of 12.5 cm for treatment of a PTV (shaded area) with the 10 MV photon beam using the standard field (dashed lines) and a 1.4 cm shorter field combined with BIM (solid lines). Depicted are the 20, 50, 90 and 95% isodose levels. *b* Corresponding dose profiles in superior-inferior direction along the central axis.

Figure 5.5 shows similar results for another PTV treated with the 10 MV photon beam. For the standard field and the intensity modulated field measured isodose distributions are compared in figure 5.5a. Predicted and measured dose profiles in superior-inferior direction along the central axis are depicted in figure 5.5c for both fields. For the standard field Cadplan predicts a minimum dose in the entire PTV of 95%, but in reality this value was less than 90% in the most superior end of the tumor volume (dashed lines in figures 5.5a, c). By selecting the length and the weight of the boost fields according to the rules mentioned in the previous section, underdosages in the most inferior and most superior parts of the PTV could be avoided with BIM, in spite of the reduced field length (solid lines in figures 5.5a, c). For BIM, measured and predicted isodose distributions are compared in figure 5.5b. Due to the inaccurate model in Cadplan for the increased lateral secondary electron transport in lung, the difference between predicted and measured doses equals 10% at the ends of the PTV. The higher dose differences compared with the standard field, which were about 5%, are due to the shorter field length used for BIM, resulting in a shorter distance between the PTV ends and the field edge. Application of BIM may result in a maximum dose of



- Figure 5.5 a* Measured isodose distributions in lung equivalent material at a depth of 12.5 cm for treatment of a PTV (shaded area) with the 10 MV photon beam using the standard field (dashed lines) and a 1.4 cm shorter field combined with BIM (solid lines). Depicted are the 20, 50, 90 and 95% isodose levels.
- b* Comparison between the measured isodose distribution for the BIM treatment (solid lines) and the distribution predicted by our Cadplan treatment planning system (dashed lines). Depicted are the 20, 50, 90, 95, 100 and 105% isodose levels.
- c* Measured dose profiles in superior-inferior direction along the central axis for the standard field (dashed line) and BIM (solid line) and corresponding dose profiles predicted by our treatment planning system (dots and squares respectively).

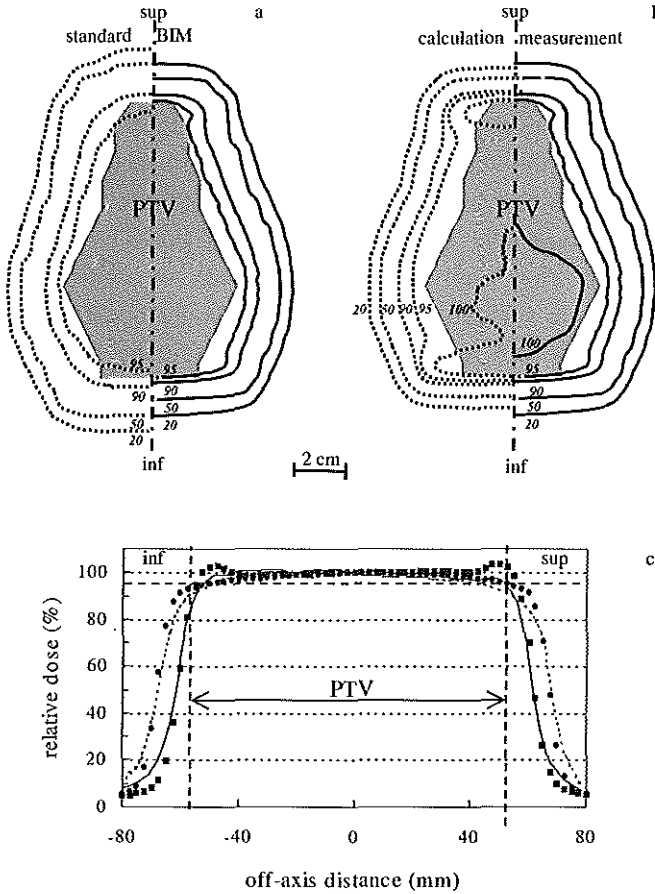


Figure 5.6 a Measured isodose distributions in lung equivalent material at a depth of 12.5 cm for treatment of a PTV (shaded area) with the 6 MV photon beam using the standard field (dashed lines) and with a 1.4 cm shorter field combined with BIM (solid lines). Depicted are the 20, 50, 90 and 95% isodose levels.

b Comparison between the measured isodose distribution for the BIM treatment (solid lines) and the distribution predicted by our Cadplan treatment planning system (dashed lines). Depicted are the 20, 50, 90, 95 and 100% isodose levels.

c Measured dose profiles in superior-inferior direction along the central axis for the standard field (dashed line) and BIM (solid line) and corresponding dose profiles predicted by our treatment planning system (dots and squares respectively).

110% near the ends of the PTV according to the treatment plan (see figure 5.5c), but in reality this value never exceeded 107% in any of our measurements.

In figure 5.6 dose distributions for treatment of an identical PTV as in figure 5.5, using the 6 MV photon beam, are depicted. Again Cadplan predicts a minimum dose in the entire PTV of 95% for the standard field, but in reality this value was only 91% (dashed lines in figures 5.6a, c). Due to the sharper 95-50% dose fall-off for 6 MV, a shorter length for the boost fields (1.6 instead of 2.3 cm) could be used compared with the previous example when applying BIM. Moreover, in accordance to the rules mentioned in the previous subsection, a lower weight for the boost fields was adequate to get a minimum dose of 95% in the PTV (solid lines in figures 5.6a, c). BIM reduced the 50-95% penumbra by 0.9 cm along the central axis in both the superior-inferior direction and in the corners of the treatment field. Measured and predicted isodose distributions for BIM are depicted in figure 5.6b. Due to the smaller effect of increased lateral secondary electron transport in lung for 6 MV, the differences between predicted and measured doses did generally not exceed 6%, yielding a maximum dose in the PTV of less than 105% according to the treatment plan.

5.3.5 Comparison of dose distributions in the tumor geometry for standard fields and intensity modulated fields

Compared with the lung geometry, the 95-50% dose fall-off is sharper in the tumor geometry (1.6 instead of 1.9 cm for 10 MV), due to the penetration of secondary electrons generated in the edges of the high density GTV into the low density lung tissue of the PTV (see figure 5.7). As a result, the 95% isodose does encompass the PTV for the standard field (field margin 1.5 cm), both for the 6 and the 10 MV photon beams. However, by applying BIM, a similar dose distribution in the PTV can be obtained with a reduction in field length of 1.4 cm. Due to the lateral secondary electron transport from the GTV into the penumbra regions, the dose calculations of the treatment planning system are more accurate in the tumor geometry than in the lung geometry; the difference between calculated and measured doses is reduced to a maximum of 5% for 10 MV. Therefore, the weight of the boost fields for 10 MV may be reduced so that the planned minimum dose on the superior and inferior ends of the PTV just exceeds 100% of the isocenter dose, like for the 6 MV photon beam.

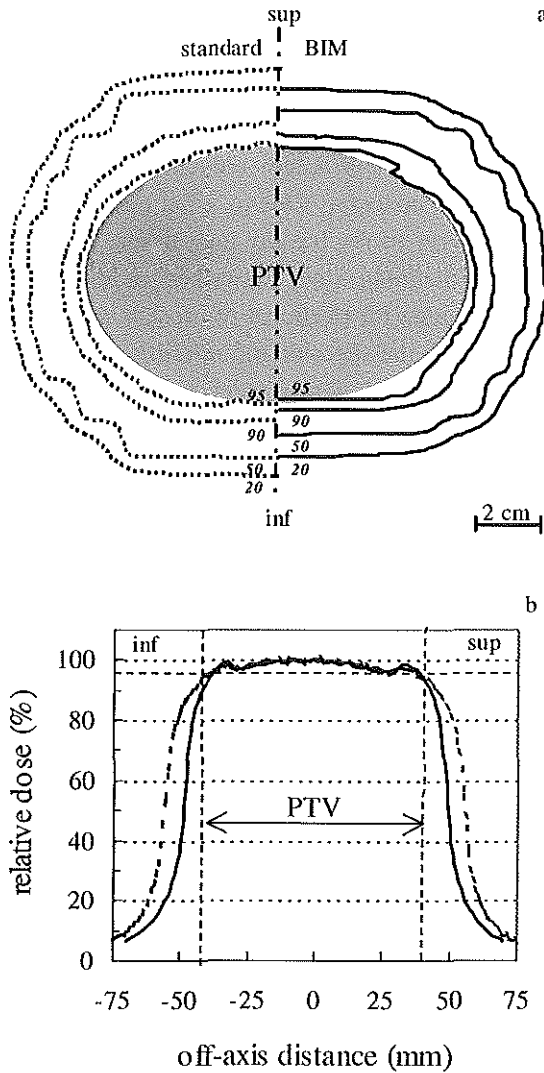


Figure 5.7 a Measured isodose distributions for treatment of the PTV (shaded area) in the 'tumor geometry' (depicted in figure 5.2) at a depth of 8 cm with the 10 MV photon beam using the standard field (dashed lines) and a 1.4 cm shorter field combined with BIM (solid lines). Depicted are the 20, 50, 90 and 95% isodose levels.

b Corresponding dose profiles along the central axis in superior-inferior direction.

5.4 Conclusions

The results of this dosimetric study show that, in spite of the increased lateral secondary electron transport in lung tissue, BIM can effectively be used for penumbra enhancement and superior-inferior field length reduction in lung cancer treatments, whilst achieving adequate tumor coverage. Due to a field length reduction of 1.4 cm, BIM yields reduced dose delivery to the healthy lung tissue, as was demonstrated by the results of our treatment planning study described in the previous chapter. In contrast to the use of this technique for treatment of prostate cancer patients, the boost fields which are superimposed on the superior and inferior ends of the treatment fields have to be longer and of a higher weight in order to compensate for the effects of increased lateral secondary electron transport in lung tissue. The Cadplan treatment planning system does not correctly account for this increased lateral electron transport, but practical rules for selecting the length and the weight of the applied boost fields could be derived to circumvent this problem. Using these rules, underdosages in the superior and inferior parts of the PTV could be avoided in spite of the reduction in field lengths with respect to the fields used in our present treatment technique. In contrast, with the present standard technique for lung cancer treatments, underdosages in the superior and inferior ends of the PTV do usually occur, despite the use of superior-inferior field margins of 1.5 cm or larger and a minimum PTV dose of 95% of the isocenter dose as predicted by the treatment planning system. Clearly, there is a pressing need for more accurate dose calculation algorithms which correctly model the effect of electron density on lateral secondary electron transport, in order to enable quantification of the actual dose delivery in clinical lung cancer treatments, e.g. by using dose volume histograms and (normal) tissue complication probabilities. The availability of correct dose volume histograms may also facilitate the design of dose escalation studies for lung cancer treatments. Due to the sharper beam penumbræ around the superior and inferior field edges, clinical application of the proposed BIM technique puts higher demands on the accuracy of the definition of the GTV in superior and inferior direction and the inclusions of adequate margins between the GTV and the PTV to account for patient set-up inaccuracies and internal organ motion due to breathing.

In this dosimetric study the advantages of BIM for penumbra enhancement and field length reduction in superior-inferior direction were demonstrated for single fields. By realizing these effects for every single beam, this technique can effectively be used in coplanar lung treatments.

Chapter 6
**Leaf trajectory calculation for dynamic multileaf collimation
to realize optimized fluence profiles**

Adopted from the original article by MLP Dirx, BJM Heijmen and JPC van Santvoort, published in *Phys. Med. Biol.* 43: 1171-1184, 1998.

6.1 Introduction

Dose distributions can often be significantly improved by applying intensity modulated X-ray beams, calculated by means of inverse treatment planning techniques [12,17,56,68,91,104,114,134,137,164,166-168]. Using customized beam profiles, the high dose region can often be conformed more closely to the target volume, reducing the dose delivered to surrounding critical organs and normal structures. Moreover, for some tumor sites, e.g. in the head and neck region, a more homogeneous dose distribution in the target volume can be obtained.

One way of realizing intensity modulated beam profiles is the use of compensators. However, compensators have several drawbacks. First of all, their production is labor-intensive and time consuming. Since they have to be changed manually for each treatment field, their use is time consuming during treatment delivery as well. For this reason, only a limited number of compensators can generally be used in clinical practice. Another drawback is the need for models to accurately include scattered photons and beam hardening, as produced by the compensators, in the dose calculations.

A second way to produce intensity modulated beams is the superpositioning of a number of partially overlapping, static, irregularly shaped fields produced with a multileaf collimator (MLC). Examples of this method have been described in chapters 3 and 4 and by Bortfeld *et al* [13] and Galvin *et al* [51], Fraass *et al* [50] and de Neve *et al* [35,36]. Probably the most flexible way is the use of dynamic multileaf collimation, scanning beams or a combination of both techniques [28,57,135,136,138,147,158,165,169].

For dynamic multileaf collimation, several analytical algorithms have been described in recent years for the calculation of the required leaf trajectories to realize an optimized fluence profile employing the sliding window technique [29,135,138,147]. This technique is based on moving each leaf pair of the MLC independently but unidirectionally across the treatment field while the beam is on, effectively sweeping apertures of variable widths across the field.

To reduce leakage radiation between adjacent leaves of a multileaf collimator, all commercially available MLCs have a so-called tongue-and-groove arrangement (see figure 6.1). A disadvantage of such an arrangement is that it can yield serious underdosages both in the case of superpositioning of multiple static fields and for dynamic multileaf collimation [112,158]. Recently, van Santvoort and Heijmen [158] have presented a method for leaf trajectory calculation for dynamic multileaf collimation, which fully avoids tongue-and-groove underdosage effects by synchronization of the trajectories of adjacent leaves. Webb *et al* [169] refined this

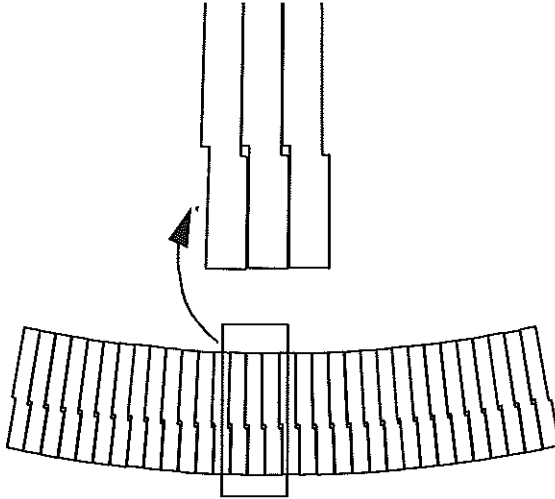


Figure 6.1 Tongue-and-groove arrangement of the MM50 multileaf collimator.

method by allowing also partial synchronization, accounting for the effect of increased leaf transmission in the tongue-and-groove area.

In the article of van Santvoort and Heijmen [158] leaf transmission and collimator scatter were not accounted for. In this chapter an iterative algorithm for leaf trajectory calculation is presented that does take into account transmission and collimator scatter, while still avoiding tongue-and-groove underdosage effects. To assess the accuracy of this algorithm in combination with the Cadplan 3D treatment planning system (Varian-Dosetek), predicted absolute dose distributions for optimized fluence profiles were compared with dose distributions measured for the 25 MV photon beam of the MM50 Racetrack Microtron using dynamic multileaf collimation. The required leaf trajectories resulted from calculations with the presented algorithm. Prediction of dose distributions was performed using the pencil beam algorithm as implemented in the Cadplan system [140,142].

6.2 Iterative algorithm for leaf trajectory calculation

Starting point for the calculations are optimized fluence profiles $F_{\text{opt}}(k,x)$ for all leaf pairs k , expressed in monitor units and calculated by inverse treatment planning techniques, taking into account off-axis variations in the primary beam fluence profile

of the accelerator. A fluence of 1 MU corresponds to the fluence that results in a dose delivery of 1 cGy at the depth of dose maximum in water for a static $10 \times 10 \text{ cm}^2$ field using a source to surface distance of 100 cm. The optimized fluence profiles are realized with the sliding window technique with the leaves moving across the field from left to right.

The iterative calculation of the leaf trajectories is started by assuming that for each leaf pair k the required monitor unit profile $MU_0(k,x)$, defining for each position x the number of monitor units that one of the two leaves of a leaf pair should not block x in order to realize $F_{opt}(k,x)$, is equal to the optimized fluence profile, i.e.:

$$MU_0(k, x) = F_{opt}(k, x) \quad (6.1)$$

In iteration step i , the leaf trajectories for all leaves are determined from the profiles MU_{i-1} using the method described by Van Santvoort and Heijmen [158]. Next, forward calculations of the resulting fluence profiles F_i are performed, taking into account both collimator scatter and leaf transmission (see also figure 6.2):

$$F_i(k, x) = \int_{MU_{R,i}(x)}^{MU_{L,i}(x)} S_{c,i}(k, MU) dMU + T \left[MU_{tot,i} - [MU_{L,i}(k, x) - MU_{R,i}(k, x)] \right] \quad (6.2)$$

For each leaf pair k , the first term of equation 6.2 describes the fluence delivered to position x while it is unblocked by the opposing leaves, i.e. during the period that the right leaf has passed position x (i.e. $MU_{R,i}(k,x)$ monitor units after the irradiation started) and the left leaf has not yet reached this position (i.e. $MU_{L,i}(k,x)$ monitor units after the irradiation started). The collimator scatter factors $S_c(k,MU)$ for the irregularly shaped fields at times MU are derived from measured values for rectangular fields. For each leaf pair k , the leaf opening at time MU is determined. Together with the field length, defined by the collimator blocks, the leaf opening of pair k defines a rectangular field. The collimator scatter factor of this rectangular field, obtained by interpolation of measured values, is taken as the collimator scatter factor $S_c(k,MU)$.

The second term in equation 6.2 describes the fluence contributions due to the effective transmission under the moving leaves during the periods that x is blocked by one of the two leaves of a leaf pair. This effective transmission includes both transmission through the leaves and the effect of extra-focal radiation, originating from the periphery of the focus at the target and from the collimator blocks [63,142]. $MU_{tot,i}$ is the total number of monitor units needed to realize the fluence profile.

The calculated fluence profiles in iteration i , $F_i(k,x)$, are compared with the optimized profiles $F_{opt}(k,x)$, and the MU-profiles are adjusted for the next iteration:

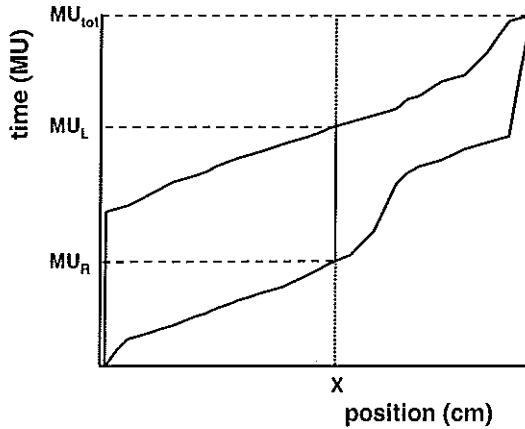


Figure 6.2 Example of required leaf trajectories to generate an optimized fluence profile using dynamic multileaf collimation. MU_R and MU_L indicate the number of monitor units after which respectively the right and the left leaf arrive at position x ; MU_{tot} indicates the total number of monitor units required to generate the fluence profile.

$$MU_i(k, x) = MU_{i-1}(k, x) - (F_i(k, x) - F_{opt}(k, x)) \quad (6.3)$$

The iteration continues until for each position and leaf pair the difference between the realized and the optimized fluence profile is less than a predetermined tolerance level or until the overall difference, indicated by the rms deviation, is not decreasing significantly between successive iterations.

6.3 Materials and methods

6.3.1 Measurement of collimator scatter factors

Collimator scatter factors needed for leaf trajectory calculations have been measured for rectangular fields using an RK chamber (volume 0.13 cc), vertically positioned in a brass build-up cap with a cylindrical side wall of 2 gcm^{-2} and a front wall of 10 gcm^{-2} [89]. In order to have the radiation field fully encompassing the used build-up cap, the source-to-surface distance was extended from 100 to 250 cm for the smallest fields. For fields with leaf openings of less than 1 cm, measurements were also performed with

TLD, positioned in a build-up cap with side and front walls of the same thicknesses as mentioned before, but with a smaller outer diameter. Measurements were performed on the beam axis for leaf openings ranging from 0.4 to 10 cm and field lengths of 5, 10 and 15 cm.

To verify the method, explained in section 6.2, for calculation of collimator scatter factors for the long, narrow and irregularly shaped fields observed in dynamic multileaf collimation, collimator scatter factors have also been measured for many of those fields. Leaf settings for the irregularly shaped fields were derived from optimized fluence profiles using the algorithm described in the previous section. For the measurements the leaf positions were shifted so that the two middle leaf pairs were centered around the beam axis. The measurements were performed with an RK-chamber on the beam axis using the same experimental set-up as for the rectangular fields.

In the method presented in section 6.2 the collimator scatter factor is assumed to be independent of position within the field. To verify this assumption, doses were measured in the center of fields of $1.6 \times 10 \text{ cm}^2$, centered around off-axis positions of 2.5, 5, 7.5, 10 and 12.5 cm. Each dose, normalized to the dose for the on-axis $1.6 \times 10 \text{ cm}^2$ field, was compared with the corresponding normalized primary fluence profile as measured with the leaves and collimator blocks completely opened. All measurements were performed with the RK-chamber vertically positioned in the build-up cap mentioned above.

6.3.2 Measurement of transmission through the leaves

The transmission through the leaves has been measured in a water phantom (RFA-300, manufactured by Scanditronix Medical AB) using a linear diode array consisting of 11 p-type diodes, and with film, irradiated perpendicularly to the beam axis in a polystyrene phantom [153]. In the latter case, measured optical densities were converted into doses by applying a sensitometric curve determined for the beam axis of a $10 \times 10 \text{ cm}^2$ field using the same set-up. Measurements were made for a $0 \times 10 \text{ cm}^2$ field, i.e. with the leaves fully closed and the collimator blocks set to an opening of 10 cm. The transmission was determined by normalizing the results to the dose measured at the same position for a $10 \times 10 \text{ cm}^2$ field, using the same number of monitor units. For all measurements the source to surface distance was 100 cm.

6.3.3 Realization of fluence profiles at the MM50 Racetrack Microtron

The dual gantry MM50 Racetrack Microtron is equipped with a double focused multileaf collimator suited for shaping both photon and electron beams [46,71]. Projected at isocenter, the leaves have a width of 1.25 cm and a range of travel of 16 cm from the beam axis to 14 cm across it. The maximum leaf speed is 1 cm s^{-1} and the maximum dose rate is 5 MU s^{-1} . Arbitrary fluence profiles can be generated clinically using dynamic multileaf collimation, which is fully integrated in the clinical treatment mode. For DMLC, a treatment field is divided into a number of so-called subsegments. The first subsegment (start segment) defines the positions of the leaves when the irradiation is started, the last one (stop segment) defines their positions when the beam is turned off. Additional, intermediate subsegments are used to change the speed of the leaves during the irradiation. While the number of monitor units associated with a subsegment is delivered, each leaf moves with an appropriate constant velocity (cm/MU), calculated by the control system of the accelerator, to the position defined for the next subsegment. By definition, the number of monitor units for the stop segment is zero. The maximum number of allowed subsegments equals 48.

For realization at the accelerator, the continuous leaf trajectories, as calculated with the method described in section 6.2, are subdivided into 48 subsegments. A simple method for this segmentation would be based on an identical number of monitor units for each subsegment. However, using this method, unnecessary subsegments may then be defined in periods that the velocities of the leaves do not change significantly, leaving too few segments to accurately account for large velocity changes in other periods, resulting in substantial deviations between calculated continuous leaf trajectories and segmented leaf trajectories. To minimize these deviations another method for segmentation is used. In this method, the calculated velocity changes of the leaves are ranked from high to low. To define the intermediate subsegments additional to the start and stop segment, the times at which the 46 highest velocity changes occur are then used. However, defining two separate subsegments at nearly the same time of the irradiation does not substantially improve the accuracy of segmented leaf trajectories. Therefore, one refinement was made to the described method. The number of monitor units associated with a subsegment should be at least $\text{MU}_{\text{tot}} / 2(N-1)$. (MU_{tot} indicates the number of monitor units needed to realize the fluence profile and N is the number of subsegments.) Definition of the 46 intermediate subsegments is then based on the previous mentioned ranking of velocity changes, while skipping segmentations that would be too close to previous segmentations, as defined above.

The leaf positions and monitor units for each subsegment are transferred to the MM50 by network and are stored in the patient database.

During a DMLC treatment the leaf positions are verified every 0.08 seconds by comparing the actual values, measured with potentiometers, with the prescribed positions. In case for one of the leaves the deviation exceeds the preset tolerance level for more than a preselected number of subsequent measurements, the treatment is terminated. Presently, these tolerance levels have been set to 0.2 cm and to 3 times, in order to avoid that a treatment is unnecessarily terminated in case a leaf position appears to deviate strongly from its prescribed position due to electronic spikes on the readout signal. For reasons of treatment time efficiency and potential hardware problems with the leaves during DMLC operation, 0.2 cm was also chosen as the leaf position tolerance for the Varian MLC at the Memorial Sloan-Kettering Cancer Center [92].

6.3.4 Dosimetric verification of leaf trajectory calculations

The method for leaf trajectory calculation was tested for the 25 MV photon beam of the MM50 Racetrack Microtron for a wide range of fluence profiles. Both model cases and real clinical cases were studied. To verify the method for leaf trajectory calculation, absolute dose distributions were measured for fields realized with the calculated leaf trajectories. These measured dose distributions were compared with calculated dose distributions derived from corresponding optimized fluence profiles by convolution with a pencil beam [140,142], as implemented in the Cadplan treatment planning system. Relative dose profiles were measured in a water phantom at different depths, using a linear diode array consisting of 11 p-type diodes, and with film, irradiated perpendicularly to the beam axis in a polystyrene phantom. In the latter case, measured optical densities were converted into doses by applying a sensitometric curve as described before. For all measurements the source to surface distance was 100 cm. Absolute dose measurements, needed for normalization of the relative dose profiles, were performed with an ionization chamber in a relatively flat part of the beam profile.

6.4 Results and discussion

6.4.1 Collimator scatter factors needed for leaf trajectory calculation

In figure 6.3, measured collimator scatter factors, determined relative to a $10 \times 10 \text{ cm}^2$ field, are depicted for the 25 MV photon beam of the MM50. It was verified that within the accuracy of the measurements the collimator scatter factor did not depend on the

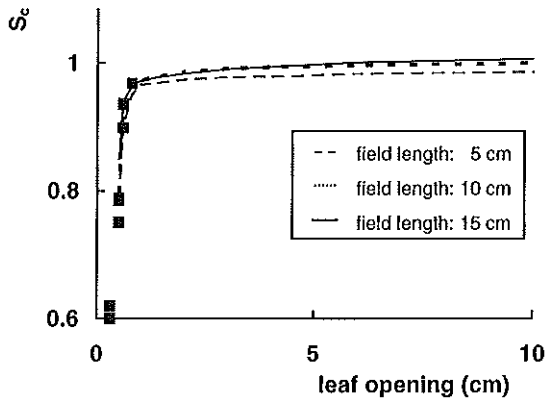


Figure 6.3 Measured collimator scatter factors for rectangular fields with field lengths of 5, 10 and 15 cm respectively using an RK chamber (lines) or TLD (points).

detector type (RK chamber or TLD) and the source-to-surface distance (100 or 250 cm). It is clear that for a fixed field length the variation of the collimator scatter factor is rather small (less than 4%) for leaf openings larger than 0.8 cm. This variation is in agreement with previously described results [180] when no flattening filter is present, like on the MM50. For smaller leaf openings the collimator scatter factor decreases dramatically. Using a similar measurement technique as suggested by Huang *et al* [60], it was concluded that backscatter of radiation into the monitor chamber is absent for the MM50. Therefore, the large decrease in collimator scatter factors for small field openings should be explained by blocking of photons originating from the periphery of the focus at the target as described by Zhu and Bjärngård [180].

6.4.2 Verification of predicted collimator scatter factors for irregularly shaped fields and off-axis positions

Measured and predicted collimator scatter factors have been compared for 116 different irregularly shaped fields. Since the measurements were made on the beam axis, the average predicted collimator scatter factor for the two leaf pairs adjacent to the beam axis was used in this comparison. As an example the shapes of six irregularly shaped fields and the corresponding measured and predicted collimator scatter factors are depicted in figure 6.4.

Figure 6.5 shows a histogram of the observed ratios between the measured and predicted values for leaf openings of 0.7 cm and larger (N=112). On average, this ratio

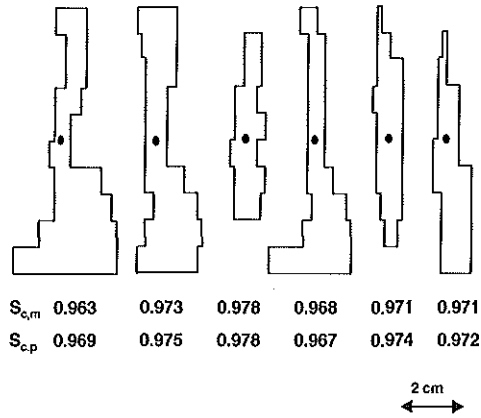


Figure 6.4 Examples of irregularly shaped fields used to verify our method to predict the collimator scatter factor. $S_{c,m}$ and $S_{c,p}$ are measured and predicted collimator scatter factors in the indicated points respectively.

equals 0.996 ± 0.003 (1 SD), which means that our model makes a small overestimation of the S_c factors. One reason for this rather good agreement is the fact that very irregularly shaped apertures are avoided as a result of the synchronization of the leaf trajectories (see section 6.2).

For leaf openings smaller than 0.7 cm differences between predicted and measured collimator scatter factors up to 5% have been observed. However, from figure 6.3 it is clear that these deviations can already be explained by an error of 0.05 cm in the actual

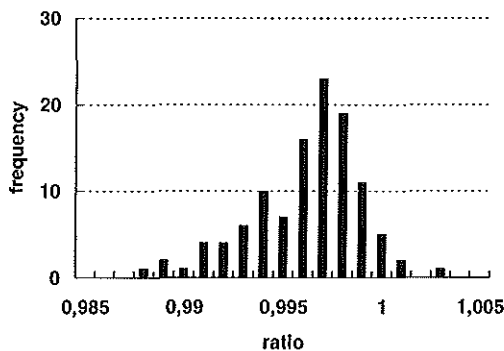


Figure 6.5 Observed ratios between measured and predicted on-axis collimator scatter factors for 112 irregularly shaped fields with on-axis openings of 0.7 cm or larger.

leaf openings. A small deviation of the detector from the center of the fields can explain these deviations as well. Generally, when using dynamic multileaf collimation, the leaf openings are larger than 0.7 cm during most of the treatment. Only for the first and last few monitor units the leaf openings are smaller, resulting in a less accurate prediction of the collimator scatter factor. This inaccuracy does only affect the accuracy of the calculated fluences in the penumbra regions of the fields.

The normalized doses for the off-axis positioned $1.6 \times 10 \text{ cm}^2$ fields (see section 6.3.1) agreed within 0.6% with the normalized primary fluence profile. Therefore, in equation 6.2 on-axis collimator scatter factors can indeed be used for off-axis positions. More in general, the validity of using on-axis measured S_c factors in off-axis positions is confirmed by the close on- and off-axis agreement between calculated and predicted dose profiles (see section 6.4.5).

6.4.3 Effective transmission through the leaves

For the 25 MV photon beam of the MM50, both film and diode measurements yielded an (average) transmission through the leaves of 0.8% at a depth of 3.5 cm. The interleaf leakage was less than 2%.

Assuming a negligible extra-focal radiation, the first comparisons of measured and predicted dose distributions for intensity modulated beams were made using a value for the effective transmission T in equation 6.2 of 1%. A systematic underestimation of the predicted dose distributions was then found. In later runs, the effective transmission was used as a tuning parameter. It was concluded that the best overall agreement could be achieved assuming an effective transmission of 2%, which by coincidence equals the interleaf leakage (see above). This value is only slightly higher than the 1.5% that was used by Storchi *et al* [142] in their calculation for dynamic wedges on Varian Clinacs.

6.4.4 Iterative calculation of leaf trajectories

In figure 6.6, a typical example is presented of the results of our iterative method for leaf trajectory calculation. As indicated in the previous subsection, a value for the effective transmission T of 2% was applied in equation 6.2. For each monitor unit, the collimator scatter factors $S_c(k, \text{MU})$ as used in equation 6.2 were determined by interpolation from the data in figure 6.3 using the field length and the leaf opening (see section 6.2). After one iteration, large differences (up to 10%) are observed between

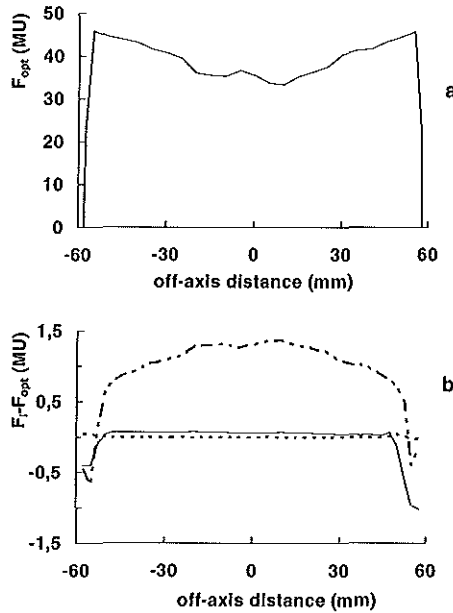


Figure 6.6 a Example of an optimized fluence profile.
 b Differences between realised and optimized fluence profiles after 1, 2 and 7 iterations, indicated by dashed, solid and dotted lines respectively.

the realized fluence profile F_i and the optimized fluence profile F_{opt} . Generally, after a second iteration these differences are already reduced to less than 0.2 MU, except at the edges of the field. This is related to the very small leaf openings at the beginning and at the end of the irradiation, resulting in S_c factors that strongly deviate from 1. Generally after 3 to 10 iterations, the differences between the realized and optimized fluence profiles are less than 0.1 MU for all points within the treatment field, except for those with an optimized fluence less than 2% of the total number of monitor units needed to realize the profile. Such a low fluence can never be realized due to the unavoidable transmission through the leaves.

After segmentation in 48 subsegments, the agreement between the realized and optimized fluence profiles generally remains within 0.5 MU for most points within the field. An increase in the maximum number of subsegments, requiring a modification of the control software of the accelerator, will improve the accuracy after segmentation. In the meantime, dose distributions can be derived from the segmented fluence profiles, to make sure that the remaining differences between the segmented and the optimized fluence profiles do not yield clinically unacceptable results.

6.4.5 Dosimetric verification of leaf trajectory calculation

In figure 6.7, a comparison is made between measured and predicted absolute dose profiles at depths of 3.5, 10 and 20 cm for three 1D model cases, i.e. with identical modulated fluence profiles for all leaf pairs. The field length was 10 cm for the first two fluence profiles and 12.5 cm for the third one.

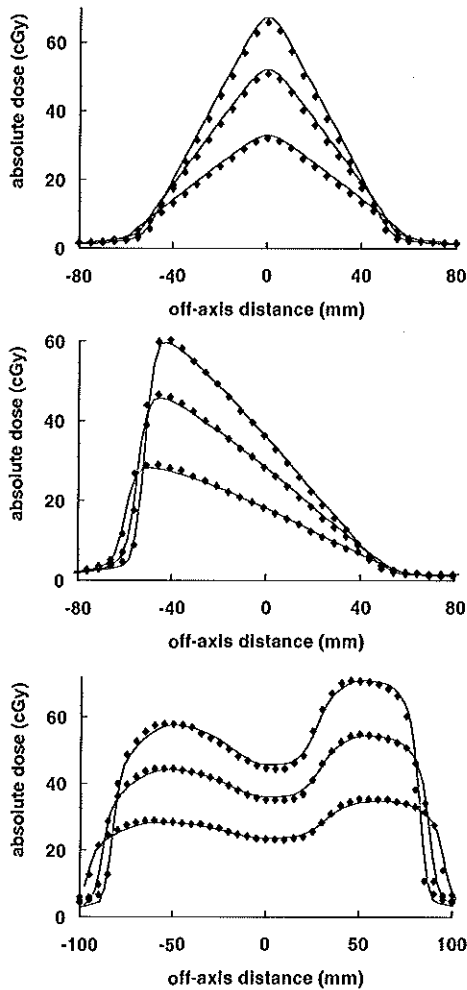


Figure 6.7

Comparison between measured and calculated absolute dose profiles, indicated by dots and lines respectively, at depths of 3.5, 10 and 20 cm for three 1D model cases.

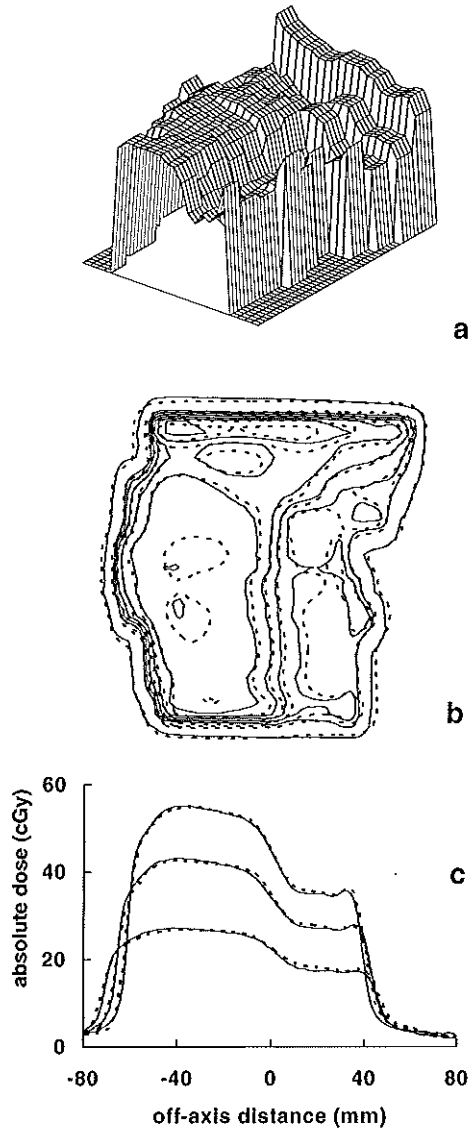


Figure 6.8

- a* Optimized fluence profile for treatment of a patient with prostate cancer.
- b* Comparison between measured and calculated isodose distributions, indicated by solid and dashed lines respectively, at a depth of 35 mm. Depicted are the 10, 30, 35, 40, 45, 50 and 55 cGy dose levels.
- c* Comparison of measured and calculated dose profiles, indicated by solid and dashed lines respectively, along the central axis at depths of 3.5, 10 and 20 cm.

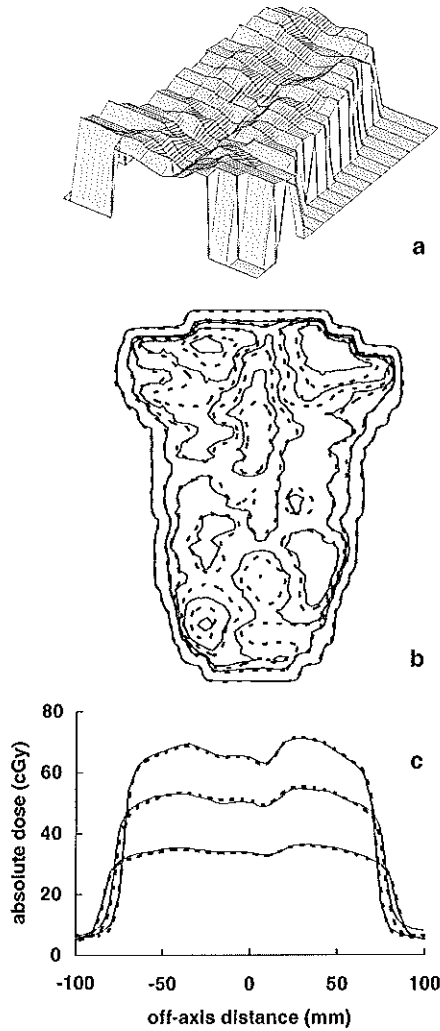


Figure 6.9

- a Optimized fluence profile for the elective treatment of a patient with head and neck cancer.
- b Comparison between measured and calculated isodose distributions, indicated by solid and dashed lines respectively, at a depth of 35 mm. Depicted are the 20, 60, 65, 70, and 75 cGy dose levels.
- c Comparison of measured and calculated dose profiles, indicated by solid and dashed lines respectively, along the central axis at depths of 3.5, 10 and 20 cm.

Figures 6.8 and 6.9 show the results for two clinical cases: an optimized fluence profile used for treatment of a prostate cancer patient (figure 6.8a) and one used for the elective treatment of a patient with a head and neck cancer (figure 6.9a). Figures 6.8b and 6.9b show the isodose distributions for a depth of 3.5 cm. In figures 6.8c and 6.9c dose profiles at an off-axis distance of 0.7 cm (through the middle of a leaf pair) and at depths of 3.5, 10 and 20 cm are compared. For all cases, measured and predicted dose distributions agreed within 2%, or within 0.2 cm in regions with a high dose gradient.

6.5 Conclusions

An iterative method for leaf trajectory calculation is described which takes into account transmission and collimator scatter, while avoiding tongue-and-groove underdosage effects. To achieve a maximum difference between optimized and realized fluence profiles of 0.1 MU for each point within the treatment field, generally less than 10 iterations are necessary, taking only a few seconds on a HP9000/C110 workstation. Absolute dose measurements show that the accuracy of our method for leaf trajectory calculation in combination with the dose calculation algorithm of the Cadplan 3D planning system is adequate for clinical application.

Chapter 7
**Testing of the stability of intensity modulated beams
generated with dynamic multileaf collimation,
applied to the MM50 Racetrack Microtron**

Adopted for the original manuscript by MLP Dirkx and BJM Heijmen, to be published
in *Med. Phys.* 27 (12), 2000.

7.1 Introduction

Treatment plans can often be significantly improved by applying intensity modulated X-ray fields, calculated by means of inverse treatment planning techniques [12,16,17,56,68,91,104,114,134,137,164,166-168]. Especially for concave shaped targets, the use of optimized beam profiles generally allows a closer conformation of the high dose region to the target volume, while reducing the dose in surrounding critical organs and normal structures. A flexible way of delivering intensity modulated beam profiles is dynamic multileaf collimation (DMLC) with the sliding window technique [29,40,135,138,147,158]. This technique is based on a continuous, independent and unidirectional movement of each leaf pair of a multileaf collimator (MLC) across the treatment field, while the beam is on. In the previous chapter a method for calculation of the required leaf trajectories to realize optimized intensity modulated beam profiles was presented. Using an iterative method, leaf transmission and collimator scatter were accounted for and tongue-and-groove underdosage effects could be fully avoided. For the MM50 Racetrack Microtron (Scanditronix Medical AB) it was demonstrated that measured absolute dose distributions resulting from the calculated leaf trajectories and dose distributions predicted with the dose calculation algorithm of the Cadplan 3D planning system (Varian) generally agreed within 2%, or 0.2 cm in regions with high dose gradients.

Before implementing DMLC in their clinical practice, Chui *et al* [28] and LoSasso *et al* [92] designed and conducted tests to examine the mechanical accuracy of a Varian multileaf collimator in DMLC mode and its impact on the dose delivery of intensity modulated beams realized with DMLC. As a final test before starting patient treatment with DMLC on our MM50 Racetrack Microtron, some of these tests were also performed. Complementary dosimetrical tests were performed to verify, (i) the long term stability of intensity modulated beam profiles, (ii) the stability of these profiles subject to gantry rotation, and (iii) the sensitivity of DMLC treatments to treatment interrupts, e.g. caused by an error detected by the treatment machine.

7.2 Methods and materials

7.2.1 Dynamic multileaf collimation at the MM50 Racetrack Microtron

The dual gantry MM50 Racetrack Microtron is equipped with a double focused multileaf collimator. Due to the scanning beam principle and the helium in the treatment head, the MLC can be used for shaping of both photon and electron beams

[46,71]. Projected at isocenter, the leaves have a width of 1.25 cm and a range of travel of 15.5 cm from the beam axis to 14 cm across it, yielding a maximum field size of 31x40 cm². Servomotors control the leaf movement. For each leaf the actual leaf position is derived from a potentiometer reading. Redundant readout is not available. The maximum leaf speed is 1 cm s⁻¹.

The MLC of the MM50 is calibrated by successively positioning the leaves at five positions (-14, -7, 0, 7 and 15 cm) using the light field, and storing the corresponding readouts of the potentiometers in a file. To position a leaf at an intermediate position, a linear interpolation between the stored calibration values is used. When setting up an MLC field, a driving command is sent by the MLC control system to the servomotor of each leaf. The actual readout of the corresponding potentiometers is used as a feedback for leaf positioning. Based on the setup of 1237 static fields, it has been demonstrated that the precision of the MLC control system in terms of static field definition is within 0.05 cm at 97% confidence level [108].

Arbitrary fluence profiles can be generated using dynamic multileaf collimation, which is fully integrated in the clinical treatment mode of the MM50. The profiles are generated with fixed doserates, which are the same as those used for static fields. The applied doserate is 3.3 MU s⁻¹ for the 10 MV photon beam and 5 MU s⁻¹ for the 25 MV beam. For DMLC, a treatment field is divided into a number of so-called subsegments. The first subsegment (start segment) defines the positions of the leaves when the irradiation is started, the last one (stop segment) defines their positions when the beam is turned off. Additional, intermediate subsegments are used to change the speed of the leaves during the irradiation. While the number of monitor units associated with a subsegment is delivered, each leaf moves with an appropriate constant velocity (cm/MU), calculated by the control system of the accelerator, to the position defined for the next subsegment. By definition, the number of monitor units for the stop segment is zero. During a DMLC treatment the leaf positions are verified every 0.08 seconds by comparing the actual values, measured with potentiometers, with the prescribed positions. In case for one of the leaves the deviation exceeds the preset tolerance level for more than a preselected number of subsequent measurements, the irradiation is stopped. These tolerance levels, which do not effect the leaf position accuracy, have been set to 0.2 cm and to 3 times, in order to avoid that a treatment is unnecessarily terminated in case a leaf position appears to deviate strongly from its prescribed position due to electronic spikes on the readout signal. For reasons of treatment time efficiency and potential hardware problems with the leaves during DMLC operation, 0.2 cm was also chosen as the leaf position tolerance for the Varian MLC at the Memorial Sloan-Kettering Cancer Center [92].

In addition to the leaf position verification every 0.08 seconds during a DMLC

delivery, the actual leaf positions and the number of monitor units delivered by the treatment unit are logged in a file every two seconds. By comparing these data with the prescribed leaf trajectories, the accuracy of the realized leaf positions at fixed times during the treatment can be assessed retrospectively.

The required leaf trajectories to realize an optimized intensity modulated beam profile by dynamic multileaf collimation are calculated using the algorithm that was described in the previous chapter, including leaf transmission and collimator scatter. A sliding window technique is applied in which the leaves are moving across the field from left to right. The leaf motions of adjacent leaf pairs are synchronized to avoid underdosage effects in the tongue-and-groove overlap [158]. The calculated leaf trajectories and corresponding monitor units are transferred to the MM50 by network and are stored in the patient database.

7.2.2 Stability of leaf positioning in DMLC mode

In DMLC mode the dose delivered in the treatment field is directly affected by the width of the sliding gap sweeping across the field. Recently, Budgell *et al* demonstrated that realization of intensity modulated beam profiles, calculated by inverse planning, using dynamic multileaf collimation, definitely requires a leaf position accuracy better than 1 mm, to avoid large dose errors, both in regions with relatively flat beam profiles and in regions with high dose gradients [20]. To verify the accuracy and stability of leaf positioning in the DMLC mode of the MM50 Racetrack Microtron, we implemented a quality assurance test as proposed by Chui *et al* [28]. In our version, a $0.1 \times 40 \text{ cm}^2$ slit beam was swept across the field. At 7 cm intervals, each leaf pair was forced to stop during 100 MU, yielding narrow hot spots. Film measurements were performed in a polystyrene phantom using the 25 MV photon beam. The films were positioned perpendicularly to the beam axis at the depth of dose maximum, at 100 cm from the focus. If the leaves were positioned correctly, film measurements would show straight dark lines at equal distances, on top of a light background. The accuracy of leaf positioning could be assessed within 0.05 cm by viewing the films on a light box. Smaller leaf positioning errors could be detected after scanning the films on a Lumiscan 75 laserdensitometer (Lumisys), using a spot size of 0.014 cm. A sensitometric curve, derived from films irradiated in a static $10 \times 10 \text{ cm}^2$ field with various numbers of monitor units, using the same experimental setup as described above, was applied to convert measured optical densities into doses.

The stability of gap widths was investigated by dose measurements in the center of a uniform $10 \times 10 \text{ cm}^2$ field that was delivered dynamically by sweeping a $0.4 \times 10 \text{ cm}^2$ slit

beam as proposed by LoSasso *et al* [92]. A NE 2571 ionization chamber was used, which was positioned at a depth of 5 cm in a polystyrene phantom. The source to surface distance was 100 cm. To correct for output variations (i.e. cGy/MU-ratio) of the accelerator in static fields, both in time and for different gantry angles, each measured dose value was divided by the dose measured in the center of the corresponding static 10x10 cm² field. Due to the narrow leaf gap used in this experiment, the measured dose was highly sensitive to the exact gap width; a deviation of only 0.01 cm would result in a dose difference of about 2.5% [92].

7.2.3 Long term dosimetric stability

Day-to-day variations in dose distributions realized with DMLC were assessed by performing dose measurements with an ionization chamber and with a SRI-100 electronic portal imaging device (EPID) for gantry angle 0°. The SRI-100 is a fluoroscopic system, basically consisting of a fluorescent screen, two mirrors and a CCD camera [1,163]. The CCD-chip consists of 512 x 256 pixels, with a pixel size projected at isocenter of about 0.05 x 0.08 cm². The distance from the focus to the fluorescent screen is 160 cm. For the 10 MV photon beam, measurements were performed at an effective depth of 2 cm and for the 25 MV beam at a depth of 2.5 cm [121]. The EPID has favorable characteristics for dosimetric applications: on-axis pixel values reproduce within 0.5% and, after correction for observed on-axis fluctuations, off-axis pixel values reproduce within 0.2% [38,59]. Except for verification and correction of the daily patient setup during a radiotherapy treatment, the EPID is used for dosimetric quality control measurements and in-vivo dosimetry in our institution [38,59,76,77,118,121-124].

In our present application, signals were integrated on the CCD chip during periods of 240 ms. The final image was derived by averaging 120 successive camera frames which were only corrected for dark current, measured just before irradiation started. Acquisition of 120 frames allowed full coverage of the beam-on time for the DMLC fields that were tested. The portal images were analyzed by calculating average pixel values in areas of 0.4x0.8 cm². Relative dose profiles were derived by normalizing these pixel values to the measured pixel value in a reference point in a relatively flat part of the beam profile. The dose in this reference point was measured with an ionization chamber positioned at the depth of maximum dose in a waterequivalent phantom. To enable a correction for day-to-day variations in the output (i.e. cGy/MU-ratio) of the accelerator, the dose in the center of a static 10x10 cm² field for 200 MU was measured as well.

7.2.4 Dosimetric stability under gantry rotation

To investigate the influence of gravity on delivered dose profiles, intensity modulated beam profiles were realized under different gantry angles. Relative dose profiles, normalized to a reference point, were measured using the SRI-100 (see previous subsection) and a linear diode array (Scanditronix Medical AB) attached to the collimator. The diode array consists of 11 p-type diodes with a spacing of 2.5 cm. For the measurements, a final resolution of 0.25 cm was achieved by moving the array and repeating the DMLC delivery ten times. The dose in the reference point was measured in a polystyrene phantom at the depth of maximum dose, using a NE 2571 ionization chamber.

7.2.5 Sensitivity to treatment interrupts

Generally, effects of acceleration and deceleration of the leaves are neglected in calculation methods to derive leaf trajectories required to generate optimized intensity modulated beam profiles [40,135,138,147]. If these effects are significant, deviations in dose profiles may be observed when during a DMLC treatment the leaf movement is forced to stop due to an interrupt by the treatment machine, and is restarted afterwards. To analyze these effects, films (Kodak XV), which were positioned perpendicularly to the beam axis in a polystyrene phantom at 5 cm depth, were irradiated. The source to surface distance was 100 cm. Measured optical densities were converted into doses by applying a sensitometric curve (see subsection 7.2.2 for more details). For this test a 2D intensity modulated beam profile was used with identical 1D fluence profiles for groups of five adjacent leaf pairs, allowing the effect of treatment interrupts to be analyzed carefully for different 1D beam profiles at the same time. In total 190 monitor units were delivered. To allow multiple fluctuations on each fluence profile, each treatment was interrupted manually three times and restarted afterwards. The films were normalized to the dose in the center of a flat profile, being one of the 1D fluence profiles. Measured dose profiles were compared with dose profiles for uninterrupted treatments.

7.3 Results and discussion

7.3.1 Stability of leaf positioning in DMLC mode

Figure 7.1 shows part of a film irradiated with the sweeping 0.1 cm wide slit beam. By viewing these films on a light box it was concluded that in an 80 days period the stability of leaf positioning was within 0.05 cm. During this period no recalibration of the leaves was necessary. Variations in optical density, e.g. visible in figure 7.1 at the bottom left, point at small differences (<0.05 cm) in gap widths related to the accuracy of leaf calibration. For these narrow slit beams, the measured optical density is highly dependent on the actual gap width, because the beam focus is partly blocked by the leaves, affecting the number of photons that can reach the film [40].

During a period of 80 days, dose measurements were performed in the center of a uniform 10x10 cm² field, as realized by sweeping a 0.4 cm wide slit beam across the treatment field, at gantry angle 0°. Measured dose values were corrected for the measured day-to-day dose variation in the center of the static 10x10 cm² field, and (arbitrarily) normalized to the average corrected dose in the 80 days study period. As shown in figure 7.2, the variation in dose was only 0.4% (1SD), pointing at an excellent stability of the gap width in time (<0.01 cm).

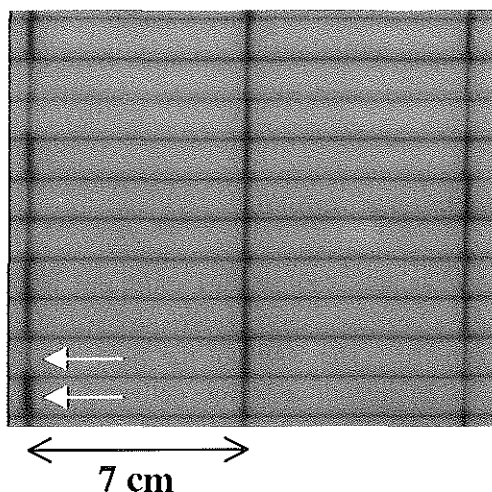


Figure 7.1

Part of a verification film used to study the accuracy of leaf positioning and gap widths. The arrows point at a line with a low optical density and a line with a high optical density, related to a slightly smaller and a slightly larger gap width than intended.

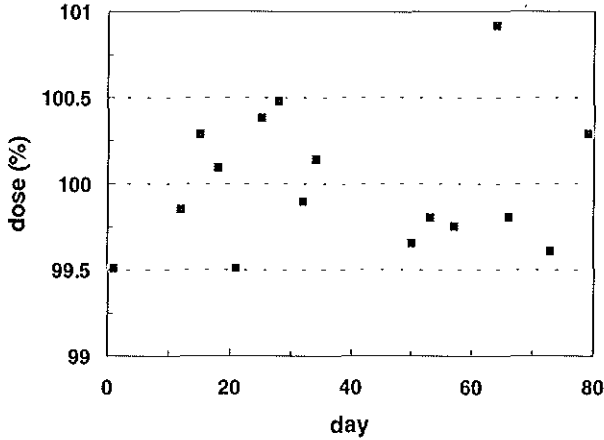


Figure 7.2 Stability of the dose in the center of a uniform $10 \times 10 \text{ cm}^2$ field, realized by scanning a $0.4 \times 10 \text{ cm}^2$ slit beam. The average measured dose in the 80 days study period was set to 100%.

Dose measurements in uniform $10 \times 10 \text{ cm}^2$ fields, realized with the sweeping 0.4 cm wide slit beam at gantry angles 0° , 90° , 180° and 270° , were used to investigate the variation in gap width subject to gantry rotation. After correction for the dose variation in the static $10 \times 10 \text{ cm}^2$ field subject to gantry rotation, a maximum dose difference between the four gantry angles of 2% was found in the field center, indicating that the variation in gap width subject to gantry rotation is less than 0.01 cm as well.

7.3.2 Long term dosimetric stability

The long term dosimetric stability was verified using one intensity modulated beam from a treatment plan for a prostate cancer patient, derived in a pre-clinical treatment planning study (see figure 7.3). The width of the field was 12 cm. To realize this intensity modulated field, 136 monitor units were delivered.

In figure 7.4, the long term stability of the dose in the reference point of the intensity modulated field (see figure 7.3), measured with the ionization chamber, is depicted, after correction for measured day-to-day dose variations in the center of a static $10 \times 10 \text{ cm}^2$ field and (arbitrarily) normalization to the average corrected dose in the 100 days study period. The results show a variation of only 0.2% (1 SD), which is within the accuracy of the measurements, indicating that the stability in dose for the DMLC treatment is similar to the variation in dose for a 'standard' treatment with a static field.

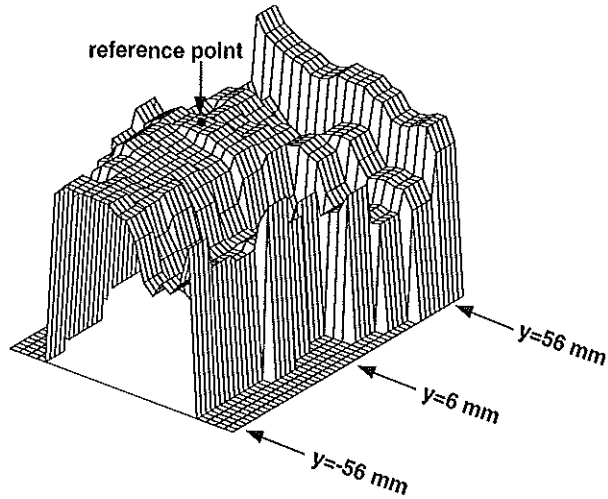


Figure 7.3 Optimized fluence profile for a patient with prostate cancer. To assess the long-term stability and gantry angle dependence of relative dose profiles, measured profiles were normalized to the dose in the indicated reference point. The arrows indicate the positions of the measured dose profiles depicted in figures 7.5 and 7.6.

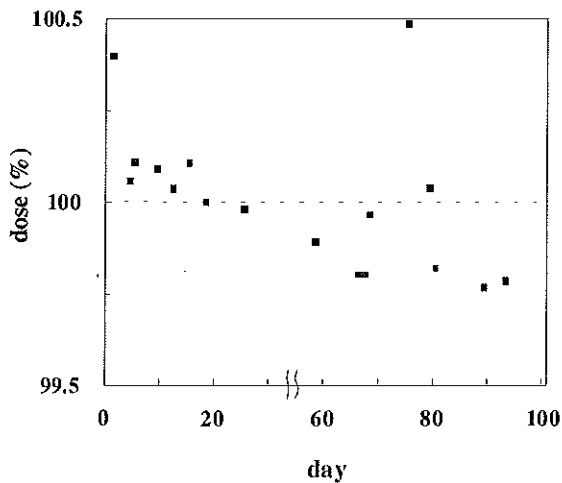


Figure 7.4 Long-term stability of the dose in the reference point indicated in figure 7.3. The average measured dose in the 100 days study period was set to 100%.

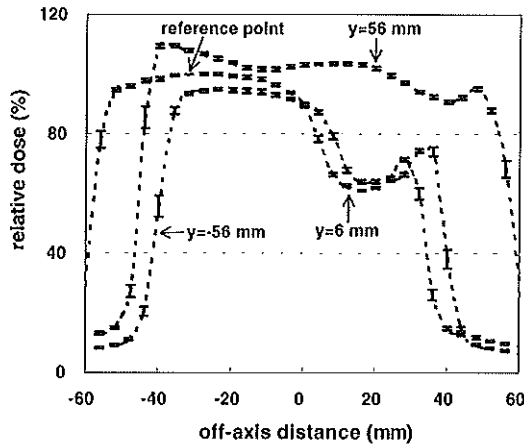


Figure 7.5 Long-term stability of dose profiles measured with the EPID and normalized to 100% in the reference point. The dashed lines show average profiles measured in the 100 days period at the three off-axis positions indicated by the arrows in figure 7.3. The error bars indicate the observed variations (± 1 SD).

In figure 7.5 average dose profiles ($N=17$) at three off-axis positions, measured with the EPID and normalized to 100% in the reference point, are depicted by dashed lines. The error bars indicate the observed variations (± 1 SD) in the 100 days study period. Apart from regions with very large dose gradients, the variations in the relative dose profiles were generally less than 1% (1 SD), which is similar to the variation in dose profiles observed during our daily dosimetric quality control measurements for static fields [38]. The larger dose variations at the field edges correspond to day-to-day variations in the measured beam penumbra of only ± 0.03 cm, which are likely due to small variations in the alignment of the EPID box with respect to the isocenter position.

7.3.3 Stability under gantry rotation

The stability of delivered dose profiles under gantry rotation was investigated for a wide range of fluence profiles using 10 and 25 MV photon beams. Both 1D model cases, i.e. with identical modulated profiles for all leaf pairs, and real 2D clinical cases were studied.

For all gantry angles, the dose in the reference point, as measured with the ionization

chamber, reproduced within 0.2% (1 SD) after correction for dose variations in the center of a static $10 \times 10 \text{ cm}^2$ field subject to gantry rotation. The smaller gantry angle dependence compared to the result mentioned in section 7.3.1 is related to the fact that, in contrast to that measurement, the sweeping leaf gaps were generally a few centimeters wide during DMLC delivery instead of 0.4 cm, reducing the impact of small deviations in the gap widths.

For the intensity modulated beam depicted in figure 7.3, the gantry angle dependence of the relative dose profiles (i.e. normalized at 100% in the reference point), measured with the EPID for a fixed collimator angle, is shown in figure 7.6. In this figure, the dashed lines show relative dose profiles measured at 0° gantry angle. Each error bar indicates the maximum of the local differences between the relative dose values measured at 90° , 180° and 270° and the corresponding dose value measured at 0° . Although no corrections were made for the potential gantry angle dependency of the beam profiles of corresponding static fields in this analysis, maximum deviations from gantry angle 0° of less than 1% were generally observed, apart from regions with large dose gradients. Therefore, the influence of gravity on dose profiles delivered with DMLC should be less than 1%. Similar results were derived from the measurements with the linear diode array.

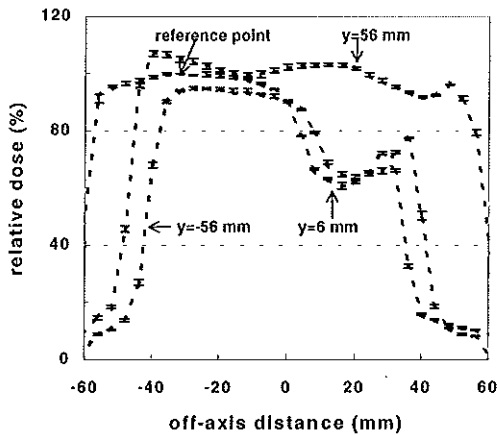


Figure 7.6 Stability of the delivered dose profiles under gantry rotation after normalization to 100% in the reference point. The dashed lines show profiles for gantry angle 0° at the three off-axis positions, indicated by the arrows in figure 7.3. The error bars show the maximum local deviations with respect to these curves for gantry angles 90° , 180° and 270° .

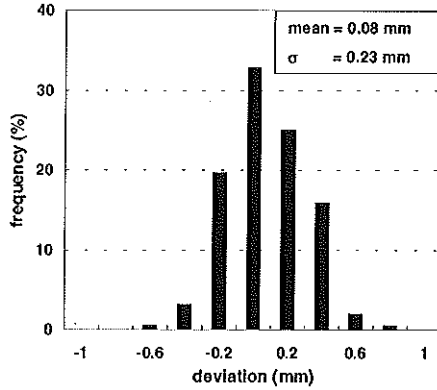


Figure 7.7 Frequency histogram of the observed deviations between the realized leaf positions as stored in the log file and the prescribed leaf positions when realizing the fluence profile indicated in figure 7.3 at gantry angle 0°.

For a DMLC treatment at gantry angle 0°, figure 7.7 shows a frequency histogram of the detected deviations between the actual leaf positions as stored in the log file and the prescribed leaf positions. On average the leaves were positioned correctly within 0.01 cm, while the deviations from the prescribed positions were only 0.023 cm (1 SD). When delivering this DMLC treatment at gantry angle 90° (with all leaves traveling in the direction of gravity) or 180°, similar deviations were observed. Only at gantry angle 270°, for which all leaves were traveling against gravity, an average shift of 0.03 cm was observed with respect to the results in figure 7.7, showing that on average the leaves were traveling with a small time delay. As shown before in subsection 7.3.1, the gap width did not change significantly under gantry rotation, indicating that the deviation in leaf positioning is similar for both the left and the right leaves when traveling against gravity. As a result, the (rather small) deviations did not affect the dose profiles delivered with DMLC, as was also demonstrated by the results in figure 7.6. After rotation of the collimator angle by 180°, similar deviations as for gantry angle 270° were also observed for gantry angle 90°.

7.3.4 Sensitivity to treatment interrupts

In figures 7.8a and 7.8b dose profiles measured during an uninterrupted DMLC treatment are depicted, after normalization to the dose in the center of the flat profile

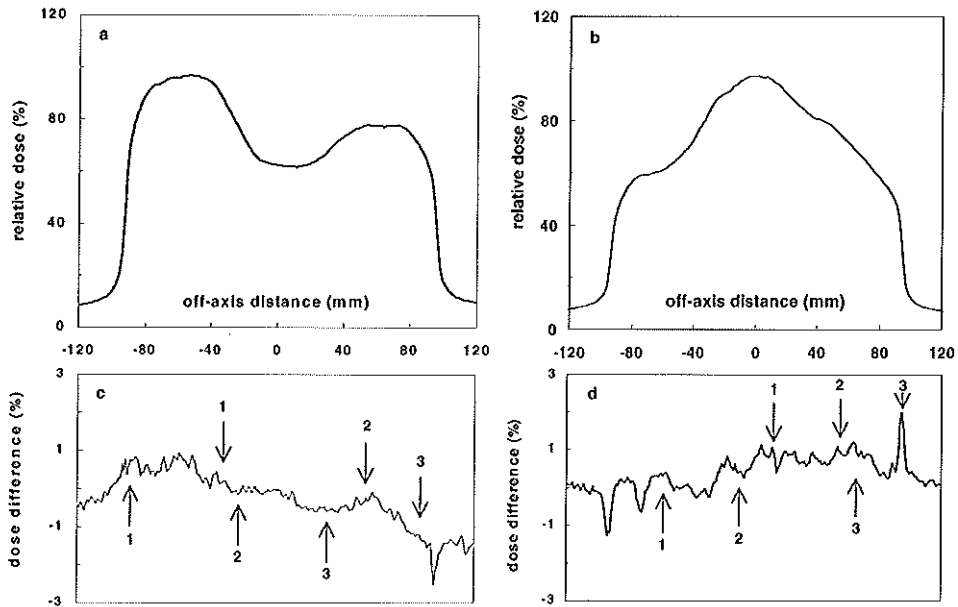


Figure 7.8 *a/b* Dose profiles measured for an uninterrupted treatment.
c/d Measured dose differences between an uninterrupted treatment and a treatment during which the leaves were forced to stop three times due to (manual) interrupts. The arrows 1-3 indicate the positions where the right and left leaves were forced to stop. Figure c corresponds to figure a and figure d to figure b.

(not depicted). The results were compared with profiles measured during treatments in which the leaves were forced to stop three times due to (manual) interrupts. In figure 7.8c and 7.8d dose differences with respect to the corresponding uninterrupted treatment are depicted. Apart from regions with a steep dose gradient, these differences were generally less than $\pm 1\%$, which is within the uncertainty of the film measurements. Even when leaves were traveling at maximum leaf speed at the time of treatment interrupt, increased deviations with respect to the uninterrupted treatment were not observed, indicating that deceleration and acceleration of the leaves have a negligible influence on the realized fluence profiles at the MM50, as was also concluded before by Spirou and Chui [135]. The results also demonstrate that a DMLC treatment can be completed correctly after an interrupt by the control system of the treatment machine has occurred.

7.4 Conclusions

The results described in the present and the previous chapters show that the accuracy and stability of leaf positioning in DMLC mode and the dosimetric accuracy and stability of intensity modulated beams, generated at the MM50 by means of dynamic multileaf collimation, is adequate for clinical introduction. Clinical application of DMLC for head and neck cancer patients and prostate cancer patients has recently started. As part of our quality control program, a method for pretreatment verification of the absolute beam fluence profiles for all treatment fields of a patient has been developed using our portal imaging device [77]. The procedure, which is described in the next chapter, simultaneously verifies the mechanical and dosimetric performance of the treatment unit, the calculation of the dose distribution by the treatment planning system, which results from derived leaf trajectories, and the correct transfer of the leaf-sequencing file to the treatment machine. In the near future an on-line, independent verification of the realized leaf trajectories will be implemented which derives the actual leaf positions in each camera frame acquired during the treatment and, in combination with the number of delivered monitor units, calculates the differences with respect to the prescribed leaf positions [5,118].

Chapter 8
**Dosimetric verification of intensity modulated beams produced
with dynamic multileaf collimation using an electronic portal
imaging device**

Adopted from the original article by KL Pasma, MLP Dirkx, M Kroonwijk, AG Visser
and BJM Heijmen, published in *Med. Phys.* 26: 2373-2378, 1999.

8.1 Introduction

Dose distributions delivered by multiple field irradiation techniques can often be significantly improved by modulating the two-dimensional intensity profile of the individual x-ray beams [12,16,17,56,68,91,104,114,134,137,164,166-168]. One technique to realize intensity modulated (IM) beam profiles, calculated by means of inverse treatment planning, is the use of dynamic multileaf collimation (DMLC) applying the 'sliding window' technique [29,40,135,138,147,158]. For this technique an algorithm for calculating the required leaf trajectories was presented in chapter 6. In 1995 the first group of patients was irradiated using DMLC at Memorial Sloan-Kettering Cancer Center, NY [86]. Recently, treatment of head and neck cancer patients with DMLC has also started in our clinic.

A disadvantage of the dynamic technique is that it is difficult to verify due to its complexity. Bortfeld *et al* have therefore proposed to produce intensity modulated beams by superpositioning a number of partially overlapping, static, irregularly shaped fields produced with the MLC [13]. Controlling the delivery of a sequence of small doses and static leaf settings was considered to be a straightforward extension of existing linear accelerator control. However, compared to DMLC generally longer treatment times are required for the static technique.

For verification of segmented beam delivery Curtin-Savard and Podgorsak proposed the use of the scanning liquid ionization chamber EPID [32]. Without a patient in the beam, portal images were acquired for each subfield of the leaf sequence and converted into a dose rate distribution. Subsequently, the images were converted into absolute dose distributions by multiplication with the corresponding monitor unit setting. Finally, the individual dose distributions were summed to produce a dose distribution at the measurement depth. These distributions were then compared with dose distributions predicted by a treatment planning system. Because of the use of the monitor unit setting, the comparison with the dose distribution of the treatment planning system is basically a verification of the relative dose distribution. The applied EPID is relatively slow in returning to its initial state. Therefore, a 60 s rest interval between measurement of subsequent segments had to be applied, yielding long overall measurement times of typically one hour. Due to the scanned signal readout and the measurement of dose rate instead of dose, the applied EPID is not suitable for high precision dosimetric verification of DMLC.

To test the reproducibility and accuracy of DMLC, the use of film has been reported [90,92,164]. At Memorial Sloan-Kettering Cancer Center film dosimetry is performed in a flat homogeneous phantom for each field prior to the first treatment. Measured dose distributions are compared with corresponding calculated dose distributions [92].

A disadvantage of film dosimetry is that it is time consuming since it requires developing and scanning of the film. Moreover, a sensitometric curve is needed to convert optical densities into doses.

CCD camera based EPIDs are a promising tool for verification of DMLC due to their high data acquisition rate and capability to measure simultaneously in all points of the treatment field [5,100,121,118]. Balter *et al* showed preliminary results of a method to derive leaf positions in each camera frame acquired during treatment delivery and to compare them with a table of prescribed leaf positions [5]. Leaf positions could be determined with an accuracy of 0.6 mm and a duty cycle of less than 1 s. A similar approach was implemented by Partridge *et al* [118]. They used a custom made EPID with image acquisition synchronized to the accelerator magnetron current pulse production, with one CCD camera frame acquired per accelerator pulse. Data were presented for a 6 MV beams. The accuracy of the leaf position measurements was 2 mm. Due to a limitation of the camera triggering hardware, the pulse rate of the linac had to be reduced. Ma *et al* calculated normalized reference images from MLC leaf sequencing files and compared these with normalized images measured with a fluoroscopic beam imaging system (BIS, Wellhöfer Dosimetrie, Schwarzenbruck, Germany) for a 6 MV photon beam [100]. This imaging system can be fastened to the blocking tray holder of a linear accelerator. It was especially designed for quality control tasks. For calculation of the reference image a measured portal image of a large open field was used. The reference image was therefore not only related to the prescribed fluence, but also contained optical distortions in the EPID system. A global correlation coefficient was used to compare the calculated reference image with the image measured with the BIS. This method can be used to verify whether leaf sequencing files have been transferred correctly to the linac control computer and whether the treatment can be correctly executed without machine faults. Transmission through the leaves (both intraleaf and interleaf) was not taken into account and a simple empirical method was used to model extrafocal scatter. Despite these limitations, they concluded that it was possible to detect uncertainties of less than 0.05 cm in leaf positioning during DMLC.

The above described methods to verify leaf motion cannot be used to check whether the calculated leaf trajectories do indeed generate the *absolute* beam fluence profiles used in treatment planning. In this paper a new method is presented for a pre-treatment verification of these absolute beam fluence profiles utilizing a commercially available CCD camera based fluoroscopic EPID. In the absence of the patient EPID images are acquired for all beams produced with DMLC. These images are then converted into two-dimensional dose distributions and compared with calculated dose distributions. The calculations are performed with a pencil beam algorithm as implemented in a

commercially available treatment planning system using the same absolute beam fluence profiles as used in the treatment planning system for calculation of the patient dose distributions. In this paper results are presented for intensity modulated 10 and 25 MV photon beams; both model cases and real clinical cases were studied. Absolute dose profiles measured with the EPID were also compared with ionization chamber measurements. Preliminary results on measurements of absolute dose distributions in IM fields produced with DMLC have been reported [121].

8.2 Materials and methods

8.2.1 EPID and ionization chamber dose measurements

The applied EPID is a Philips SRI-100 (Philips Medical Systems), which basically consists of a fluorescent screen, two mirrors and a CCD camera. The fluorescent screen is a 1.65 mm thick stainless steel plate coated with a layer of gadolinium oxysulphide. To reduce the detection of high-energy electrons generated in patients, an extra 1 mm thick stainless steel slab has been mounted on the standard fluorescent screen [121]. The added slab hardly affects the image quality [76]. The acquired images may be used both for set-up verification and for *in vivo* dosimetry [77,123]. The EPID has a fixed focus to fluorescent screen distance of 160 cm. Technical details of the EPID have been described by Visser *et al* and Althof *et al* [1,163].

Image acquisition is performed with a procedure written in the macro command language that comes with the system. The integration time on the CCD chip was set to 240 ms and 120 camera frames were accumulated in the frame store memory. The read out time needed to transmit a frame from the CCD to the frame grabber (during which no signal is accumulated) is 80 ms. The final image is the mean of the integrated camera frames, corrected for the dark current measured prior to the irradiation. In the original procedure image acquisition starts automatically when the measured pixel values in the center of the camera frame exceed a threshold, i.e. when the beam is switched on. For the DMLC measurements described in this paper, image acquisition was started manually, since the leaves block the pixels in the center of the image at the start of the irradiation, when using the sliding window technique. The procedure was discussed in detail by Pasma *et al* [121].

Due to sagging of the EPID structure, the field center can shift slightly. To correct the image for this shift, the position of the field center was derived using the position of the field borders in an EPID image of a (static) square field and was stored in a lookup table. Raw EPID images of 512x256 pixels were then resampled to arrays of 64x64

elements; each element represents a region of interest with an area of $0.5 \times 0.5 \text{ cm}^2$ projected at isocenter. Conversion of these arrays into absolute dose distributions was performed in three steps. Acquired images were first corrected for the non-linear response of the system [118,121]. Subsequently, the image was corrected for the optical 'cross talk' by deconvolving it with a point spread function [59,121]. Finally, the resulting array was divided by an array that accounts for relative EPID sensitivity [121]. The system was calibrated once. The observed day-to-day variation of the EPID response per unit of delivered dose is 0.4% (1σ) [122]. Due to radiation damage to the CCD chip the EPID response gradually decreases ($\sim 3\%$ /year) [123]. This decrease was carefully monitored and corrected for by using the daily acquired images for the quality control of the absolute output and field flatness of the scanning photon beams of the MM50 (see chapter 2) and the two weekly output checks with an ionization chamber.

Dose measurements were also performed with a N31002 ionization chamber (PTW, Freiburg, Germany). The ionization chamber was inserted in a polystyrene mini-phantom [118] at a depth of 2.0 cm for the 10 MV beam and at 2.5 cm for the 25 MV beam. For those depths, it was experimentally found that the variations in the on-axis response of the EPID (EPID pixel value/portal dose measured with the ionization chamber) were minimal for field sizes ranging from 3×3 up to $18 \times 18 \text{ cm}^2$ and polystyrene absorber thicknesses ranging from 0 up to 35 cm. For a 25 MV photon beam the mean of the standard deviations of the EPID response for all field sizes was 0.4% [121]. The mini-phantom was scanned in an empty RFA-300 water phantom (Scanditronix Medical AB) with the center of the ionization chamber positioned at a distance of 160 cm from the focus, which is equal to the fixed focus to fluorescent screen distance of the EPID.

8.2.2 Calculation of the dose distribution at the detector

Starting point for the calculation of the dose distribution at the fluorescent screen of the detector is the optimized beam fluence $F_{\text{opt}}(x, y)$ (in MU) to be delivered at positions (x, y) , which is the result of a computer optimization or inverse treatment planning. Using the iterative algorithm described chapter 6, leaf trajectories are then calculated, taking into account collimator scatter and the effective leaf transmission, which is the sum of the transmission through the leaves and the extra focal radiation under the moving leaves, and avoiding tongue-and-groove underdage effects [158]. Generally less than 10 iterations are necessary to minimize the difference between the optimized fluence profiles $F_{\text{opt}}(x,y)$ and the realized fluence profiles $F(x,y)$, which are used for calculation of the final dose distribution in the patient with the CadPlan 3D treatment

planning system (Varian-Dosetek).

The expected absolute dose distribution in the plane of the fluorescent screen of the EPID in absent of a patient, $D_{p,0}(x,y)$, is calculated from the realized fluence profile using the pencil beam algorithm as implemented in the CadPlan treatment planning system [140,142]. In the current implementation (CadPlan v2.7.9) the penumbra width is a linear function of the SSD. As a result, the predicted dose distributions would become inaccurate for the SSD of the detector (160 cm), which is much larger than the SSDs clinically used. Therefore, the dose distribution is calculated at 100 cm from the focus by enlarging the field with a factor of 1.6 (160/100). The dose distribution is then normalized using the calculated on axis dose in a static 16x16 cm² field for 150 MU. Finally, the absolute dose distribution is calculated using the measured cGy/MU value at the detector for a 10x10 cm² field. Dose calculations and the calibration measurement are performed at a water depth of 2 cm for the 10 MV photon beam, and at a depth of 2.5 cm for the 25 MV beam, equal to the effective measuring depths of the EPID, as discussed in section 8.2.1.

8.2.3 Realization and verification of fluence profiles

Measured and predicted dose distributions $D_{p,0}(x,y)$ were compared for the 10 and 25 MV photon beams of the MM50 Racetrack Microtron. For the 10MV beam the dose rate was 200 MU min⁻¹ and for the 25MV beam 300 MU min⁻¹. The microtron produces 200 radiation pulses per second. For all measurements the leaves moved from left to right parallel to the x-axis.

The developed method was tested for a range of fluence profiles; both model cases and real clinical cases were studied. Calculated absolute dose distributions (section 8.2.2) were compared with dose distributions derived from EPID images (section 8.2.1) and with dose profiles measured with an ionization chamber. The axes for comparisons in the leaf direction were chosen at the center of each leaf pair ($y = \pm 0.6, \pm 1.9, \pm 3.1, \dots$). Throughout the paper positions and distances are defined at the plane normal to the beam axis at 100 cm from the focus. The reported differences are the mean deviation in percent and the corresponding standard deviation in percent (i.e. mean $\pm 1 \sigma$).

8.3 Results

In figures 8.1 and 8.2 data are presented for intensity modulated 10 MV beams. Within the treatment field the leaf trajectories were identical for all leaf pairs; the presented data are for $y=0.6$ cm. Outside the penumbra region, both beams show an excellent agreement between EPID and ionization chamber measurements; the difference is only $0.3\pm 0.6\%$ (figure 8.1) and $0.1\pm 0.8\%$ (figure 8.2). The actual agreement may even be slightly better, since each ionization chamber measurement required the complete irradiation to be repeated.

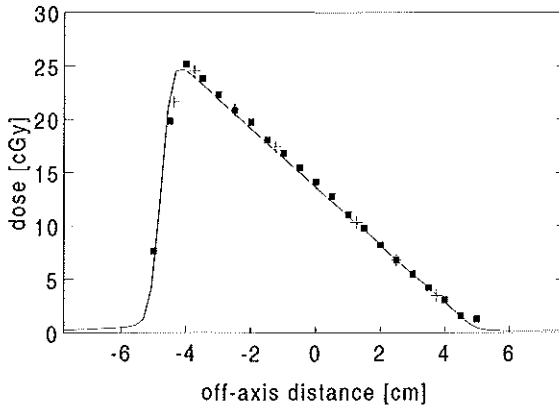


Figure 8.1 Predicted (line) and measured absolute dose profile (■ EPID, + ionization chamber) along the $y=0.6$ cm axis for a wedge profile produced with DMLC using the 10 MV photon beam.

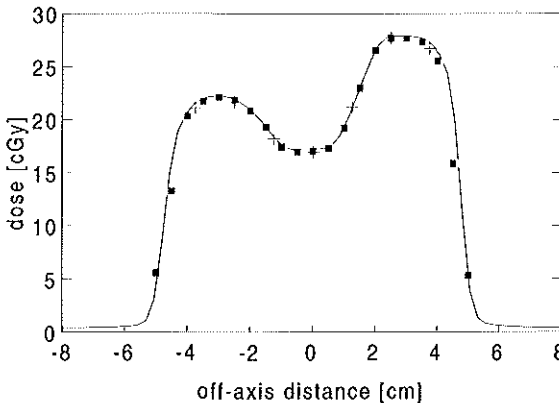


Figure 8.2 Predicted (line) and measured absolute dose profile (■ EPID, + ionization chamber) along the $y=0.6$ cm axis for an IM 10 MV photon

As concluded in the previous chapter, the short-term reproducibility of the absolute dose delivery with DMLC at the MM50 Racetrack Microtron is 0.2%. The deviations between the calculated dose profile and the profile measured with the EPID are $-2.1 \pm 1.2\%$ and $0.9 \pm 0.8\%$, respectively.

The data presented in figure 8.3 are for a beam fluence profile that was also used to generate the data in figure 8.2, but now was realized with the 25 MV beam. Again deviations between EPID and ionization chamber measurements are small: $0.2 \pm 1.3\%$. The deviation between the predicted dose profile and the profile measured with the EPID is $-1.0 \pm 0.7\%$. Similar results were found for the profile presented in figure 8.4: $0.2 \pm 1.0\%$ and $-1.0 \pm 1.4\%$ respectively.

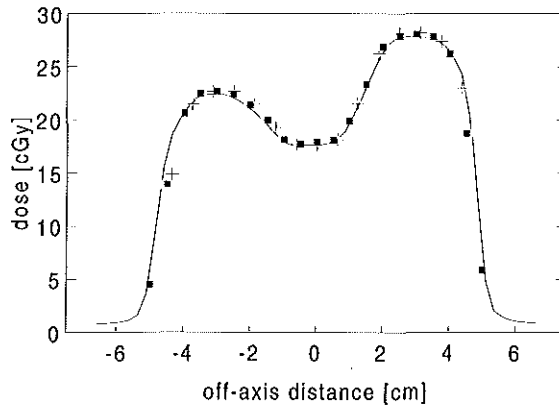


Figure 8.3 Predicted (line) and measured absolute dose profile (■ EPID, + ionization chamber) along the $y=0.6$ cm axis for an IM 25 MV beam.

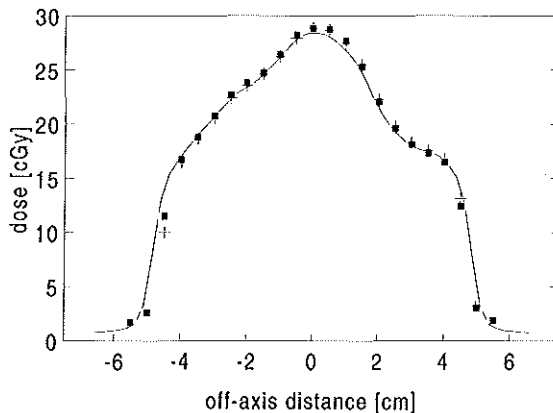


Figure 8.4 Predicted (line) and measured absolute dose profile (■ EPID, + ionization chamber) along the $y=0.6$ cm axis for an IM 25 MV beam.

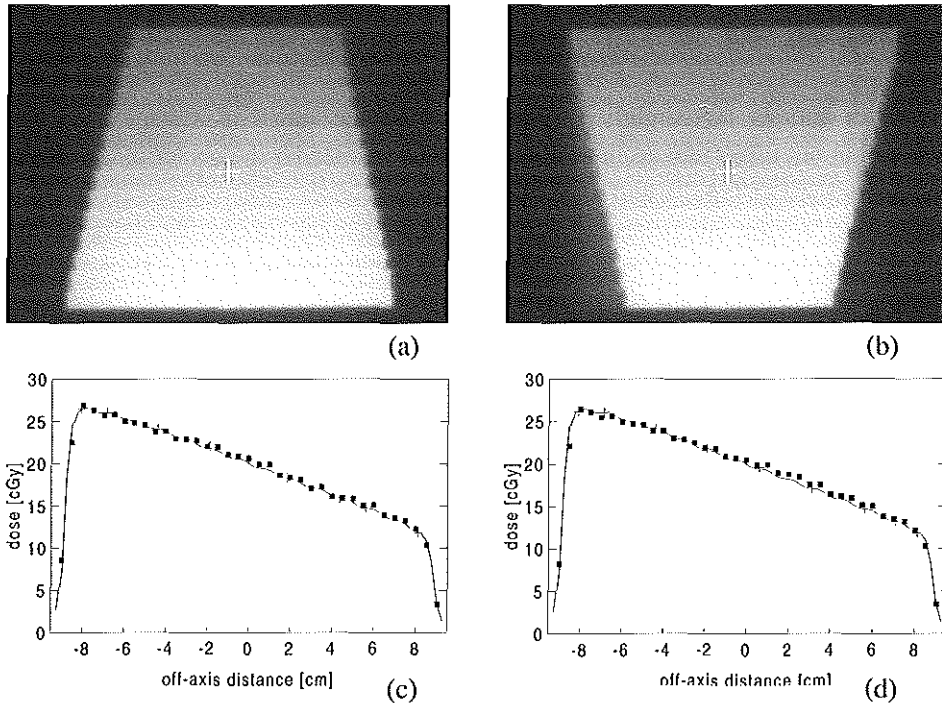


Figure 8.5 Raw EPID images of IM 25 MV photon beams are shown in (a) and (b). In (c) and (d) the corresponding measured (■ EPID, + ionization chamber) and predicted (line) absolute dose profiles along the y-axis (perpendicular to the axis along which the leaves move) are shown.

In figures 8.5a and b acquired EPID images (512x256 pixels) for two non-square IM 25 MV beams are shown. The fluence decreases in the y-direction; the dose at the top of the image is a factor of 2.2 lower than at the bottom. Due to the synchronization of leaf trajectories of adjacent leaves, underdosage (lower pixel values) do not occur in the overlap regions [158]. The small overdosage (higher pixel values) in the overlap regions of adjacent leaves are due to the interleaf leakage of about 2% (see section 6.4.3). These overdosages can be avoided using partial synchronization [169].

Figures 8.5c and d show cross sections along the y-axis (normal to the axis along which the leaves move) of the two-dimensional dose profile derived from the EPID images shown in figures 8.5a and b respectively. Corresponding predicted dose profiles and dose profiles measured with an ionization chamber are included. For the first field (figure 8.5a) the deviation between EPID and ionization chamber measurements was

$0.2 \pm 1.1\%$ and for the second field (figure 8.5b) $0.4 \pm 2.0\%$. The deviations between the predicted profile and the EPID measurements were $-0.9 \pm 1.7\%$ and $-1.4 \pm 1.7\%$, respectively.

Standard deviations are slightly increased due to the interleaf leakage that was measured but not taken into account in the calculations. Under the center of the leaves the deviations are $-0.7 \pm 1.2\%$ and $-0.4 \pm 1.6\%$, respectively.

In figure 8.6 results are presented for a two-dimensional IM profile designed for treatment of a prostate cancer patient. The deviation between the predicted profile and the profile measured with the EPID is $0.5 \pm 1.1\%$.

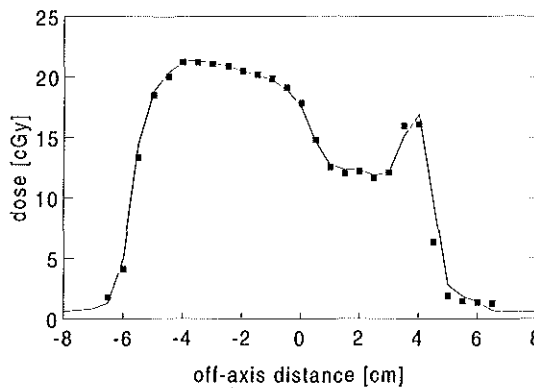


Figure 8.6 Predicted (line) and with the EPID measured (■) absolute dose profile along the $y = -1.9$ cm axis of a lateral IM 25 MV photon beam for a prostate cancer patient.

8.4 Discussion and conclusions

A procedure for pre-treatment verification of absolute beam fluence profiles realized with DMLC was developed and tested. The time required to verify an IM beam is about two minutes, which is much shorter than any other dosimetric technique. The EPID system only has to be calibrated once. The agreement between calculations and EPID measurements and between EPID and ionization chamber measurements was within 2% (1σ). The procedure allows an overall verification of (i) the calculation of the final dose distribution, corresponding to the calculated leaf trajectories (including the models to incorporate collimator scatter and leaf transmission), (ii) the correct transfer of the leaf sequencing file to the treatment machine and (iii) the mechanical

and dosimetric performance of the treatment unit. It is not always possible to distinguish between these types of errors using only portal images. Previously published DMLC verification methods with EPIDs only verified leaf motion [5,118] or relative dose profiles [100]. The excellent agreement between our EPID and ionization chamber measurements in all cases shows that the read out time of 80 ms (during which no signal is collected) has no detectable effect; the data acquisition rate is sufficiently high [100].

In the near future the developed method will be extended to enable verification of DMLC during patient treatment. Acquisition of portal images suitable for dosimetric verification of DMLC can be fully integrated into existing imaging routines for patient set-up verification, without introducing an increase in the overall treatment time [77]. Preliminary results on measurements of portal dose images (PDI), i.e. the dose distribution behind a patient in a plane normal to the beam axis, in an IM beam have been reported [121]. The calculation of a PDI for a patient irradiated with an IM beam is a relatively simple extension of existing methods [120]. The relation is $D_p(x,y)=D_{p,0}(x,y) \cdot T(x,y)$, with $D_p(x,y)$ the predicted portal dose at position (x,y) beneath the patient, $D_{p,0}(x,y)$ the predicted portal dose in absence of the patient (as described in section 8.2.2), and $T(x,y)$ the predicted transmission through the patient using the planning CT-data. [123]. A potential problem is to distinguish between deviations in predicted and measured PDIs due to machine faults and differences due to deviations between the patient anatomy during acquisition of the planning CT scan and during treatment delivery. For prostate cancer patients we have observed that deviations in patient anatomy introduce large local differences between predicted and measured PDIs [77]. Machine faults are likely to produce a constant difference over the whole irradiation field. In case of malfunctioning of a single leaf, the difference will be limited to the beam's eye view of that leaf.

Chapter 9
General discussion

9.1 Introduction

The main objective of this thesis was the development and clinical implementation of intensity modulated treatment techniques using a multileaf collimator. Secondly, fast methods for dosimetrical quality control of (i) intensity modulated treatment fields, and (ii) an advanced treatment unit like the MM50 were developed, which were based on measurements with an electronic portal imaging device (EPID).

In this section, the clinical application of different techniques for delivery of intensity modulated beams using a multileaf collimator will shortly be reviewed and advantages and disadvantages will be summarized. Next, the impact of treatment uncertainties in intensity modulated radiotherapy (IMRT) will be discussed in more detail. Finally, the issue of dosimetrical quality control of IMRT will be addressed.

9.2 Clinical implementation of IMRT techniques using a multileaf collimator

9.2.1 *Static intensity modulation techniques*

The use of static intensity modulation does not necessarily require inverse treatment planning; improved treatment plans may also be achieved by using forward planning. Examples have been described in chapter 3 and 4 of this thesis. At the University of Michigan, the use of static intensity modulated treatment techniques based on forward planning started already in 1994. In their treatment planning system UmPlan, special tools for defining segments within a treatment field were implemented in order to achieve a homogeneous dose distribution in the target volume [50]. For each treatment field, generally only small numbers of additional segments (1 or 2) were required, thereby minimally increasing the treatment delivery complexity and treatment time. They have implemented multi-segmented intensity modulation for nearly all tumor sites, including prostate, liver, abdomen, lung, breast and chest wall, head and neck and brain [44,50]. They use this technique in dose escalation studies, e.g. for patients with a brain tumor in which the dose to the central part of the tumor volume (GTV+0.5 cm margin) has step-wise been increased from 70 to 100 Gy, without increasing the dose to the outer part of the planning target volume and the surrounding normal brain tissue [150,162]. A similar technique of static beam intensity modulation has also been implemented by Pickett *et al* to escalate the dose to regions inside the prostate with tumor cells, as defined by the combined use of magnetic resonance imaging (MRI) and magnetic resonance spectroscopy (MRS), to 90 Gy, without increasing the dose to the

rectum and the bladder [126].

Another approach for implementing segmented intensity modulation by means of forward planning techniques has been developed by de Neve *et al* for various tumor sites [36,37]. For treatment of tumors with a similar geometry and anatomical location they defined class solutions, describing the beam parameters, penumbra margins and segmentation rules to be used for plan optimization. Segments were designed based on the patient anatomy, thereby increasing the number of segments in the vicinity of the projection of sensitive structures. Recently, automatic optimization tools have been developed to assign weights to individual beam segments using a biophysical object function [34].

Clinical introduction of step and shoot techniques based on inverse planning started only a few years ago. At this time this technique is used for different tumor sites at a limited number of centers around the world, like in Heidelberg [127] and San Francisco [160].

9.2.2 *Dynamic intensity modulation*

Clinical application of dynamic multileaf collimation for realization of intensity modulated fields started in 1995 at Memorial Sloan-Kettering Cancer Center, NY at a Varian accelerator. Originally they used the technique in their dose escalation study for prostate cancer patients [90,179], but in the meantime the application has been extended to other tumor sites, like primary nasopharynx cancer [61]. In our clinic dynamic multileaf collimation was introduced clinically in 1999 for treatment of head and neck cancer patients at the MM50 Racetrack Microtron, replacing compensators, which were used before [155]. Recently, we have implemented this technique for treatment of prostate cancer patients as well, using the inverse planning module Helios in our treatment planning system Cadplan for calculation of optimized fluence profiles.

9.2.3 *Rotational intensity modulation techniques*

Clinical application of the Peacock MiMiC started in Houston in 1994 [55]. Since then, the system has been introduced in many other institutes, especially in the United States. Till now only one system has been installed in Europe, at the University Hospital of Brussels [159]. The system is especially suited for treatment of patients with brain and head and neck cancer, but other tumor sites like prostate cancer have been treated as well [55].

Last year, the clinical use of intensity modulated arc therapy (IMAT) using a multileaf collimator has been started at the University of Maryland Medical School for treatment of patients with head and neck cancer [178].

9.2.4 Comparison of techniques for intensity modulation with a MLC

Each of the different techniques described before has advantages and disadvantages. Compared to dynamic multileaf collimation, static intensity modulation is often assumed to be implemented more easily and safely in clinical practice, considering it a straightforward extension of the use of the multileaf collimator as a static beam shaping device. But static multileaf collimation generally requires longer treatment times, because the beam is interrupted during the set-up of the different MLC segments. To reduce the overall treatment times for the step-and-shoot technique, improvements have recently been made in accelerator design by several manufactures, allowing a faster set-up and verification of succeeding subfields, taking a few seconds only. However, to reach acceptable treatment times it still remains important to limit the number of segments for each treatment field, yielding a resolution limitation.

Compared to static intensity modulation, optimized intensity modulated fields can often be realized more precise by using dynamic multileaf collimation, especially when the optimized fluence profiles have steep dose gradients. It is still under debate whether this is clinically relevant or not. In a treatment planning study for different brain tumors, Keller *et al* [72] showed that differences in the final dose distribution were only very small when realizing each treatment field by dynamic multileaf collimation or by the superpositioning of 5 to 7 static beam segments.

For static intensity modulation, leaf-sequencing algorithms may yield very small beam segments or segments with isolated leaf openings. To achieve accurate dose delivery, this puts high demands on the mechanical accuracy of the MLC, on the applied dose calculation algorithms and on models to include collimator scatter effects. For dynamic multileaf collimation this problem may be avoided to a large extend by synchronizing the leaf trajectories [158,169]), which also avoids tongue-and-groove underdosage effects.

Compared to static and dynamic intensity modulation with a limited number of beam angles, rotational intensity modulation techniques are often capable in producing superior dose distributions [160], because they offer a higher degree of freedom to avoid sensitive structures by spreading out the dose over other normal structures. However, due to the slice-by-slice approach, intensity modulation with the Peacock MiMic generally requires much longer treatment times compared to static and dynamic

intensity modulation techniques. Moreover, slice-by-slice intensity modulated beam delivery, as with the Peacock MiMic, is very sensitive to patient movements during the treatment. Small patient movements of only 1 mm can already result in errors in the delivered dose of 25% or more [23,96]. These disadvantages do not apply to IMAT. Because most of the target will be in the beam while rotating the gantry, treatment delivery with IMAT is rather efficient. For most clinical sites, an optimal treatment requires less than five arc rotations, making the delivery time of IMAT comparable to the time required for conventional treatment techniques [15,178]. Moreover, the patient does not need to be moved during the treatment, avoiding the problem of beam abutment between slices and the risk of under- or overdosages related to that. Finally, IMAT can be implemented on an existing linear accelerator with an MLC, without requiring additional hardware.

9.3 Impact of treatment uncertainties in IMRT

In chapters 3 and 4 a BIM technique was presented for penumbra enhancement around the superior and inferior field edges. Sharper beam penumbræ were realized by delivering additional beam fluence in the most superior and inferior parts of the treatment field. Similarly, inverse treatment planning techniques often yields optimized fluence profiles with increased fluence levels at the edges of the treatment field and close to the projection of sensitive structures. Due to the sharper beam penumbræ, smaller penumbra margins may be applied for definition of the treatment fields, yielding a reduced dose delivery to surrounding normal tissues. As a result, the use of intensity modulation allows for a (further) reduction in the risk of side effects for several tumor sites and for dose escalation in the treatment of others. However, to avoid geometrical misses of the target volume, the smaller treatment fields put higher demands on the accuracy of the definition of the GTV and the CTV and the inclusions of adequate margins between the CTV and the PTV to account for patient set-up inaccuracies and internal organ motion [62].

9.3.1 Delineation of the target volume

A CT scan is still generally used for definition of the target volume. However, due to insufficient visibility and contrast in the CT images and the difficulty to define the extend of potential microscopic spread of the tumor, large variations in target delineation have been reported for various tumor sites, both between different

physicians and between several delineations of one physician at different times [24,48, 87,133,152]. Often, the accuracy of the target definition can be improved by adding other imaging modalities like MRI, MRS, PET or SPECT [3,111,128,149]. Because these modalities lack information on electron densities, which is required for treatment planning, delineated volumes should always be transferred to a CT scan. To minimize the risk of errors in this process, automatic 3D matching tools to overlay images of different modalities, which have been developed by several groups [73,125,157], should become more generally available. Furthermore, new protocols and procedures should be developed to use these imaging modalities to achieve a reduction in tumor delineation variations.

9.3.2 Set-up accuracy and organ motion

In the past decade many studies have been performed to quantify the accuracy of patient set-up using megavoltage imaging with a portal imaging device. Both off-line [7,8,33] and on-line correction [3,35,97,154,146] protocols have been developed to reduce set-up errors, which should be taken into account when defining the PTV. For safe application of IMRT the use of these techniques will become more crucial. As an extension of the verification technique described in the previous chapter, a study will be started in our clinic to combine the use of megavoltage imaging for patient set-up verification with in-vivo dosimetry during DMLC treatments, allowing verification of the actual dose delivery of intensity modulated beams during patient treatment.

A problem with megavoltage imaging is that the tumor volume itself is generally not visible in the portal images. Instead the geometrical verification of the tumor is often based on surrounding bony structures. A solution for this problem is to implant radio-opaque markers in the tumor volume [3,9,161], but this is not easily possible for all tumor sites. It is common that treatment plans are designed using a single CT scan of the patient. However, to be able to compensate for inter-fraction motion, additional CT scans can be made at the first treatment days. In the William Beaumont Hospital, this technique is used to design an effective PTV, formed by the hull of the delineated tumor volume in the initial treatment planning CT scan and in 4 succeeding scans [171]. Depending on the observed intra-fraction variations, one decides whether a patient is suitable for IMRT and/or dose escalation. For those patients a new treatment plan is then designed based on the effective PTV. Another approach, which might be suitable especially for patients with larger inter-fraction motions, is to acquire a CT scan prior to each treatment fraction. To enable this, a helical CT scanning capability will be available in the tomotherapy unit that is being developed at the University of

Wisconsin [49]. At William Beaumont Hospital a kilovoltage cone beam CT option has been installed at one of their accelerators, which allows for the generation of full volumetric CT slices after one gantry rotation, without the need of patient displacement [64].

In recent years several methods have been developed to incorporate the impact of patient set-up errors and organ motion in the final dose distribution [98,106,145]. Application of this technique may be very important, especially when applying IMRT, since more accurate information on the actual dose delivery during an entire treatment course for both the target volume and normal tissues lying nearby is obtained and potential over- or underdosages can be quantified. Moreover, algorithms which incorporate (random) errors for patient set-up and organ motion in the inverse planning process have been published [88,91]

When delivering intensity modulated beams, one should also be aware of the impact of intra-fraction organ motion e.g. due to respiration. In contrast to static field treatments without intensity modulation, where intra-fraction organ motion only effects the field boundaries by broadening the effective dose fall-off, the interplay of organ motion and field shape variation during an IMRT treatment can distort the desired fluence profile within the treatment field significantly, yielding under- or overdosages up to 100% [177]. This problem is not only restricted to dynamic and rotational treatments; significant hot and cold spots may also arise at the boundaries of subfields which are superimposed in static intensity modulation techniques. To minimize the organ motion due to respiration, the use of the deep-inspiration breath hold technique [58] or active breathing control [170] is proposed. Especially for lung cancer patients, these treatment techniques are not always well tolerated. Alternatively, the treatment delivery can be gated, by switching on the treatment device at a predetermined phase of the breathing cycle, and switching it off at other phases [78,79]. But gating will result in a prolonged treatment time.

9.3.3 Geometrical misalignment of the treatment unit parameters

Geometrical misalignment of treatment unit parameters may have a large impact on the dose delivered within an intensity modulated field. Especially a high accuracy in leaf positioning is required to avoid under- or overdosages [20,92]. When using dynamic multileaf collimation, the dose delivered in the treatment field is directly related to the width of the sliding gap sweeping across the treatment field, as explained in chapter 7. Based on simulations, Budgell *et al* recently concluded that the realization of intensity modulated beam profiles, calculated by inverse planning, definitely require a leaf

position accuracy better than 1 mm, to avoid large dose errors, both in regions with a relatively homogeneous beam profile and in regions with high dose gradients [20]. As was demonstrated in chapter 7 and by others [20,92], modern control systems of a multileaf collimator allow for a stability in leaf positioning well within 0.01 cm. Therefore, the leaf position accuracy is mainly affected by the accuracy of the leaf calibration, which should be verified regularly, e.g. on a two-weekly basis. For this purpose, a quality control test using a narrow sweeping leaf gap, as proposed by LoSasso [92] and applied in chapter 7, is very useful, allowing deviations in leaf calibration of 0.05 cm to be detected. Additionally, as was shown in chapter 7, the stability in gap width may be verified within 0.01 cm by performing dose measurements in a uniform field, realized by sweeping a 0.4 cm wide slit across the field.

The impact of misalignment of the gantry and collimator angle on dose distributions delivered by IMRT has been investigated, both for single beams on a phantom [94] and for clinical multi-beam treatment plans [30,174]. The magnitude of dose errors due to gantry misalignment increase proportional with the distance to the isocenter plane; in the isocenter plane itself no dose errors exist. For a single beam, dose errors of more than 10% may be observed at 10 cm from the isocenter plane when the gantry angle has been misaligned by 1° [94]. These dose errors do not only occur at the boundaries of the treatment field, like for static fields, but also inside the treatment field, especially for highly modulated fluence profiles. To minimize the errors associated to gantry angle misalignment, the isocenter should therefore be placed close to the center of the target, if possible. Misalignment of the collimator angle has a smaller impact on the dose distribution and the dose errors are mainly concentrated to the boundaries of the treatment field. In the studies of Convery and Rosenbloom [30] and Xing *et al* [174] the impact of angular misalignments on dosimetric quantities, like the minimum, maximum and average doses and dose volume histograms for the target and sensitive organs was investigated for clinical treatment plans. They demonstrated that errors in gantry and collimator angle positions of less than 1° have only small impacts on the delivered dose distribution for clinical IMRT plans. In contrast, the accuracy of patient positioning was demonstrated to be of much greater importance.

9.4 Dosimetrical verification of IMRT

9.4.1 *Verification by dose measurements*

Within the treatment field, intensity modulated beams, calculated by inverse treatment planning techniques, generally show large variations in the optimized fluence profile. For dose calculations, this puts higher demands on the accuracy of the algorithms implemented in treatment planning systems. At this time, the different leaf sequencing algorithms that were developed have only been validated for a limited number of treatment fields and tumor sites. Moreover, the delivery of intensity modulated beams by either of the methods described in section 9.2 is certainly more complex compared to conventional treatments. For these reasons a pre-treatment dosimetrical verification of the intensity modulated beams for each individual patient is definitely required for the time being. In literature, two different approaches have been described. In the first approach, the dose distribution for individual treatment fields is verified by using film, ionization chambers, TLD or a portal imaging device [21,100,122]. For each beam direction, the measured dose distribution is then compared with the calculated dose distribution resulting from the expected fluence profile of the optimized beam. A second approach is the verification of the entire IMRT plan at once by irradiating some special phantom with all intensity modulated fields [95,127,151]. In this phantom measurements may be performed simultaneously at different parallel planes using film, TLD and/or ionization chambers. Also gel dosimetry has been applied for quantifying the accuracy of the 3D dose distribution [110,117]. Measured dose distributions are compared with calculated dose distributions in the phantom using the fluence maps and beam directions, which result from the optimized treatment plan of the patient.

Because an accurate verification of the entire treatment plan of a patient is most relevant, application of the second approach seems to be preferred. For rotational techniques, it is probably also the only practical solution to verify the dose delivery. However, the treatment plan of a patient is not verified directly, because the phantom and the patient are generally quite differently shaped. Consequently, there is no direct correlation between the accuracy of the phantom measurements and the patient treatment plan. Moreover, due to the contribution of all treatment fields to the final dose distribution, reasons for observed deviations between calculated and measured dose profiles are often hardly identified. In case single fields are verified the interpretation of observed differences between measured and calculated dose distributions is more straightforward, especially when a flat, homogeneous phantom perpendicular to the beam axis is used for the measurements.

The process of dosimetrical verification of IMRT plans should be fast and accurate to

allow a large number of patients to be treated safely with IMRT, without requiring excessive effort and time for quality control. In contrast to other measurement techniques like film, the use of an electronic portal imaging device is a very powerful tool for absolute dosimetry in this respect, as was demonstrated in chapter 8. Using this method accurate verification of absolute 2D dose distributions is possible within a few minutes.

9.4.2 Independent verification of monitor units for IMRT

Generally the number of monitor units required for a patient treatment is calculated by the treatment planning system. As part of the quality control program these numbers are often verified using an independent calculation method. But, in contrast to conventional treatments, an intuitive verification of the number of monitor units is no longer possible for IMRT due to the increased complexity of the treatment technique. Algorithms for monitor unit verification, which are presently used for conventional treatments, do not apply for IMRT either. Therefore, as part of the patient specific quality control, the absolute dose delivered to a patient by intensity modulated fields is generally verified by dose measurements in a phantom, as described before. Recently, methods that are suitable for monitor unit verification for IMRT have been described, applying the leaf sequencer file (which, like for the MM50, includes the leaf settings for each MLC subfield and the corresponding number of monitor units) to be used for the patient treatment [80,173]. In the future a similar, independent check of the monitor units to be delivered in each treatment field might replace the dose measurements for individual patients.

9.5 Concluding remarks

Although the clinical application of IMRT is still limited around the world, new implementations are rapidly increasing nowadays, because of the improvements that can be achieved in terms of dose delivery to the tumor volume and sensitive structures. Due to the increased complexity, clinical implementation of IMRT is labour intensive at this stage, limiting the number of patients that can be treated with this technique. In the next couple of years, methods for planning, delivery and automatic verification of IMRT treatments will certainly be extended and further integrated, allowing this technique to be applied for larger numbers of patients and tumor sites.

Summary

Introduction

Although investigations on computer optimization of radiotherapy treatment planning (inverse planning) have demonstrated that dose distributions can often be conformed tightly to a target volume by customizing the beam intensity profiles within the treatment field, clinical application of intensity modulated radiotherapy has just been started in a limited number of institutes around the world. At the Daniel den Hoed Cancer Center studies on the development and clinical implementation of intensity modulated conformal radiotherapy started after clinical introduction of the MM50 Racetrack Microtron. Both static and dynamic intensity modulation using a multileaf collimator were investigated. Results of these studies have been described in this thesis.

Static beam intensity modulation

In axial co-planar treatments with multiple fields, the penumbrae of the superior and inferior field edges of all treatment fields overlap, yielding broad overall penumbrae in these regions. Therefore, large field margins are generally needed for definition of the superior and inferior field borders to avoid underdosages in the superior and inferior ends of the planning target volume (PTV). Chapters 3 and 4 deal with a technique for penumbra enhancement at the superior and inferior field edges using static beam intensity modulation (BIM). The intensity modulated x-ray beams, generated with a multileaf collimator, include narrow boost fields to increase the dose in the superior and inferior ends of the PTV. Due to penumbra enhancement the length of all treatment fields could be reduced, while still achieving a minimum dose in the PTV of 95% of the prescribed dose. As a result of the reduced field lengths, the dose delivery to critical structures could often be reduced. The benefits of this BIM technique with respect to our (previous) standard technique have been assessed in a treatment planning study for prostate cancer patients (chapter 3) and lung cancer patients (chapter 4), using our Cadplan 3D treatment planning system. For prostate cancer patients application of the BIM technique allowed a field length reduction of 1.6 cm, generally yielding smaller volumes of rectum and bladder in the high dose region. For lung cancer patients the field lengths could be reduced by 1.4 cm for all patients. Due to reduced dose delivery to the healthy lung tissue, application of BIM allowed a potential for dose escalation of 6 to 7 Gy on average, without increasing the predicted incidence of pneumonitis. For 2 of the 12 patients in the treatment planning study, the estimated allowed dose escalation even exceeded 15 Gy. All dose escalations would be possible without exceeding the spinal cord tolerance dose.

The accuracy of our Cadplan treatment planning system for calculating dose distributions for the BIM technique was validated by dose measurements. Relative dose distributions for the narrow boost fields generally agreed within 2% or 2 mm with dose distributions, which were calculated by Cadplan. For accurate monitor unit calculations, the phantom scatter table as used in Cadplan had to be modified using measured data for square fields smaller than $4 \times 4 \text{ cm}^2$.

In the treatment planning study for lung cancer patients a treatment planning system was used that did not correctly account for the increased lateral secondary electron transport in lung tissue. Therefore, before starting clinical implementation of the BIM technique for lung cancer patients, extensive dosimetrical measurements were required (i) to assess the accuracy of our Cadplan 3D treatment planning system for the proposed BIM technique in lung treatments, (ii) to adapt the proposed BIM technique to account for increased lateral electron transport, and (iii) to define practical rules for designing treatment plans with the Cadplan treatment planning system. The results, presented in chapter 5, show that, by increasing the length and the weight of the boost fields applied in the BIM technique, to compensate for increased lateral secondary electron transport in lung tissue, a field length reduction of 1.4 cm is indeed possible. Practical rules could be derived for designing the BIM plans using our Cadplan planning system.

Reduced dose delivery to critical structures with the proposed BIM technique, related to the decreased superior-inferior field lengths, is not typical for the treatment techniques applied in our clinic; improved treatment plans are to be expected for all coplanar techniques. Nowadays, BIM is routinely applied in our clinic at different treatment units for treatment of prostate cancer patients and head and neck cancer patients. The extra time needed for set-up and delivery of the boost fields is usually less than 1 minute. Treatment plans for the BIM technique are easily obtained by 'forward' treatment planning; sophisticated computer optimization algorithms are not required.

Dynamic beam intensity modulation

Chapter 6 describes an algorithm for the calculation of the required leaf trajectories to generate optimized intensity modulated beam profiles by means of dynamic multileaf collimation (DMLC). The algorithm iteratively accounts for leaf transmission and collimator scatter, and fully avoids tongue-and-groove underdosage effects. The accuracy of this algorithm in combination with the dose calculation algorithm of our Cadplan treatment planning system has been assessed by comparing absolute dose distributions for optimized fluence profiles with dose distributions measured on the MM50 Racetrack Microtron, using the calculated leaf trajectories. Both theoretical and

clinical cases generally yielded an agreement within 2%, or 2 mm in regions with a high dose gradient, showing that the accuracy is adequate for clinical application. As a final test before starting patient treatment using dynamic multileaf collimation, the stability of intensity modulated beam profiles, generated at the MM50 Racetrack Microtron using DMLC, was investigated, (i) in time, (ii) subject to gantry rotation and (iii) in case of treatment interrupts, e.g. caused by an error detected by the treatment machine. The results, presented in chapter 7, show that the absolute dose in a reference point, situated in a relatively flat part of the beam profile, reproduced within 0.2% (1σ) over a period of 100 days. During this period variations in the relative beam profiles were generally less than 1% (1σ), except for regions with very large dose gradients. A similar reproducibility was measured for different gantry angles, showing that gravity has a negligible influence. No significant deviations between uninterrupted and interrupted treatments could be observed, indicating that the effects of acceleration and deceleration of the leaves are negligible and that a DMLC treatment can be finished correctly after a treatment interrupt. In the meantime, patient treatment using dynamic multileaf collimation has been started in our clinic at the MM50 for head and neck cancer patients and prostate cancer patients.

Dosimetric quality control using an EPID

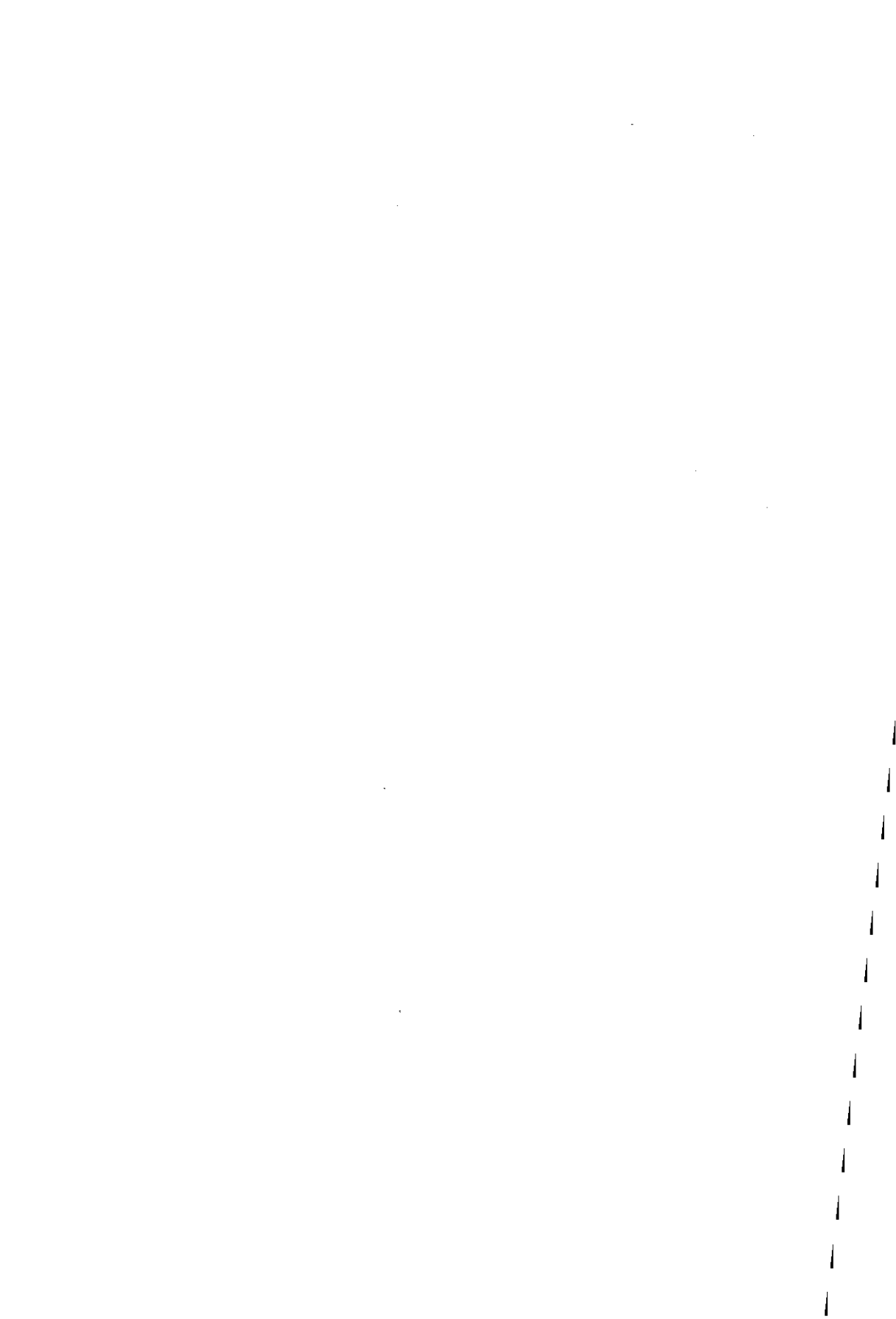
A complex treatment machine like the MM50 Racetrack Microtron definitely requires extensive dosimetric quality control. Chapter 2 describes a method for fast and daily dosimetric checks of the absolute output and the beam fluence profile of scanned photon beams at different gantry angles using an electronic portal imaging device (EPID). Open beams are checked for four gantry angles and for gantry angle 0° a wedged field is checked as well. The performance and analysis of the measurements take less than 10 minutes. It is demonstrated that the applied EPID is well suited for these dosimetric measurements due to its excellent stability, linearity and reproducibility. Daily measurements over a ten months period have demonstrated that the 2D fluence profile of the 25 MV photon beam of the MM50 is very stable in time, showing a maximum deviation of 2.8%. In this period, a deviation in the absolute output of 6% was detected once, proving the importance of these daily checks, because no interlock in the MM50 would have prevented patient treatment with this strongly deviating output. Based on the results of this study, and on clinical requirements regarding acceptability of deviations of beam characteristics, a protocol for these daily tests was developed, including action levels for additional investigations and, if necessary, adjustments of beam characteristics.

Delivery of intensity modulated beams using dynamic multileaf collimation is rather

complex and therefore requires extensive quality control before patient treatment is started. In chapter 8, a new method for pre-treatment verification of all intensity modulated beam profiles for a patient is presented based on absolute dose measurements with a fluoroscopic electronic portal imaging device. Prior to the first treatment fraction of the patient an EPID image is acquired for each treatment field and then converted into a two-dimensional dose distribution. This dose distribution is compared to a dose distribution calculated with the pencil beam algorithm as implemented in our Cadplan treatment planning system, using the same absolute beam fluence profile as used for calculation of the patient dose distribution. The method allows an overall verification of (i) the calculation of the dose distribution by the treatment planning system, using the leaf trajectories derived with the algorithm described in chapter 6, (ii) the correct transfer of the leaf sequencing file to the treatment unit, and (iii) the mechanical and dosimetrical performance of the treatment machine. For both theoretical and clinical examples using 10 and 25 MV photon beams, the accuracy of this method for pre-treatment verification was demonstrated by an agreement within 2% (1σ) between both calculated dose distributions and EPID measurements and between EPID and ionization chamber measurements. The time required to verify an intensity modulated beam is about 2 minutes, which is much shorter than for other dosimetrical techniques.

IMRT in clinical practice

In the general discussion of the last chapter different methods to realize intensity modulated beam profiles using a multileaf collimator are compared. Because in IMRT the dose delivery is generally more closely conformed to the tumor volume, the position of the tumor volume during treatment delivery should be well known. Some uncertainties that are related to this, like the accuracy of target delineation, the patient setup accuracy and detection of internal organ motion, are discussed. Finally, the dosimetrical verification of IMRT is addressed in more detail.



Samenvatting

Inleiding

Bij de toepassing van radiotherapie voor behandeling van patiënten met kanker gaat het erom dat er voldoende dosis wordt afgegeven in het tumorvolume om de tumorcellen te doden en dat de dosis in het gezonde weefsel zo laag mogelijk wordt gehouden om de kans op bijwerkingen van de behandeling te beperken. Onderzoek naar de toepassing van computeroptimalisatie bij het maken van behandelplannen voor radiotherapie (inverse planning) heeft aangetoond dat het gebruik van patiëntspecifieke intensiteitsgemoduleerde bundelprofielen over het algemeen de beste mogelijkheden biedt om de dosisafgifte te beperken tot het tumorvolume. Echter tot op heden wordt intensiteitsgemoduleerde radiotherapie (IMRT) wereldwijd slechts in een beperkt aantal behandelcentra toegepast.

Na de ingebruikname van het MM50 Racetrack Microtron, een bestralingsapparaat dat uitermate geschikt is voor de toepassing van geavanceerde bestralingstechnieken, zijn binnen de Daniel den Hoed Kliniek studies van start gegaan naar de ontwikkeling en klinische implementatie van IMRT. Hierbij is zowel statische als dynamische intensiteitsmodulatie middels een multileaf collimator onderzocht. Dit proefschrift beschrijft de resultaten van dit onderzoek.

Statische intensiteitsmodulatie

In axiale, coplanaire bestralingen met meerdere velden overlapt de dosisafval aan de craniale en caudale zijde van ieder bestralingsveld, hetgeen resulteert in minder scherpe totale dosisgradiënten. Bij de bepaling van de bestralingsvelden in craniale en caudale richting moeten hierdoor meestal brede veldmarges worden toegepast om te voorkomen dat de meest craniale en caudale gedeeltes van het beoogde doelvolumen (PTV) ondergedoseerd worden. In de hoofdstukken 3 en 4 wordt een techniek beschreven, gebruikmakend van statische bundel intensiteitsmodulatie (BIM), waarmee scherpere dosisgradiënten kunnen worden gerealiseerd in cranio-caudale richting. In deze BIM techniek wordt in de meest craniale en caudale gedeeltes van het PTV extra dosis afgegeven door gebruik te maken van smalle velden, die worden gevormd middels de multileaf collimator, met een laag gewicht. Als gevolg van de scherpere dosisgradiënten kan de lengte van ieder bestralingsveld worden gereduceerd, terwijl in het PTV toch minimaal 95% van de voorgeschreven dosis wordt afgegeven. De reductie van de veldlengte leidt veelal tot een verminderde dosisafgifte in het gezonde weefsel. Met het Cadplan 3D planningsysteem zijn studies uitgevoerd om de voordelen van de BIM techniek ten opzichte van de (oude) standaard behandeltechniek te bepalen bij patiënten met prostaat- en longkanker. Toepassing van de BIM techniek maakt bij

patiënten met prostaatkanker (hoofdstuk 3) een reductie van de lengte van ieder bestralingsveld met 1.6 cm mogelijk, waardoor over het algemeen een kleiner deel van blaas en rectum een hoge dosis krijgt. Bij patiënten met longkanker (hoofdstuk 4) kan de lengte van ieder bestralingsveld met 1.4 cm worden verminderd, met als gevolg een lagere dosisafgifte in gezond longweefsel. Toepassing van de BIM techniek biedt daarmee de mogelijkheid om de dosis in de tumor met gemiddeld 6 tot 7 Gy te verhogen, zonder het risico op bijwerkingen (pneumonitis) te vergroten. Voor twee van de twaalf patiënten in de planningstudie bleek zelfs een verhoging van de tumordosis met meer dan 15 Gy mogelijk. Voor alle patiënten was deze verhoging van de tumordosis mogelijk zonder dat de tolerantiedosis van het ruggenmerg werd overschreden.

Om de nauwkeurigheid te bepalen waarmee het Cadplan planningsysteem de dosisverdelingen voor de BIM techniek berekent, zijn er dosismetingen verricht in water. De gemeten relatieve dosisverdelingen voor de smalle boostvelden kwamen over het algemeen binnen 2% of 2 mm overeen met de dosisverdelingen die door Cadplan werden berekend. Om een correcte absolute dosisberekening te krijgen moest de tabel met fantoom scatterfactoren die door Cadplan wordt gebruikt, worden aangepast voor velden kleiner dan $4 \times 4 \text{ cm}^2$.

De toename van het laterale elektrontransport in weefsel met een lage elektronendichtheid, zoals longweefsel, wordt door het planningsysteem Cadplan niet correct in rekening gebracht. Alvorens over te gaan tot klinische toepassing van de BIM techniek bij patiënten met longkanker werd er daarom eerst een uitgebreid dosimetrisch onderzoek uitgevoerd. Het doel van deze studie was om (i) vast te stellen wat de nauwkeurigheid is van de dosisvoorspellingen voor de BIM techniek door Cadplan, (ii) te bepalen hoe de BIM techniek moet worden aangepast om te corrigeren voor het toegenomen laterale elektrontransport in longweefsel, en (iii) om praktische regels vast te stellen waarmee BIM behandelplannen voor patiënten met longkanker met Cadplan kunnen worden gemaakt. De resultaten van deze studie, beschreven in hoofdstuk 5, laten zien dat de lengte en het gewicht van de boostvelden, die in de BIM techniek worden toegepast, moeten worden vergroot om te compenseren voor de toegenomen laterale elektronenverstrooiing. In dat geval blijkt een reductie van de veldlengte met 1.4 cm inderdaad mogelijk, zonder dat er delen van het PTV worden ondergedoseerd.

Reductie van de dosisafgifte in kritieke organen, als gevolg van een verminderde cranio-caudale veldlengte, door toepassing van de beschreven BIM techniek, is niet typisch voor de bestralingstechnieken die in ons instituut worden toegepast. Verbeterde behandelplannen kunnen worden verwacht voor alle coplanaire bestralingstechnieken. Momenteel wordt de BIM techniek veelvuldig toegepast in ons instituut bij de

bestraling van patiënten met KNO- en prostaatumoren op verschillende bestralings-toestellen met een multileaf collimator. De extra tijd voor het instellen en afgeven van de boostvelden is meestal minder dan één minuut. Behandelplannen voor de BIM techniek kunnen eenvoudig worden verkregen met 'voorwaartse' planning. Gecomplieerde computeroptimalisatie algoritmen zijn hiervoor niet vereist.

Dynamische intensiteitsmodulatie

In hoofdstuk 6 is een algoritme beschreven om de leafbewegingen te berekenen waarmee een geoptimaliseerd intensiteitsgemoduleerde profiel middels dynamische multileaf collimatie (DMLC) kan worden gerealiseerd. Via een iteratieve berekeningsmethode corrigeert dit algoritme voor transmissie door de leaves en collimator verstrooiing. Daarnaast wordt voorkomen dat er in het overlap gebied van twee naastliggende leaves onderdoseringen ontstaan als gevolg van de 'tongue-en-groove' constructie. De nauwkeurigheid van dit algoritme in combinatie met het Cadplan planningsysteem is bepaald door voor een groot aantal intensiteits-gemoduleerde profielen absolute dosisverdelingen te berekenen en deze te vergelijken met dosisverdelingen die op de MM50 werden gemeten, gebruikmakend van de berekende leafbewegingen. Voor zowel theoretische als klinische intensiteitsprofielen komen gemeten en berekende dosisprofiel over het algemeen binnen 2% overeen, behalve in gebieden met een sterke dosisgradiënt waar een overeenkomst binnen 2 mm wordt gevonden. Voor klinische toepassingen is deze nauwkeurigheid voldoende.

Alvorens dynamische multileaf collimatie klinisch toe te gaan passen, is de stabiliteit van intensiteitsgemoduleerde velden, die op de MM50 worden gerealiseerd middels dynamische multileaf collimatie, onderzocht, (i) gedurende een langere tijdsperiode, (ii) bij bestraling vanuit verschillende bundelhoeken, en (iii) na onderbreking van de bestraling, bijvoorbeeld vanwege een door het bestralingsstoestel gedetecteerde fout. De resultaten van dit onderzoek zijn beschreven in hoofdstuk 7. Gedurende een periode van honderd dagen blijkt de absolute dosis in een referentiepunt, gelegen in een relatief vlak gedeelte van een intensiteitsgemoduleerd veld, binnen 0.2% (1σ) te reproduceren. Binnen deze tijdsperiode waren de relatieve dosisprofielen meestal binnen 1% reproduceerbaar, behalve in gebieden met een grote dosisgradiënt. Voor bestralingen vanuit verschillende bundelhoeken werd een vergelijkbare reproduceerbaarheid in de dosisprofielen gemeten, wat aantoont dat de zwaartekracht een verwaarloosbare invloed heeft. Ook waren er geen aantoonbare verschillen tussen dosisprofielen die werden gemeten bij een ononderbroken en onderbroken bestraling. Hieruit blijkt dat versnelling en vertraging van de leaves geen noemenswaardige invloed heeft op de leafbewegingen en dat een DMLC bestraling correct kan worden voltooid na een

onderbreking van de bestraling. Intussen is de klinische toepassing van DMLC op de MM50 van start gegaan bij bestraling van patiënten met KNO- en prostaattumoren.

Dosimetrische kwaliteitscontrole met een EPID

Het klinisch gebruik van een complex bestralingstoestel als het MM50 Racetrack Microtron vereist een uitgebreidere dosimetrische kwaliteitscontrole dan veelal gebruikelijk is. In hoofdstuk 2 is een methode beschreven waarmee dagelijks snel de absolute output en het bundelprofiel van een scannende fotonenbundel kunnen worden geverifieerd bij bestraling vanuit verschillende bundelhoeken, gebruikmakend van een megavolt afbeeldingsstelsel (MVA). Open bundels worden geverifieerd voor vier bundelhoeken en voor één hoek wordt tevens een wigveld gecontroleerd. Het uitvoeren en analyseren van deze metingen neemt minder dan tien minuten in beslag. Door zijn uitstekende stabiliteit, lineariteit en reproduceerbaarheid blijkt het MVA-systeem uitermate geschikt te zijn voor dosismetingen. Dagelijkse metingen gedurende een periode van tien maanden hebben aangetoond dat het relatieve bundelprofiel van de 25 MV fotonenbundel van de MM50 zeer stabiel is. De maximale variatie in dosis bleek slechts 2.8% te bedragen. Gedurende deze periode werd eenmaal een afwijking in de absolute dosis van 6% aangetoond, hetgeen het belang van deze dagelijkse metingen bewijst, omdat geen van de alarmeringssystemen van de MM50 patiëntenbehandeling met deze sterk afwijkende output had voorkomen. Gebaseerd op de resultaten van dit onderzoek en de voor klinische toepassingen toelaatbare variaties in bundelkarakteristieken, is een protocol opgesteld voor de dagelijkse kwaliteitscontrole met MVA, waarin tevens wordt aangegeven bij welke afwijkingen aanvullend onderzoek noodzakelijk is en de bundelkarakteristieken zonnodig moeten worden aangepast.

Patiëntenbehandeling met intensiteitsgemoduleerde velden middels dynamische multileaf collimatie, is tamelijk complex en vereist daarom uitgebreide kwaliteitscontrole alvorens een patiëntenbestraling van start gaat. In hoofdstuk 8 wordt een methode beschreven voor de dosimetrische verificatie van intensiteits-gemoduleerde bundels, die wordt uitgevoerd met een MVA-systeem. Voor de eerste bestraling van een patiënt wordt voor ieder bestralingsveld een MVA-beeld opgenomen. Het MVA-beeld wordt omgerekend naar een absolute 2D dosisverdeling die wordt vergeleken met de voorspelde dosisverdeling voor het betreffende bestralingsveld. De dosisvoorspelling wordt gedaan met het algoritme dat ook in het Cadplan planningsstelsel geïmplementeerd is, gebruikmakend van hetzelfde absolute bundelprofiel dat ook voor de berekening van de dosisverdeling in de patiënt wordt toegepast. Deze methode biedt de mogelijkheid om gelijktijdig (i) de berekening van de dosisverdeling door het planningsstelsel te verifiëren, die is gebaseerd op de

leafbewegingen die met het in hoofdstuk 6 beschreven algoritme worden afgeleid, (ii) te controleren of de file waarin de berekende leafbewegingen worden beschreven correct naar het bestralingstoestel is overgestuurd, en (iii) te bepalen of het bestralingstoestel mechanisch en dosimetrisch correct is afgesteld. Voor 10 en 25 MV fotonenbundels blijken, voor zowel theoretische als klinische intensiteitsgemoduleerde velden, de voorspelde dosisverdelingen en de dosisverdelingen gemeten met MVA, en de dosisverdelingen gemeten met MVA en met een ionisatievat, binnen 2% (1σ) overeen te komen. Dit toont de nauwkeurigheid van deze methode aan voor dosimetrische controle van intensiteitsgemoduleerde velden. Per bundel kost deze controle ongeveer 2 minuten, wat veel sneller is dan met andere dosimetrische meettechnieken.

IMRT in klinische praktijk

In de algemene discussie in het laatste hoofdstuk worden verschillende technieken om intensiteitsgemoduleerde bundels middels een multileaf collimator te realiseren vergeleken. Doordat de dosisafgifte tijdens IMRT veelal beter tot het doelvolume kan worden beperkt, is het van groot belang dat de lokalisatie van de tumor tijdens de bestraling met grote nauwkeurigheid bekend is. Problemen die hierbij een rol spelen zijn ondermeer de intekennauwkeurigheid van het tumorvolume, de positioneringsnauwkeurigheid van de patiënt en de beweging van het doelvolume in de patiënt. Tot slot wordt nader ingegaan op de dosimetrische verificatie van IMRT.

Bibliography

- 1 Althof VGM, de Boer JCJ, Huizenga H, Stroom JC, Visser AG and Swanenburg BN. 'Physical characteristics of a commercial electronic portal imaging device'. *Med. Phys.* 23: 1845-1855, 1996.
- 2 Arriagada R, Le Chevalier T, Quoix E *et al.* 'Effect of chemotherapy on locally advanced non-small cell lung carcinoma: a randomized study of 353 patients'. *Int. J. Radiat. Oncol. Biol. Phys.* 20: 1183-1190, 1991.
- 3 Badiozamani KR, Wallner K, Cavanagh W, and Blasko J. 'Comparability of CT-based and TRUS-based prostate volumes'. *Int. J. Radiat. Oncol. Biol. Phys.* 43: 375-378, 1999.
- 4 Balter JM, Sandler HM, Lam K, Bree RL, Lichter AS and Ten Haken RK. 'Measurement of prostate movement over the course of routine radiotherapy using implanted markers'. *Int. J. Radiat. Oncol. Biol. Phys.* 31: 113-118, 1995.
- 5 Balter JM, McShan DL, Kim J and Fraass BA. 'Automated on-line verification of dynamic multileaf collimator configuration using a computer controlled radiotherapy system'. *Med. Phys.* 24: 1002, 1997 (abstr.).
- 6 Bax DP, Verlinde PH, Storchi P, Woudstra E and Puurunen H. 'Evaluation of the accuracy of the calculation of irregular photon fields in a radiotherapy planning system'. *Radiother. Oncol.* 37 (suppl. 1): S13, 1995 (abstr.).
- 7 Bel A, van Herk M, Bartelink M and Lebesque V. 'A verification procedure to improve patient set-up accuracy using portal images'. *Radiother. Oncol.* 29: 253-260, 1993.
- 8 Bel A, Vos PH, Rodrigus PT, Creutzberg CL, Visser AG, Stroom JC and Lebesque JV. 'High-precision prostate cancer irradiation by clinical application of an offline patient setup verification procedure, using portal imaging'. *Int. J. Radiat. Oncol. Biol. Phys.* 35: 321-332, 1996.
- 9 Bergstrom P, Lofroth PO and Widmark A. 'High-precision conformal radiotherapy (HPCRT) of prostate cancer: a new technique for exact positioning of the prostate at the time of treatment'. *Int. J. Radiat. Oncol. Biol. Phys.* 42: 305-311, 1998.
- 10 Biggs PJ and Shipley WU. 'A beam width improving device for a 25 MV X ray beam'. *Int. J. Radiat. Oncol. Biol. Phys.* 12: 131-135, 1986.
- 11 Blomquist M, S  therberg, Karlsson M and Zackrisson B. 'Scanned intensity modulation for 50 MV photons'. *Phys. Med. Biol.* 43: 1185-1197, 1998.
- 12 Bortfeld ThR, B  rkelbach J, Boesecke R and Schlegel W. 'Methods of image reconstruction from projections applied to conformation radiotherapy'. *Phys. Med. Biol.* 35: 1423-1434, 1990.
- 13 Bortfeld ThR, Kahler DL, Waldron TJ and Boyer AL. 'X-ray field compensation with multileaf collimators'. *Int. J. Radiat. Oncol. Biol. Phys.* 28:

- 723-730, 1994.
- 14 Boyer A, Geis P, Grant W *et al.* 'Modulated beam conformal therapy for head and neck tumors'. *Int. J. Radiat. Oncol. Biol. Phys.* 39: 227-236, 1997.
 - 15 Boyer AL and Yu CX. 'Intensity-modulated radiation therapy with dynamic multileaf collimators'. *Semin. in Radiat. Oncol.* 9: 48-59, 1999.
 - 16 Brahme A, Roos JE, and Lax I. 'Solution of an integral equation encountered in rotation therapy'. *Phys. Med. Biol.* 27: 1221-1229, 1982.
 - 17 Brahme A. 'Optimization of stationary and moving beam radiation therapy techniques'. *Radiother. Oncol.* 12: 129-140, 1988.
 - 18 British Journal of Radiology, supplement 25. 'Central Axis Depth Dose Data for Use in Radiotherapy', 1996.
 - 19 Brugmans MJP, van der Horst A, Lebesque JV, Mijnheer BJ. 'Beam intensity modulation to reduce the field sizes for conformal irradiation of lung tumors: a dosimetric study'. *Int. J. Radiat. Oncol. Biol. Phys.* 43: 893-904, 1999.
 - 20 Budgett GJ, Mott JHL, Williams PC and Brown KJ. 'Requirements for leaf position accuracy for dynamic multileaf collimation'. *Phys. Med. Biol.* 45: 1211-1227, 2000.
 - 21 Burman C, Chui CS, Kutcher G, Leibel S, Zelefsky M, LoSasso T, Spirou S, Wu Q, Yang J, Stein J, Mohan R, Fuks Z and Ling CC. 'Planning, delivery, and quality assurance of intensity-modulated radiotherapy using dynamic multileaf collimator: a strategy for large-scale implementation for the treatment of carcinoma of the prostate'. *Int. J. Radiat. Oncol. Biol. Phys.* 39: 863-873, 1997.
 - 22 Carol MP. 'Peacock: a system for planning and rotational delivery of intensity modulated fields'. *Int. J. Imag. Sys. Tech.* 6: 56-61; 1995.
 - 23 Carol MP, Grant W III, Bleier AR, Kania AA, Targovnik HS, Butler EB and Woo SW. 'The field-matching problem as it applies to the Peacock three-dimensional conformal system for intensity modulation'. *Int. J. Radiat. Oncol. Biol. Phys.* 34: 183-187, 1996.
 - 24 Cazzaniga LF, Marinoni MA, Bossi A, Bianchi E, Cagna E, Cosentino D, Scandolaro L, Valli M and Frigerio M. 'Interphysician variability in defining the planning target volume in the irradiation of prostate and seminal vesicles'. *Radiother. Oncol.* 47: 293-296, 1998.
 - 25 Chen Z, Wang X, Bortfeld T, Mohan R and Reinstein L. 'The influence of scatter on the design of modulations'. *Med. Phys.* 22: 1727-1733, 1995.
 - 26 Choy H, Yee L and Cole BF. 'Combined-modality therapy for advanced non-small cell lung cancer: Paclitaxel and thoracic irradiation'. *Semin. Oncol.* 22: 38-44, 1995.

- 27 Chui CS, LoSasso T and Spirou S. 'Dose calculation for photon beams with intensity modulation generated by dynamic jaw or multileaf collimators'. *Med. Phys.* 21: 1237-1244, 1994.
- 28 Chui CS, Spirou S and LoSasso T. 'Testing of dynamic multileaf collimation'. *Med. Phys.* 23: 635-641, 1996.
- 29 Convery DJ and Rosenbloom ME. 'The generation of intensity-modulated fields for conformal radiotherapy by dynamic multileaf collimation'. *Phys. Med. Biol.* 37: 1359-1374, 1992.
- 30 Convery DJ and Rosenbloom ME. 'Treatment delivery accuracy in intensity-modulated conformal radiotherapy'. *Phys. Med. Biol.* 40: 979-999, 1995.
- 31 Cox JD, Azarnia N, Byhardt RW *et al.* 'A randomized phase I/II trial of hyperfractionated radiation therapy with total doses of 60.0 Gy to 79.2 Gy: Possible survival benefits with ≥ 69.6 Gy in favorable patients with RTOG stage III non-small cell lung carcinoma: report of RTOG 83-11'. *J. Clin. Oncol.* 8: 1543-1555, 1990.
- 32 Curtin-Savard AJ and Podgorsak EB. 'Verification of segmented beam delivery using a commercial electronic portal imaging device'. *Med. Phys.* 26: 737-742, 1999.
- 33 De Boer JCJ and Heijmen BJM. 'An optimal off-line set-up correction protocol based on numerical simulations with measured set-up data of 600 prostate cancer patients'. In: *Proceedings of the XIIIth ICCR (International Congress on the use of Computers in Radiation Therapy)*. Edited by W Schlegel and T Bortfeld (Springer-Verlag Berlin Heidelberg 2000), pp. 553-555.
- 34 De Gerssem W, Claus F, Vakaet L, Remouchamps V, Vanhoutte I, Van duyse B, Vermael S, De Wagter C and De Neve W. 'General anatomy based segmentation for intensity modulated radiotherapy of head and neck cancer'. In: *Proceedings of the XIIIth ICCR (International Congress on the use of Computers in Radiation Therapy)*. Edited by W Schlegel and T Bortfeld (Springer-Verlag Berlin Heidelberg 2000), p. 207.
- 35 De Neve W, Van den Heuvel F, Coghe M, Verellen D, De Beukeleer M, Roelstraete A, De Roover P, Thon L and Storme G. 'Interactive use of on-line portal imaging in pelvic radiation'. *Int. J. Radiat. Oncol. Biol. Phys.* 25: 517-524, 1993.
- 36 De Neve W, De Wagter C, De Jaeger K, Thienpont M, Colle C, Derycke S and Schelfhout J. 'Planning and delivering high doses to targets surrounding the spinal cord at the low neck and upper mediastinal levels: static beam segmentation technique executed by a multileaf collimator'. *Radiother Oncol*,

- 40: 271-279, 1996.
- 37 De Neve W, De Gerssem W, Derycke S, De Meerleer G, Moerman CM, Bate MT, Van Duyse B, Vakaet L, De Deene Y and Mersseman B. 'Clinical delivery of intensity modulated conformal radiotherapy for relapsed or second-primary head and neck cancer using a multileaf collimator with dynamic control'. *Radiother. Oncol.* 50: 301-314, 1999.
- 38 Dirx MLP, Kroonwijk M, de Boer JCJ and Heijmen BJM. 'Daily dosimetric quality control of the MM50 Racetrack Microtron using an electronic portal imaging device'. *Radiother. Oncol.* 37: 55-60, 1995.
- 39 Dirx MLP, Heijmen BJM, Korevaar GA, van Os MJH, Stroom JC, Koper PCM and Levendag PC. 'Field margin reduction using intensity modulated X-ray beams formed with a multileaf collimator'. *Int. J. Radiat. Oncol. Biol. Phys.* 38: 1123-1127, 1997.
- 40 Dirx MLP, Heijmen BJM and van Santvoort JPC. 'Leaf trajectory calculation for dynamic multileaf collimation to realise optimised fluence profiles'. *Phys. Med. Biol.* 43: 1171-1184, 1998.
- 41 Dirx MLP, van Ingen KM, Kroonwijk M and Heijmen BJM. 'Reproducibility of intensity modulated beams generated with dynamic multileaf collimation (DMLC)'. *Radiother. Oncol.* 48: S186, 1998 (abstr.).
- 42 Dirx MLP, Essers M, van Sörnsen de Koste JR, Senan S and Heijmen BJM. 'Beam intensity modulation for penumbra enhancement in the treatment of lung cancer'. *Int. J. Radiat. Oncol. Biol. Phys.* 44: 449-454, 1999.
- 43 Dosoretz DE, Katin MJ, Blitzer PH *et al.* 'Medically inoperable lung carcinoma: the role of radiation therapy'. *Sem. Radiat. Oncol.* 6: 98-105, 1996.
- 44 Eisbruch A, Marsch LH, Martel MK, Ship JA, Ten Haken R, Pu AT, Fraass BA and Lichter AS. 'Comprehensive irradiation of head and neck cancer using conformal multisegmental fields: assessment of target coverage and noninvolved tissue sparing'. *Int. J. Radiat. Oncol. Biol. Phys.* 41:559-568, 1998.
- 45 Ekstrand KE and Barnes WH. 'Pitfalls in the use of high energy X-rays to treat tumors in the lung'. *Int. J. Radiat. Oncol. Biol. Phys.* 18: 249-252, 1990.
- 46 Essers M, Eggen M, Binnekamp D, Creutzberg CL and Heijmen BJM. 'Chest wall irradiation with MLC shaped photon and electron fields'. *Int. J. Radiat. Oncol. Biol. Phys.* 48: 1201-1213, 2000.
- 47 Evans PM, Hansen VN and Swindell W. 'The optimum intensities for multiple static multileaf collimator field compensation'. *Med. Phys.* 24: 1147-1156, 1997.
- 48 Fiorino C, Reni M, Bolognesi A, Cattaneo GM, and Calandrino R. 'Intra- and

- inter-observer variability in contouring prostate and seminal vesicles: implications for conformal treatment planning'. *Radiother. Oncol.* 47: 285-292, 1998.
- 49 Fitchard EF, Aldridge JS, Reckwerdt PJ *et al.* 'Registration of synthetic tomotherapy projection data sets using cross-correlation'. *Phys. Med. Biol.* 43: 1645-1657, 1998.
- 50 Fraass BA, Kessler ML, McShan DL, Marsh LH, Watson, BA, Dusseau WJ, Eisbruch A, Sandler HM and Lichter AS. 'Optimization of clinical use of multisegment intensity-modulated radiation therapy for high-dose conformal therapy'. *Seminars in Radiat. Oncol.* 9: 60-77, 1999.
- 51 Galvin JM, Chen XG and Smith RM. 'Combining multileaf fields to modulate fluence distributions'. *Int. J. Radiat. Oncol. Biol. Phys.* 27: 697-705, 1993.
- 52 Goor C, Scalliet P, Van Meerbeeck J. *et al.* 'A phase II study combining gemcitabine with radiotherapy in stage III NSCLC'. *Ann. Oncol.* 7: 101, 1996 (abstr.).
- 53 Graham MV, Purdy JA, Emami B, Emami B, Matthews JW and Harms WB. 'Preliminary results of a prospective trial using three-dimensional radiotherapy for lung cancer'. *Int. J. Radiat. Oncol. Biol. Phys.* 33: 993-1000, 1995.
- 54 Graham MV, Jahanzeb M, Dresler C.M *et al.* 'Results of a trial with topotecan dose escalation and concurrent thoracic radiation therapy for locally advanced, inoperable non-small cell lung cancer'. *Int. J. Radiat. Oncol. Biol. Phys.* 36: 1215-1220, 1996.
- 55 Grant W and Woo SY. 'Clinical and financial issues for intensity modulated radiation therapy delivery'. *Sem. in Radiat. Oncol.* 9: 99-107, 1999.
- 56 Gustafsson A, Lind BK, Brahme A *et al.* 'A generalized pencil beam algorithm for optimization of radiation therapy'. *Med. Phys.* 21:343-356, 1994
- 57 Gustafsson A, Lind BK, Svensson R and Brahme A. 'Simultaneous optimization of dynamic multileaf collimation and scanning patterns or compensation filters using a generalized pencil beam algorithm'. *Med. Phys.* 22: 1141-1156, 1995.
- 58 Hanley J, Debois MM, Mah D, Magaras GS, Raben A, Rosenzweig K, Mychalczak B, Schwartz LH, Gloeggler PJ, Lutz W, Ling, CC, Leibel SA, Fuks Z and Kutcher GJ. 'Deep inspiration breath-hold technique for lung tumors: the potential value of target immobilization and reduced lung density in dose escalation'. *Int. J. Radiat. Oncol. Biol. Phys.* 45: 603-611, 1999.
- 59 Heijmen BJM, Pasma KL, Kroonwijk M, Althof VGM, de Boer JCJ, Visser AG and Huizenga H. 'Portal dose measurements in radiotherapy using an electronic portal imaging device (EPID)'. *Phys. Med. Biol.* 40: 1943-1955,

- 1995.
- 60 Huang PH, Chu J and Bjärngard BE. 'The effect of collimator backscatter radiation on photon output of linear accelerators'. *Med. Phys.* 14: 268-269, 1987.
- 61 Hunt MA, Zelefsky MJ, Chui CS, LoSasso T, Wolden S, Rosenzweig KE, Chong L, Amols H and Leibel SA. 'Intensity modulated radiotherapy for primary nasopharynx cancer'. *Int. J. Radiat. Oncol. Biol. Phys.* 45 (suppl 1): 276, 1999.
- 62 ICRU: Report No. 50, Prescribing, recording and reporting photon beam therapy. International Commission on Radiation Units and Measurements, Bethesda, MD, 1994.
- 63 Jaffray DA, Battista JJ, Fenster A and Munro P. 'X-ray sources of medical linear accelerators: Focal and extra-focal radiation'. *Med. Phys.* 20: 1417-1427, 1993.
- 64 Jaffray DA, Drake DG, Moreau M *et al.* 'Radiographic and tomographic localization of bone and soft targets on a clinical accelerator'. *Int. J. Radiat. Oncol. Biol. Phys.* 45: 773-789, 1999.
- 65 James HV, Atherton S, Budgell GJ, Kirby MC and Williams PC. 'Verification of dynamic multileaf collimation using an electronic portal imaging device.' *Phys. Med. Biol.* 45: 495-509, 2000.
- 66 Jiang SB and Ayyangar KM. 'On compensator design for photon beam intensity-modulated conformal therapy.' *Med Phys.* 25: 668-675, 1998.
- 67 Källman P, Lind B K, Eklöf A and Brahme A. 'Shaping of arbitrary dose distributions by dynamic multileaf collimation'. *Phys. Med. Biol.* 33: 1291-1300, 1988.
- 68 Källman P, Lind B K and Brahme A. 'An algorithm for maximizing the probability of complication-free tumour control in radiation therapy'. *Phys. Med. Biol.* 37: 871-890, 1992.
- 69 Karlsson M, Nyström H and Svensson H. 'Electron beam characteristics of the 50-MeV Racetrack Microtron'. *Med. Phys.* 19: 307-315, 1992.
- 70 Karlsson M, Nyström H and Svensson H. 'Photon beam characteristics of the MM50 Racetrack Microtron and a new approach for beam quality determination'. *Med. Phys.* 20: 143-149, 1993.
- 71 Karlsson M and Zackrisson B. 'Matching of electron and photon beams with a multileaf collimator'. *Radiother. Oncol.* 29: 317-326, 1993.
- 72 Keller-Reichenbecher M.A., Bortfeld T, Levegrün S, Stein J, Preiser K and Schlegel W. 'Intensity modulation with the "step and shoot" technique using a commercial MLC: a planning study'. *Int. J. Radiat. Oncol. Biol. Phys.* 45:

- 1315-1324; 1999.
- 73 Kessler ML, Li K and Meyer C. 'Automated image registration using mutual information for both affine and thin-plate spline geometric transformations'. In: *Proceedings of the XIIth ICCR (International Congress on the use of Computers in Radiation Therapy)*. Edited by W Schlegel and T Bortfeld (Springer-Verlag Berlin Heidelberg 2000), pp. 96-98.
- 74 King SC, Acker JC, Kussin PS, *et al.* 'High-dose, hyperfractionated, accelerated radiotherapy using a concurrent boost for the treatment of non-small cell lung cancer: Unusual toxicity and promising early results'. *Int. J. Radiat. Oncol. Biol. Phys.* 36: 593-599, 1996.
- 75 Knöös T, Ahnesjö A, Nilsson P and Weber L. 'Limitations of a pencil beam approach to photon dose calculations in lung tissue'. *Phys. Med. Biol.* 40: 1411-1420, 1995.
- 76 Kroonwijk M, Pasma KL, Quint S, Visser AG and Heijmen BJM. 'Development and clinical implementation of in-vivo dosimetry using an electronic portal imaging device'. In: *Proceedings of the XIIth ICCR (International Congress on the use of Computers in Radiation Therapy)*. Edited by D D Leavitt and G Starkschall (Medical Physics Publishing, Madison, WI, 1997), pp. 276-278.
- 77 Kroonwijk M, Pasma KL, Quint S, Koper PCM, Visser AG and Heijmen BJM. 'In vivo dosimetry for prostate cancer patients using an electronic portal imaging device (EPID): detection of internal organ motion'. *Radiother. Oncol.* 49: 125-132, 1998.
- 78 Kubo HD and Hill BC. 'Respiration gated radiotherapy treatment: a technical study'. *Phys. Med. Biol.* 41: 83-91, 1996.
- 79 Kubo HD, Len PM, Minohara S and Mostafavi H. 'Breathing-synchronized radiotherapy program at the University of California Davis Cancer center'. *Med. Phys.* 27: 346-353, 2000.
- 80 Kung JH, Chen GTY. 'Monitor units verification calculation in IMRT in patient specific dosimetry QA'. In: *Proceedings of the XIIth ICCR (International Congress on the use of Computers in Radiation Therapy)*. Edited by W Schlegel and T Bortfeld (Springer-Verlag Berlin Heidelberg 2000), pp. 292-293.
- 81 Kutcher GJ, Burman C, Brewster MS *et al.* 'Histogram reduction method for calculating complication probabilities for three-dimensional treatment planning evaluation'. *Int. J. Radiat. Oncol. Biol. Phys.* 21: 137-146, 1991.
- 82 Kwa SLS, Lebesque JV, Theuws JCM, Marks LB, Munley MT, Bentel G, Oetzel D, Spahn U, Graham MV, Drzymala RE, Purdy JA, Lichter AS, Martel

- MK and TenHaken RK. 'Radiation pneumonitis as a function of mean dose; an analysis of pooled data of 540 patients'. *Int. J. Radiat. Oncol. Biol. Phys.* 42: 1-9, 1998.
- 83 Langer CJ, Movsas B, Hudes R, Schol J, Keenan E, Kilpatrick D, Yeung C and Curran W. 'Induction paclitaxel and carboplatin followed by concurrent chemoradiotherapy in patients with unresectable, locally advanced non-small cell lung carcinoma: report of Fox Chase Cancer Center study 94-001'. *Semin. Oncol.* 24 (suppl 12), 89-95, 1997.
- 84 Lebesque JV and Keus RB. 'The simultaneous boost technique: the concept of relative normalized total dose'. *Radiother. Oncol.* 22: 45-55, 1991.
- 85 Lebesque JV, Kwa SLS, Theuws JCM *et al.* 'Radiation pneumonitis as a function of dose and volume, an analysis of pooled data of 442 patients'. *Int. J. Radiat. Oncol. Biol. Phys.* 39 (supplement): 197, 1997 (abstr.).
- 86 Leibel SA, Zelefsky MJ, Kutcher GJ, Burman CM, Mohan R, Mageras GS, Ling CC and Fuks Z. 'The biological basis and clinical application of three-dimensional conformal external beam radiation therapy in carcinoma of the prostate'. *Semin. Oncol.* 21: 580-597, 1994.
- 87 Leunens G, Menten J, Weltens C, Verstraete J, and van der Schueren E. 'Quality assessment of medical decision making in radiation oncology: variability in target volume delineation for brain tumours'. *Radiother. Oncol.* 29: 169-175, 1993.
- 88 Li JG and Xing L. 'Inverse planning incorporating organ motion'. *Med. Phys.* 27: 1574-1578, 2000.
- 89 Li XA, Soubra M, Szanto J and Gerig LH. 'Lateral electron equilibrium and electron contamination in measurements of head-scatter factors using miniphantoms and brass caps'. *Med. Phys.* 22: 1167-1170, 1995.
- 90 Ling CC, Burman C, Chui CS, Kutcher GJ, Leibel SA, LoSasso T, Mohan R, Bortfeld T, Reinstein L, Spirou S, Wang, XH, Wu Q, Zelefsky M, Fuks Z. 'Conformal radiation treatment of prostate cancer using inversely-planned intensity-modulated photon beams produced with dynamic multileaf collimation'. *Int. J. Radiat. Oncol. Biol. Phys.* 35: 721-730, 1996.
- 91 Löf J, Lind BK and Brahme A. 'An adaptive control algorithm for optimization of intensity modulated radiotherapy considering uncertainties in beam profiles, patient set-up, and internal organ motion'. *Phys. Med. Biol.* 43:1605-1628, 1998.
- 92 LoSasso T, Chui CS and Ling CC. 'Physical and dosimetric aspects of a multileaf collimation system used in dynamic mode for implementing intensity modulated radiotherapy'. *Med. Phys.* 25: 1919-1927, 1998.

- 93 Lovelock DMJ, Chui CS, Kutcher GJ and Mohan R. 'Analysis of the photon beam treatment planning data for a scanning beam machine'. *Med. Phys.* 21: 1969-1977, 1994.
- 94 Low DA, Zhu XR, Purdy A and Söderström S. 'The influence of angular misalignment on fixed-portal intensity modulated radiation therapy'. *Med. Phys.* 24:1123-1139, 1997.
- 95 Low DA, Chao KS, Mutic S, Gerber RL, Perez CA and Purdy JA. 'Quality assurance of serial tomotherapy for head and neck patient treatments'. *Int. J. Radiat. Oncol. Biol. Phys.* 42: 681-92, 1998.
- 96 Low DA, Mutic S, Dempsey JF, Markman J, Goddu SM and Purdy JA. 'Abutment region dosimetry for serial tomotherapy'. *Int. J. Radiat. Oncol. Biol. Phys.* 45:193-203, 1999.
- 97 Luchka K and Shalev S. 'Pelvic irradiation of the obese patient: a treatment strategy involving megavoltage simulation and intratreatment setup corrections'. *Med. Phys.* 23: 1897-1902, 1996.
- 98 Lujan AE, Ten Haken RK, Larsen EW and Balter JM. 'Quantization of setup uncertainties in 3D dose calculations'. *Med. Phys.* 26: 2397-2402, 1999.
- 99 Lyman JT and Wolbarst AB. 'Optimization of radiation therapy III: A method of assessing complication probabilities from dose-volume histograms'. *Int. J. Radiat. Oncol. Biol. Phys.* 13: 103-109, 1987.
- 100 Ma L, Geis PB and Boyer AL. Quality assurance for dynamic multileaf collimator modulated fields using a fast beam imaging system. *Med. Phys.* 24: 1213-1220, 1997.
- 101 Ma L, Boyer AL, Xing L and Ma CM. 'An optimized leaf-setting algorithm for beam intensity modulation using dynamic multileaf collimation'. *Phys. Med. Biol.* 43: 1629-1643; 1998.
- 102 Mackie TR, Holmes T, Swerdloff S, Reckwerdt P, Desay JO, Yang J, Paliwal B *et al.* 'A new concept for the delivery of dynamic conformal radiotherapy'. *Med. Phys.* 20:1709-1719, 1993.
- 103 Mackie TR, Balog J, Ruchala K, Shephard D, Aldridge S, Fitchard E, Reckwerdt P, Olivera G, McNutt T and Mehta M. 'Tomotherapy'. *Sem. In Radiat. Oncol.* 9: 108-117, 1999.
- 104 Magaras GS and Mohan R. 'Application of fast simulated annealing for optimization of conformal radiation treatments'. *Med Phys.* 20: 639-647, 1993.
- 105 Mageras GS, Fuks Z, O'Brien J, Brewster LJ, Burman C, Chui CS, Leibel SA, Ling CC, Masterson ME, Mohan R and Kutcher GJ. 'Initial clinical experience with computer-controlled conformal radiotherapy of the prostate using a 50 MeV Medical Microtron'. *Int. J. Radiat. Oncol. Biol. Phys.* 30: 971-978,

- 1994.
- 106 Mageras GS, Fuks Z, Leibel SA, Ling CC, Zelefsky MJ, Kooy MH, van Herk M and Kutcher GJ. 'Computerized design of target margins for treatment uncertainties in conformal radiotherapy'. *Int. J. Radiat. Oncol. Biol. Phys.* 43: 437-445, 1999.
- 107 Martel MK, Ten Haken RK, Hazuka MB, *et al.* 'Dose-volume histogram and 3-D treatment planning evaluation of patients with pneumonitis'. *Int. J. Radiat. Oncol. Biol. Phys.* 28: 575-581, 1994.
- 108 Masterson ME, Mageras GS, LoSasso T, Jöreskog E, Larsson LG, Tsiraskis B, Febo R, Mohan R, Ling CC, Leibel SA, Fuks Z and Kutcher GJ. 'Preclinical evaluation of the reliability of a 50 MeV Racetrack Microtron'. *Int. J. Radiat. Oncol. Biol. Phys.* 28: 1219-1227, 1994.
- 109 McNutt TR, Mackie TR and Paliwal BR. 'Analysis and convergence of the iterative convolution/superposition dose reconstruction technique for multiple treatment beams and tomotherapy'. *Med. Phys.* 24:1-12, 1997.
- 110 Meeks SL, Bova FJ, Maryanski MJ, Kendrick LA, Ranade MK, Buatti JM and Friedman WA. 'Image registration of BANG gel dose maps for quantitative dosimetry verification'. *Int. J. Radiat. Oncol. Biol. Phys.* 43: 1135-1141, 1999.
- 111 Milosevic M, Voruganti S, Blend R, Alasti H, Warde P, McLean M, Catton P, Catton C, and Gospodarowicz M. 'Magnetic resonance imaging (MRI) for localization of the prostatic apex: comparison to computed tomography (CT) and urethrography'. *Radiother. Oncol.* 47: 277-284, 1998.
- 112 Mohan R. 'Field shaping for three-dimensional conformal radiation therapy and multileaf collimation'. *Seminars in Radiat. Oncol.* 5: 86-99, 1995.
- 113 Mohan R, Wu Q, Wang X and Stein, J. 'Intensity modulation, optimization, lateral transport of radiation, and margins'. *Med. Phys.* 23: 2011-2021, 1996.
- 114 Morill SM, Lane RG, Jacobson F and Rosen II. 'Treatment plan optimization using constrained simulated annealing'. *Phys. Med. Biol.* 36: 1341-1361, 1991.
- 115 Murray N, Coy P, Pater JL, *et al.* 'Importance of timing of thoracic irradiation in the combined modality treatment of limited stage lung cancer'. *J. Clin., Oncol.* 11: 336-344, 1993.
- 116 Nath R, Agostinelli AG, Gignac CE and Schultz RJ. 'Improvement of small field penumbra and dose distributions on a 4 MV accelerator'. *Int. J. Radiat. Oncol. Biol. Phys.* 7: 957-959, 1981.
- 117 Oldham M, Bauster I, Lord C, Smith TAD, Mcjury M, Warrington AP, Leach MO and Webb S. 'An investigation into the dosimetry of a nine-field tomotherapy irradiation using BANG-gel dosimetry'. *Phys. Med. Biol.* 43: 1113-1142, 1998.

- 118 Partridge M, Evans PM, Mosleh-Shirazi A and Convery D. 'Independent verification using portal imaging of intensity-modulated beam delivery by the dynamic (MLC) technique'. *Med. Phys.* 25:1872-1879, 1998.
- 119 Pasma KL, Kroonwijk M, Visser AG and Heijmen BJM. 'Portal dose measurements with a video-based electronic portal imaging device using a deconvolution algorithm'. In: *Proceedings of the XIIth ICCR (International Congress on the use of Computers in Radiation Therapy)*. Edited by D D Leavitt and G Starkschall (Medical Physics Publishing, Madison, WI, 1997), pp. 282-284.
- 120 Pasma KL, Heijmen BJM, Kroonwijk M and Visser AG. 'Portal dose image (PDI) prediction for dosimetric treatment verification in radiotherapy I: An algorithm for open beams'. *Med. Phys.* 25: 830-840, 1998.
- 121 Pasma KL, Kroonwijk M, de Boer JCJ, Visser AG and Heijmen BJM. 'Accurate portal dose measurements with a fluoroscopic electronic portal imaging device (EPID) for open and wedged beams and dynamic multileaf collimation.' *Phys. Med. Biol.* 43: 2047-2060, 1998.
- 122 Pasma KL, Dirkx MLP, Kroonwijk M, Visser AG and Heijmen BJM. 'Dosimetric verification of intensity modulated beams produced with dynamic multileaf collimation using an electronic portal imaging device'. *Med. Phys.* 26: 2373-2378, 1999.
- 123 Pasma KL, Kroonwijk M, Quint S, Visser AG and Heijmen BJM. 'Transit dosimetry with an electronic portal imaging device (EPID) for 115 prostate cancer patients'. *Int. J. Radiat. Oncol. Biol. Phys.* 45:1297-1303, 1999.
- 124 Pasma KL, Kroonwijk M, van Dieren EB, Visser AG and Heijmen BJM. 'Verification of compensator thicknesses using a fluoroscopic electronic portal imaging device'. *Med. Phys.* 26: 1524-1529, 1999.
- 125 Petti KL, Kessler ML, Fleming T and Pitluck S. 'An automated image-registration technique based on multiple structure matching'. *Med. Phys.* 21: 1419-1426, 1994.
- 126 Pickett B, Vigneault E, Kurlhanewicz J, Verhey L, Roach M. 'Static field intensity modulation to treat a dominant intra-prostatic lesion to 90 Gy compared to seven field 3-dimensional radiotherapy'. *Int. J. Radiat. Oncol. Biol. Phys.* 43:921-929, 1999.
- 127 Rhein B, Grosser KH, Haering P and Bortfeld T. 'Experience with dosimetric verification of intensity modulated radiotherapy (IMRT) at the German cancer research center'. *Int. J. Radiat. Oncol. Biol. Phys.* 45 (suppl 1): 408, 1999 (abstr.).
- 128 Roach M, Faillace-Akazawa P, Malfatti C, Holland J, and Hricak H. 'Prostate

- volumes defined by magnetic resonance imaging and computerized tomographic scans for three-dimensional conformal radiotherapy'. *Int. J. Radiat. Oncol. Biol. Phys.* 35: 1011-1018, 1996.
- 129 Robertson JM, Ten Haken RK, Hazuka MB *et al.* 'Dose escalation for non-small cell lung cancer using conformal radiation therapy'. *Int. J. Radiat. Oncol. Biol. Phys.* 37:1079-1085, 1997.
- 130 Rosander S, Sedlacek M and Wernholm O. 'The 50 MV Racetrack Microtron at the Royal Institute of Technology Stockholm'. *Nucl. Inst. Meth.* 204: 1-20, 1982.
- 131 Saunders MI, Dische S, Barrett A *et al.* 'Continuous hyperfractionated accelerated radiotherapy (CHART) versus conventional radiotherapy in non-small cell lung cancer: a randomized multicentre trial'. *Lancet* 350: 161-165, 1997.
- 132 Schaake-Koning C, van den Bogaert W, Dalesio, Festen J, Hoogenhout J, van Houtte P, Kirkpatrick A, Koolen M, Maat B and Nijs A. 'Effects of concomitant cisplatin and radiotherapy on inoperable non-small-cell lung cancer'. *New Engl. J. Med.* 326: 524-530, 1992.
- 133 Senan S, van Sornsen de Koste J, Samson M, Tankink H, Jansen P, Nowak PJ, Krol AD, Schmitz P and Lagerwaard FJ. 'Evaluation of a target contouring protocol for 3D conformal radiotherapy in non-small cell lung cancer'. *Radiother. Oncol.* 53: 247-255, 1999.
- 134 Söderström S and Brahme A. 'Optimization of the dose delivery in a few field techniques using radiobiological objective functions'. *Med. Phys.* 20: 1201-1210, 1993.
- 135 Spirou SV and Chui CS. 'Generation of arbitrary intensity profiles by dynamic jaws or multileaf collimators'. *Med. Phys.* 21: 1031-1041, 1994.
- 136 Spirou SV and Chui CS. 'Generation of arbitrary intensity profiles by combining the scanning beam with dynamic multileaf collimation'. *Med. Phys.* 23: 1-8, 1996.
- 137 Spirou SV and Chui CS. 'A gradient inverse planning algorithm with dose volume constraints'. *Med. Phys.* 25: 321-333, 1998.
- 138 Stein J, Bortfeld T, Dörschel B and Schlegel W. 'Dynamic X-ray compensation for conformal radiotherapy by means of multi-leaf collimation'. *Radiother. Oncol.* 32: 163-173, 1994.
- 139 Storchi P and Woudstra E. 'Calculation models for determining the absorbed dose in water phantoms in off-axis planes of rectangular fields of open and wedged photon beams'. *Phys. Med. Biol.* 40: 511-527, 1995.
- 140 Storchi P and Woudstra E. 'Calculation of irregular photon fields using pencil beam kernels derived from basic beam data'. *Phys. Med. Biol.* 41: 637-656, 1996.

- 141 Storchi P and van Gasteren JJM. 'A table of phantom scatter factors of photon beams as a function of quality index and field size'. *Phys. Med. Biol.* 41: 563-571, 1996.
- 142 Storchi P, Woudstra E, Verlinde P, Johansson P A and Samuelsson A. 'Calculation of absorbed dose distributions from dynamic wedges'. *Phys. Med. Biol.* 43: 1497-1506, 1998.
- 143 Stroom JC and Storchi PRM. 'Automatic calculation of three-dimensional margins around treatment volumes in radiotherapy planning'. *Phys. Med. Biol.* 42: 745-753, 1997.
- 144 Stroom JC, Korevaar GA, Koper PCM *et al.* 'Multiple two-dimensional versus three-dimensional PTV definition in treatment planning for conformal radiotherapy'. *Radiother. Oncol.* 47: 297-302, 1998.
- 145 Stroom J, de Boer JCJ, Huizenga H and Visser AG. 'Inclusion of geometrical uncertainties in radiotherapy treatment planning by means of coverage probability'. *Int. J. Radiat. Oncol. Biol. Phys.* 43: 905-919, 1999.
- 146 Stroom JC, Olofsen-van Acht MJ, Quint S, Seven M, de Hoog M, Creutzberg CL, de Boer HC and Visser AG. 'On-line set-up corrections during radiotherapy of patients with gynecologic tumors'. *Int. J. Radiat. Oncol. Biol. Phys.* 46: 499-506, 2000.
- 147 Svensson R, Källman P and Brahme A. 'An analytical solution for the dynamic control of multileaf collimators'. *Phys. Med. Biol.* 39: 37-61, 1994.
- 148 Svensson R, Åsell M, Näfstadius P and Brahme A. 'Optimization of the target, purging magnet and electron collector design for scanned high-energy photon beams'. *Phys. Med. Biol.* 43: 1091-1112, 1998.
- 149 Ten Haken RK, Thornton A.F, Sandler HM, LaVigne ML, Quint DJ, Fraass BA, Kessler ML and McShan DL. 'A quantitative assessment of the addition of MRI to CT-based, 3- D treatment planning of brain tumors'. *Radiother. Oncol.* 25: 121-133, 1992.
- 150 Ten Haken RK, Fraas BA, Lichter SA *et al.* 'A brain tumor dose escalation protocol based on effective dose equivalence to prior experience'. *Int. J. Radiat. Oncol. Biol. Phys.* 42:137-141, 1998.
- 151 Tsai JS, Wazer DE, Ling MN, Wu JK, Fagundes M, DiPetrillo T, Kramer B, Koistinen M, and Engler MJ. 'Dosimetric verification of the dynamic intensity-modulated radiation therapy of 92 patients'. *Int. J. Radiat. Oncol. Biol. Phys.* 40:1213-30, 1998.
- 152 Valicenti RK, Sweet JW, Hauck WW, Hudes RS, Lee T, Dicker AP, Waterman FM, Anne PR, Corn BW, and Galvin JM. 'Variation of clinical target volume definition in three- dimensional conformal radiation therapy for

- prostate cancer'. *Int. J. Radiat. Oncol. Biol. Phys.* 44: 931-935, 1999.
- 153 van Battum LJ and Heijmen BJM. 'Film dosimetry in water in a 23 MV therapeutic beam'. *Radiother. Oncol.* 34: 152-159, 1995.
- 154 van de Steene J, Van den Heuvel F, Bel A, Verellen D, De Mey J, Noppen M, De Beukeleer M and Storme G. 'Electronic portal imaging with 'on-line correction of setup error in thoracic irradiation: clinical evaluation'. *Int. J. Radiat. Oncol. Biol. Phys.* 40: 967-976, 1998.
- 155 van Dieren EB, Nowak PJCM, Wijners OB, van Sörnsen de Koste JR, van der Est H, *et al.* 'Beam intensity modulation using tissue compensators or dynamic multileaf collimation in three-dimensional conformal radiotherapy of primary cancers of the oropharynx and larynx including the elective neck'. *Int. J. Radiat. Oncol. Biol. Phys.* 47: 1299-1309, 2000.
- 156 van Gasteren JJM, Heukelom S, van Kleffens HJ, van der Laarse R, Venselaar JLM and Westermann CF. 'The determination of phantom and collimator scatter components of the output of megavoltage photon beams: measurement of the collimator scatter part with a beam-coaxial narrow cylindrical phantom'. *Radiother. and Oncol.* 20: 250-257, 1991.
- 157 van Herk M and Kooy HM. 'Automatic three-dimensional correlation of CT-CT, CT-MRI, and CT- SPECT using chamfer matching'. *Med. Phys.* 21: 1163-1178, 1994.
- 158 van Santvoort, JPC and Heijmen, BJM. 'Dynamic multileaf collimation without 'tongue-and-groove' underdosage effects'. *Phys. Med. Biol.* 41: 2091-2105, 1996.
- 159 Verellen D, Linthout N, Bel A, van den Berge D and Storme G. 'Initial experience with intensity modulated conformal radiation therapy for treatment of the head and neck region'. *Int. J. Radiat. Oncol. Biol. Phys.* 39: 99-114, 1997.
- 160 Verhey LJ. 'Comparison of three-dimensional conformal radiation therapy and intensity-modulated radiation therapy systems'. *Seminars in Radiat. Oncol.* 9: 78-98, 1999.
- 161 Vigneault E, Pouliot J, Laverdiere J, Roy J and Dorion M. 'Electronic portal imaging device detection of radioopaque markers for the evaluation of prostate position during megavoltage irradiation: a clinical study'. *Int. J. Radiat. Oncol. Biol. Phys.* 37: 205-212, 1997.
- 162 Vinceberg KA, Martel MK, Kessler ML, McShan DL, Kim JJ, *et al.* 'Dose escalation of brain tumors to 100+ Gy using automated IMRT optimization'. *Int. J. Radiat. Oncol. Biol. Phys.* 45 (suppl 1): 270, 1999 (abstr.).
- 163 Visser AG, Huizenga H, Althof VGM and Swanenburg BN. 'Performance of a

- prototype fluoroscopic radiotherapy imaging system'. *Int. J. Radiat. Oncol. Biol. Phys.* 18: 41-50, 1990.
- 164 Wang XH, Mohan R, Jackson A, Leibel SA, Fuls Z and Ling CC. 'Optimization of intensity-modulated 3D conformal treatment plans based on biological indices'. *Radiother. Oncol.* 37: 140-152, 1995.
- 165 Wang X, Spirou S, LoSassa T, Stein J, Chui C S and Mohan R. 'Dosimetric verification of intensity-modulated fields'. *Med. Phys.* 23: 317-327, 1996.
- 166 Webb S. 'Optimization of conformal radiotherapy dose distributions by simulated annealing'. *Phys. Med. Biol.* 34: 1349-1370, 1989.
- 167 Webb S. 'Optimization by simulated annealing of three-dimensional conformal treatment planning for radiation fields defined by a multileaf collimator: II. Inclusion of two-dimensional modulation of the X-ray intensity'. *Phys. Med. Biol.* 37: 1689-1704, 1992.
- 168 Webb S. 'Optimization of planning of intensity-modulated radiotherapy'. *Phys. Med. Biol.* 39: 2229-2246, 1994.
- 169 Webb S, Bortfeld T, Stein J and Convery D. 'The effect of stair-step leaf transmission on the 'tongue-and-groove problem' in dynamic radiotherapy with a multileaf collimator'. *Phys. Med. Biol.* 42: 595-602, 1997.
- 170 Wong JW, Sharpe MB, Jaffray DA, Kini VR, Robertson JM, Stromberg JS and Martinez AA. 'The use of active breathing control (ABC) to reduce margin for breathing'. *Int. J. Radiat. Oncol. Biol. Phys.* 44: 911-919, 1999.
- 171 Wong JW, Yan D, Jaffray DA, Edmundson G and Martinez AA. 'Interventional strategies to counter the effects of interfraction treatment variation'. In: *Proceedings of the XIIth ICCR (International Congress on the use of Computers in Radiation Therapy)*. Edited by W Schlegel and T Bortfeld (Springer-Verlag Berlin Heidelberg 2000), pp. 511-513.
- 172 Xia P, Verhey L. 'MLC leaf sequencing algorithm for intensity modulated beams with multiple static segments'. *Med Phys.* 25: 1424-1434; 1998.
- 173 Xing L, Chen Y, Li JG and Boyer AL. 'Monitor unit calculation for an intensity modulated photon field by a simple scatter-summation algorithm'. *Phys. med. Biol.* 45: N1-N7, 2000.
- 174 Xing L, Lin ZX, Donaldson SS, Le QT, Tate D, Goffinet DR, Wolden S, Ma L and Boyer AL. 'Dosimetric effects of patient displacement and collimator and gantry angle misalignment on intensity modulated radiation therapy'. *Radiother. Oncol.* 56: 97-108, 2000.
- 175 Yu CX, Du MN, Martinez AA and Wong JW. 'A method for implementing dynamic photon beam intensity modulation using independant jaws and a multileaf collimator'. *Phys. Med. Biol.* 40: 769-787, 1995.

- 176 Yu CX. 'Intensity modulate arc therapy with dynamic multileaf collimation: an alternative to tomotherapy'. *Phys. Med. Biol.* 40: 1435-1449, 1995.
- 177 Yu CX, Jaffray DA and Wong JW. 'The effects of intra-fraction organ motion on the delivery of dynamic intensity modulation'. *Phys. Med. Biol.* 43: 91-104, 1998.
- 178 Yu C, Chen DJ, Li A, Ma L, Shapard D and Sarfaraz M. 'Intensity-modulated arc therapy: clinical implementation and experience'. In: *Proceedings of the XIIIth ICCR (International Congress on the use of Computers in Radiation Therapy)*. Edited by W Schlegel and T Bortfeld (Springer-Verlag Berlin Heidelberg 2000), pp. 164-166.
- 179 Zelefsky MJ, Fuks Z, Happersett L, Lee HJ, Ling CC, Burman CM, Hunt M, Wolfe T, Venkatraman ES, Hackson A, Skwarchuk M and Leibel SA. 'Clinical experience with intensity modulated radiation therapy (IMRT) in prostate cancer'. *Radiother. Oncol.* 55: 241-250, 2000.
- 180 Zhu TC and Bjärngard BE. 'The head-scatter factor for small field sizes'. *Med. Phys.* 21: 65-68, 1994.



List of abbreviations

BEV	beam's eye view
BIM	beam intensity modulation
BIS	beam imaging system
CCD	charge coupled device
CT	computer tomography
CTV	clinical target volume
DMLC	dynamic multileaf collimation
DNA	desoxyribo nuvleic acid
DVH	dose volume histogram
EPID	electronic portal imaging device
GTV	gross target volume
ICRU	international commission of radiation units and measurements
IM	intensity modulation
IMAT	intensity modulated arc therapy
IMRT	intensity modulated radiotherapy
MiMiC	multileaf intensity modulated collimator
MLC	multileaf collimator
MM	medical microtron
MRI	magnetic resonance imaging
MRS	magnetic resonance spectroscopy
MVA	megavolt afbeelding
MVI	megavoltage imaging
NTCP	normal tissue complication
NTD	normalized total dose
PC	personal computer
PDI	portal dose image
PET	positron emission tomography
PMMA	polymethylmethacrylaat
PTV	planning target volume
RFA	radiation field analyzer
SPECT	single photon emission computed tomography
TLD	thermo luminescence dosimetry
1D	one dimensional
2D	two dimensional
3D	three dimensional

List of symbols

Be	beryllium
Cu	copper
D	dose
D_{\min}	minimum dose
D_{\max}	maximum dose
D_p	portal dose
Δ	difference
F	fluence
F_{opt}	optimized fluence
He	helium
L	length of treatment field
l	length of boost field
MU_{tot}	total number of monitor units
n	number
N	number
N_2	nitrogen
NTD_{avg}	average normalized total dose
S_c	head scatter factor
SD	standard deviation
σ	standard deviation
T	transmission
TD	tolerance dose
V	volume
V_{eff}	effective volume
w	width
W	wolfram

List of units

cc	cubic centimeter
cGy	centrigray
cm	centimeter
g	gram
Gy	gray
MeV	mega electronvolt
mm	millimeter
ms	millisecond
MU	monitor unit
MV	megavolt
s	second

Nawoord

Mijn dienstverband bij de Daniel den Hoed Kliniek begon op dezelfde dag dat ook de MM50 werd binnengehesen. Hoewel het idee om in een medische omgeving te gaan werken me op dat moment geweldig aansprak, had ik geen enkele ervaring met medische fysica of radiotherapie in het bijzonder. Ik kon dan ook niet vermoeden dat mijn werk nu, ruim acht jaar later, zou gaan leiden tot deze promotie. Dat deze mijlpijl nu toch bereikt is, heb ik mede te danken aan vele mensen met wie ik heb mogen samenwerken, of die op andere wijze een bijdrage hebben geleverd aan de totstandkoming van dit proefschrift. Enkele van hen wil ik hierbij in het bijzonder noemen.

In de eerste plaats wil ik mijn copromotor Ben Heijmen van harte bedanken. Als mijn directe begeleider heeft hij mij in de eerste periode wegwijs gemaakt binnen de fysica van de radiotherapie. Door zijn enthousiasme en gedrevenheid wist hij me steeds weer te prikkelen tot het oppakken van nieuwe onderzoeksideeën. Vele interessante en motiverende discussies, die vaak tot ver na werktijd doorgingen, lagen hieraan ten grondslag. Met zijn gezonde, kritische blik heeft hij mij geschoold in het schrijven van artikelen. Zijn oprechte belangstelling voor en betrokkenheid bij het wel en wee van collegae, waardeer ik zeer.

Bij de ontwikkeling van methoden voor dosimetrische kwaliteitscontrole met MVA heb ik prettig samengewerkt met Marco Kroonwijk, Hans de Boer en Kasper Pasma. Door het schrijven van software voor de EPID en voor de analyse van meetdata hebben zij een belangrijke bijdrage geleverd aan dit onderzoek. Daarnaast heeft Kasper het artikel uit hoofdstuk 8 van dit proefschrift geschreven.

Eerdere onderzoeksresultaten en ontwikkelde software van Jan van Santvoort waren zeer bruikbaar bij de implementatie van dynamische multileaf collimatie op de MM50. Onze vele discussies over IMRT in brede zin heb ik als plezierig en nuttig ervaren.

Bij de uitvoering van de klinische planningstudies heb ik nauw samengewerkt met diverse laboranten en artsen, met name Gert Korevaar, Marjolein van Os, John van Sörnsen de Koste, Suresh Senan, Peter Koper en mijn promotor Peter Levendag. Mede door hun inbreng en de enthousiaste medewerking van de laboranten van de MM50 wordt IMRT nu reeds enkele jaren toegepast in onze kliniek. De MM50 laboranten wil ik ook bedanken voor het vertrouwen dat ze in mij hebben gesteld. Ik hoop dat ik nog lange tijd mijn rol als 'huisfysicus' naar behoren zal kunnen vervullen.

In de afgelopen jaren zijn op de MM50 talloze metingen uitgevoerd, zowel in het kader van dit onderzoek, als ook tijdens de commissioning van de MM50 en bij reguliere kwaliteitscontroles. Vooral Norman Driver, Erik Loeff, Ben Göbel, Dirk Binnekamp en Marjolein Idzes hebben hieraan een grote bijdrage geleverd.

Voor technische ondersteuning kon ik een beroep doen op mijn collegae van MEA, met name Peter Brusche, Hans Groen, Eric Sanderse, Willem Lamprecht en Hans Bout. Door hun ervaring en inzet konden problemen op de MM50 meestal snel en adequaat worden opgelost, zodat de down-tijd tot een minimum beperkt bleef.

Mijn naaste collegae wil ik bedanken voor de prettige, ontspannen, maar tevens stimulerende werksfeer op KFI. Door de jaren heen is er een sterke onderlinge band gegroeid, mede door gezamenlijke uitjes, met de jaarlijkse survival als hoogtepunt.

In de afgelopen jaren heb ik een aantal stagiaires en afstudeerders van de Technische Hogeschool Rijswijk mogen begeleiden. Marco Kroonwijk, Arni van der Kamp, Karel van Ingen, Patrick van Gils en Gertjan van de Poel kunnen derhalve een deel van hun onderzoeksresultaten in dit proefschrift terugvinden.

Dick Fraass offered me the opportunity to visit his department during a period of three months. Being able to participate in investigations on IMRT from a quite different approach was very instructive for me. Our discussions at that time, and afterwards at different scientific meetings, inspired me a lot. I am also very honored that he was willing to take part in the opposition of this thesis.

I would like to thank all people of Scanditronix Medical, and especially Erik Jöreskog, for the fruitful cooperation during all these years, and the company for its financial contribution to this thesis.

De medewerkers van Medische Fotografie, met name Hans Vuik en Hans Kneefel, verdienen een pluim omdat ze steeds met grote snelheid en accuratesse dia's, foto's of posters wisten af te leveren voor een presentatie. Ook wanneer er op het laatste moment nog iets gewijzigd moest worden, stonden ze altijd voor mij klaar.

Mijn paranimfen Corine en Paul wil ik hartelijk danken voor hun vriendschap door de jaren heen en voor hun interesse in de vorderingen van mijn onderzoek. Vanuit zijn rol als paranimf vond Paul het vanzelfsprekend om dit proefschrift kritisch na te lezen.

Tot slot wil ik mijn familie van harte bedanken voor hun betrokkenheid en saamhorigheid. In het bijzonder ben ik veel dank verschuldigd aan mijn ouders voor de vele mogelijkheden en stimulansen die ze hebben gegeven om me steeds verder te ontwikkelen. Helaas heeft mijn vader dit de laatste jaren niet meer mogen meebeleven. Daarom wil ik aan hem dit proefschrift opdragen.

Curriculum vitae

Maarten Dirx werd geboren in Goirle op 12 februari 1966. In juni 1984 behaalde hij zijn Gymnasium β diploma aan het Pauluslyceum in Tilburg. Vervolgens studeerde hij Technische Natuurkunde aan de Technische Universiteit Eindhoven, waar hij in 1990 zijn ingenieursdiploma behaalde. Van september 1990 tot maart 1992 was hij als fysicus werkzaam bij het FOM instituut voor Plasmafysica 'Rijnhuizen' in Nieuwegein.

Sinds mei 1992 werkt hij binnen de Daniel den Hoed Kliniek. In de eerste periode was hij als projectmedewerker betrokken bij de installatie, acceptatie en klinische ingebruikname van het MM50 Racetrack Microtron. In 1994 is hij begonnen met zijn opleiding tot klinisch fysicus. Als onderdeel hiervan heeft hij in de zomer van 1996 drie maanden stage gelopen bij de University of Michigan in Ann Arbor (USA). In deze periode heeft hij zich met name beziggehouden met de planning van gesegmenteerde bestralingstechnieken voor patiënten met prostaat- en hersentumoren. Sinds februari 1997 is hij werkzaam als klinisch fysicus.

List of publications

- Dirkx MLP, Kroonwijk M, de Boer JCJ and Heijmen BJM. 'Daily dosimetric quality control of the MM50 Racetrack Microtron using an electronic portal imaging device'. *Radiother. Oncol.* 37: 55-60, 1995.
- Dirkx MLP, Heijmen BJM, Korevaar GA, van Os MJH, Stroom JC, Koper PCM and Levendag PC. 'Field margin reduction using intensity modulated X-ray beams formed with a multileaf collimator'. *Int. J. Radiat. Oncol. Biol. Phys.* 38: 1123-1127, 1997.
- Dirkx MLP, Heijmen BJM and van Santvoort JPC. 'Leaf trajectory calculation for dynamic multileaf collimation to realise optimised fluence profiles'. *Phys. Med. Biol.* 43: 1171-1184, 1998.
- Dirkx MLP, Essers M, van Sörnsen de Koste JR, Senan S and Heijmen BJM. 'Beam intensity modulation for penumbra enhancement in the treatment of lung cancer'. *Int. J. Radiat. Oncol. Biol. Phys.* 44: 449-454, 1999.
- Dirkx MLP and Heijmen BJM. 'Beam intensity modulation for penumbra enhancement and field length reduction in lung cancer treatments; a dosimetric study'. *Radiother. Oncol.* 56: 181-188, 2000.
- Dirkx MLP and Heijmen BJM. 'Testing of the stability of intensity modulated beams generated with dynamic multileaf collimation, applied to the MM50 Racetrack Microtron.' To be published in *Med. Phys.* 27 (12), 2000.
- Pasma KL, Dirkx MLP, Kroonwijk M, Visser AG and Heijmen BJM. 'Dosimetric verification of intensity modulated beams produced with dynamic multileaf collimation using an electronic portal imaging device'. *Med. Phys.* 26: 2373-2378, 1999.
- Van Sörnsen de Koste J, Voet P, Dirkx MLP, van Meerbeeck JP and Senan S. 'An evaluation of two techniques for beam intensity modulation in patients irradiated for stage III non-small cell lung cancer'. *Lung Cancer*, in press (2000).
- Heijmen BJM, Korevaar GA, Dirkx MLP, Huizinga H and Levendag PC. 'Conformatietherapie in Rotterdam: Het MM50-project'. *Klinische Fysica* 4-9, 1995/2.



